Establishment of biological test systems for metallic magnesium as a novel implant material and its interaction with bacteria, cells and tissue

Von der Fakultät für Lebenswissenschaften

der Technischen Universität Carolo-Wilhelmina zu Braunschweig

zur Erlangung des Grades eines

Doktors der Naturwissenschaften

(Dr. rer. nat.)

genehmigte

D i s s e r t a t i o n

von Muhammad Imran Rahim
aus Muzaffargarh / Pakistan

1. Referent: apl. Professor Dr. Peter Paul Mueller
2. Referentin: Professorin Dr. Susanne Engelmann
eingereicht am: 01.06.2015
mündliche Prüfung (Disputation) am: 27.08.2015

Druckjahr 2015

Vorveröffentlichungen der Dissertation

Teilergebnisse aus dieser Arbeit wurden mit Genehmigung der Fakultät für Lebenswissenschaften, vertreten durch den Mentor der Arbeit, in folgenden Beiträgen vorab veröffentlicht:

Publikationen

Rahim M. I, Eifler R, Rais B, Mueller P.P. Alkalization is responsible for antibacterial effects of corroding magnesium. Journal of Biomedical Materials Research Part A. 2015. doi: 10.1002/jbm.a.35503.

Weizbauer A, Kieke M, **Rahim M. I**, Angrisani GL, Willbold E, Diekmann J, Floerkemeier T, Windhagen H, Mueller P. P, Behrens P, Bude S. *Magnesium-containing layered double hydroxides as orthopaedic implant coating materials-An in vitro and in vivo study*. Journal of biomedical materials research Part B, Applied biomaterials. 2015. doi: 10.1002/jbm.b.33422.

Badar M, **Rahim M. I**, Kieke M, Ebel T, Rohde M, Hauser H, Behrens P, Mueller P. P. *Controlled drug release from antibiotic-loaded layered double hydroxide coatings on porous titanium implants in a mouse model.* Journal of Biomedical Materials Research Part A. 2014. doi: 10.1002/jbm.a.35358.

Badar M, Lunsdorf H, Evertz F, **Rahim M. I**, Glasmacher B, Hauser H, Mueller P. P. *Formation of an organic coat and release of corrosion microparticles from metallic magnesium implants.* doi: 10.1016/j.actbio.2013.03.012 Acta Biomater, 2013.

Rais B, **Rahim M. I**, Lienenklaus S, Weiss S, Tolle C, Seitz J-M, Menzel H, Hauser H, Mueller P. P. *Animal Test Models for Implant-Associated Inflammation and Infections*, in *Biomedical Technology*, T. Lenarz and P. Wriggers, Editors. 2015, Springer International Publishing. p. 175-187.

Tagungsbeiträge

Rahim M. I, Rais B, Kieke M. D, Evertz F, Weizbauer A, Windhagen H, Willbold E, Kietzman M,Glasmacher B, Stiesch M,Hauser H, Behrens P, Mueller P.P: *Characterization and optimization of antibacterial bacterial implants in vitro and validation in a small animal model* (Oral presentation). 48th DGBMT Annual Conference Hannover (2014).

Rahim M. I, Badar M, Hauser H and Mueller P. P: *Cells and material interaction*. (Oral presentation). 5th International PhD Symposium, Helmholtz Center for Infection Research, Braunschweig (2014).

Rahim M. I, Hauser H and Mueller P. P: *Establishment of different strategies to combat biomaterial associated infections* (Oral presentation). 4th Annual Retreat, Goslar Hahnenklee (2014)

Rahim M. I, Kieke M. D, Behrens P, Hauser H and Mueller P. P: *Nanoparticles based slow drug release coatings to combat implant-associated infections* (Oral presentation). 4th Annual Retreat, Goslar Hahnenklee (2013).

Posterbeiträge

Rahim M. I, Badar M, Kieke M. D, Ebel T, Rohde M, Behrens P, Hauser H and Mueller P. P: *Layered double hydroxide (LDH) based intrinsic and sustained drug delivery system to combat implant associated infections* (Poster). Der Deutschen Gesellschaft fur Biomaterialien (DGBM), Dresden (2014).

Rahim M. I, Rohde M, Lienenklaus S, Seitz J- M, Hauser H and Mueller P. P: *Establishment of biofilm mouse model to understand implant-associated infections* (Poster). 7th International Ph. D Symposium, Helmholtz Center for Infection Research, Braunschweig (2014).

Rahim M. I, Evertz F, Kieke M. D, Weizbauer A, Windhagen H, Willbold E, Glasmacher B, Hauser H and Mueller P. P: *Protective coatings on metallic magnesium to limit hydrogen generation* (Poster). 48th Annual Conference on Biomedical Technique, Hannover (2014).

Rahim M. I, Badar M, Kieke M. D, Heemeier T, Ehlert N, Duda F, Behrens P, Hauser H and Mueller P. P: *Establishing different strategies in the prevention of implant-associated infections* (Poster). 6th International Ph. D Symposium, Helmholtz Center for Infection Research, Braunschweig (2013).

Rahim M. I, Mueller P. P, Rhode M and Hauser H: *Evaluation and comparison of in vitro and in vivo degradation kinetics of magnesium* (Poster). 47th Annual conference on Biomedical Technique, Graz, Austria (2013).

Rahim M. I, Badar M, Mueller P. P, Kietzmann M, Weizbauer A, Glasmacher B and. Evertz F: *Ex vivo measurement of pull out force for biodegradable magnesium wires in Tibia bones* (Poster). Der Deutschen Gesellschaft fur Biomaterialien (DGBM), Handwerkskammer, Hamburg (2012).

Rahim M. I, Badar M, Mueller P. P, Hauser H, Abraham W-R and Kietzmann M: *Development of biological test systems for novel implant materials and interactions with bacteria, cells and tissues* (Poster). Summer School on Infection Research, Hotel Aquamaris, Rugen (2012).

Table of Contents

Abstract

Recently, magnesium based implants have gained increasing interest due to their degradability, biocompatibility and antibacterial properties. However, their clinical application is restricted due to unpredictable corrosion and the formation of gas cavities at the implantation site. The present study was aimed to identify efficiencies of magnesium as implant material and to find novel strategies to promote clinical applications. To identify relevant parameters and suitable degradation conditions, magnesium implants were incubated under various biological conditions. Magnesium is known to promote bone healing. We found that degradable magnesium interlocked with the bone *in vitro* in the absence of any cellular activity suggesting that at least in part this may be a purely physico-chemical process rather than a biological phenomenon. Further, a novel biomimetic degradable magnesium implant coating was established which substantially diminished the corrosion and eliminated the formation of gas cavities at the site of implantation. This coating was biocompatible with murine fibroblasts and with soft tissue in animals. Magnesium is reported antibacterial *in vitro*; however the underlying mechanism has not been defined. Therefore, antibacterial properties of magnesium were investigated and it was found that alkalization was solely responsible for antimicrobial effects. To investigate these antibacterial properties *in vivo*, magnesium implants were infected with bioluminescent strains of *P. aeruginosa* and *S. aureus* in mice. Contrary to the *in vitro* situation, magnesium implants were susceptible to bacterial adherence and led to the prolonged survival of bacteria. Such infections were highly resistant to high doses of antibiotics and to the host immune system. This is indicative of bacterial biofilm formation. Electron microscopy and biofilm specific staining clearly revealed the formation of exopolysaccharide matrix around bacteria which is typical for biofilms. Causal factors for prolonged bacteria survival appeared to be magnesium corrosion products. Hence, precautions must be taken before its future clinical applications however magnesium could be used as model to study implant-associated infections *in vivo.*

Zusammenfassung

Implantate auf Magnesiumbasis stoßen auf zunehmendes Interesse aufgrund ihrer Abbauarbeit, Biokompatibilität und antibakterielle Eigenschaften. Jedoch ist eine breite klinische Anwendung noch nicht möglich wegen unvorhersehbaren Korrosionseffekten und durch die Bildung von gasgefüllten Gewebehohlräumen an der Implantationsstelle. Die vorliegende Studie wurde durchgeführt um neue Strategien zu finden, welche die klinische Anwendung ermöglichen sollen. Um relevante Testparameter zu eruieren, wurden verschiedene Modelle untersucht. Magnesium ist zum Beispiel dafür bekannt, die Knochenheilung zu fördern. Wir fanden, dass solche Magnesiuminteraktionen mit dem Knochen auch in Abwesenheit von Zellen stattfinden, was darauf hindeutet, dass diese Interaktionen zumindest teilweise ein rein physikalisch-chemisches Phänomen sind. Außerdem wurde eine neuartige biomimetische und abbaubare Magnesiumbeschichtung gefunden, welche die anfängliche Korrosion beträchtlich verringert und die Bildung von Gashohlräumen im Gewebe eliminiert. Diese Beschichtung war biokompatibel mit murinen Fibroblastenkulturen und auch mit Weichgewebe in vivo. Weiter hat Magnesium antibakterielle Eigenschaften in vitro; wobei der zugrunde liegende Mechanismus bisher nicht bekannt war. Daher wurden antibakteriellen Eigenschaften von Magnesium untersucht und es wurde festgestellt, dass die Alkalisierung durch die Korrosion für sämtliche antimikrobiellen Wirkungen verantwortlich war. Um diese antibakteriellen Eigenschaften auch in vivo zu untersuchen, wurden Magnesiumimplantate in Mäusen infiziert mit lumineszent markierten *P. aeruginosa* und *S. aureus* Bakterien. Im Gegensatz zu den in vitro Resultaten waren Magnesiumimplantate anfällig für bakterielle Infektionen. Diese waren sehr widerstandsfähig gegenüber hohen Antibiotikadosen und auch gegenüber dem Immunsystem. Dies ist charakteristisch für bakterielle Biofilme. Elektronenmikroskopie und histologische Nachweismethoden zeigten die Bildung einer Exopolysaccharidmatrix, die für Biofilme typisch ist. Verantwortlich für das Überleben der Bakterien schienen Korrosionsprodukte zu sein. Daher müssen Vorsichtsmaßnahmen getroffen werden bevor Magnesiumimplantate für zukünftige klinische Anwendungen in Frage kommen. Andererseits könnten Magnesiumimplantate als Modell für die Erforschung von implantatassoziierten Infektionen dienen.

1 Introduction

1.1 Implant materials and their importance in medical science

An implant material is any foreign material that interacts with tissue and is primarily intended to substitute or restore the function of defect biological structure. These materials are helpful for millions of people worldwide after accidents or after suffering from chronic diseases [1-3]. Medical implants are then surgically inserted to restore the function or completely replace a missing body part [4]. These devices are artificially manufactured from biocompatible materials like stainless steel, chromium-cobalt alloys, titanium alloys, ceramic materials or polymeric materials [5-7]. For example, surgical sutures, needles, catheters, tooth fillings and bone plates are most frequently used [8,9]. Besides, biomaterials can also be made from proteins such as, glycoproteins, proteoglycans, elastin, fibrillin and extracellular matrix (ECM) [4,10]. Artificial tissue cages have been constructed from proteins to support cell growth and differentiation [11,12]. Medical implants encompass a vast variety of applications; hard or soft tissue repair or replacement, tissue regeneration and biomedical coatings [13,14]. Advances in the field of material science have led to the development of complete artificial organs such as heart, kidney and lung [15,16]. A total artificial heart can replace the functions of a normal human heart without inducing harmful effects [17]. Similarly, artificial lungs can support over 200 million people suffering with lung diseases [18]. The establishment and optimization of artificial organs is a new era in the field of health care. In most of clinical situations, hard tissue repair necessitates medical implants of high strength and stiffness. Metallic implants are preferably used due to their superior mechanical properties (strength and hardness) [19,20]. A complication with permanent implants is the requirement of revision surgery for their removal when the organs are restored [21]. This implant removal is considered invasive, particularly for old people [22]. However, biodegradable materials could overcome this unwanted surgery [23-25]. Biodegradable polymeric implants lack basic strength and stiffness therefore they cannot support hard tissue. This disadvantage shifted the main attention towards the degradable metals. Recently, degradable metallic implants have been introduced which have high stability and strength. Screws and pins made from degradable metals were already clinically used for internal bone fixation or tubular cages

used as coronary stents [26]. Iron as well as iron alloys have been proposed as degradable metallic implant material [27-29]. Still, corrosion particles released as a result of iron degradation may induce tissue irritations [27]. As an alternative, magnesium-based alloys have recently gained increasing attention as degradable metallic implants. They possess sufficient strength to support hard tissue. Magnesium-based medical devices have already demonstrated promising potential to support tissue functionalities in animal models and in human beings as well.

1.1.1 Magnesium as a potential biodegradable material

Magnesium degrades gradually inside the body and therefore can support the tissue for a time sufficient for the completion of healing process. After its exposure to physiological fluids, following chemical reaction takes place [30,31].

Anodic reaction**:** $Mg \rightarrow Mg^{2+} + 2e^-$

Cathodic reaction**:** $2H_2O + 2e^- \rightarrow H_2 + 2OH^-$

$Mg^{2+} + 2OH^- \rightarrow Mg(OH)_2$

As a degradable implant, corrosion products of magnesium are usually acceptable for host and non-allergic to surrounding tissue. Magnesium ions (Mg^{2+}) released as degradation product are excreted out of the body without inducing any harmful effects. Hydrogen produced during the reaction leads to the formation of small cavities in the surrounding tissue and no toxic effects from it have been reported so far. Magnesium corrosion is complicated phenomenon and it varies with the composition of the surrounding medium. Generally, it is fast in the presence of physiological solutions with low pH or high chloride concentration [32]. On the other hand, magnesium corrosion is slow in the presence of biological solutions in the presence of proteins and *in vivo* [33,34]. Interestingly, magnesium degradation triggers the precipitation of a corrosion layer on its surface which attracts the deposition of different elements from the surrounding environment [35,36]. With the establishment of this layer, the degradation process of magnesium also decelerates [37]. Many studies have shown that the corrosion layer is composed of the elements magnesium (Mg), oxygen (O), carbon (C), phosphorus (P), calcium (Ca) and traces of nitrogen (N) and sodium (Na) [38,39]. Calcium and phosphorus accumulating on the

surface of magnesium might be contributing to potentiate the process of new bone formation.

1.1.2 Magnesium (Mg^{2+}) as essential element for life

Mg^{2+} is essential for all living organisms. A human body of approximately 70 kg contains normally 24 g of magnesium which is equal to 1 mole. It is 4th most abundant cation of human body and the 2nd most abundant intracellular cation [40]. Normal plasma contains 0.7-1.1 mmol/l of magnesium, approximately 45% of which is protein-bound [41]. Mg^{2+} is involved in numerous biological activities. It serves as co-factor for ATP and many metabolic enzymes, co-regulator of protein synthesis and plays an important role in the stabilization of RNA and DNA structures [42]. Magnesium plays critical role in human metabolism and a slight variation in its normal blood concentration may lead to hypotension, muscular paralysis and respiratory distress [43]. Shortage of magnesium can lead to the incomplete formation of pigmented layer of eye [44]. Generally, during hypomagnesaemia (lack of magnesium in body), reserves of magnesium already stored inside bones are released in general circulation to compensate this deficiency. In case if magnesium level exceeds than its normal limits, excess amount is efficiently secreted out of the body without inducing any harmful effects on kidneys [45]. In addition, Mg^{2+} plays a critical role in the regulation of different intracellular pathways and in the activation of cell surface receptors mainly involved in human immune system. Mg^{2+} is also essentially required for activation and proliferation of blood lymphocytes in combination with Ca^{2+} [46,47]. Recently, Mg^{2+} has been reported to serve as second messenger during the pathways required for the activation of human T-lymphocytes [48]. Mg^{2+} was found to interact with magnesium transporter gene MAGT1 during T-cell activation and stimulation of epithelial cells. Therefore, disruption in the normal supply of Mg^{2+} within cells resulted into the CD4 lymhopenia, induction of severe viral infection and defective T-lymphocytes activation (Figure 1) [48]. Mg^{+2} have been reported to play an active role in the functioning of Reactive oxygen species (ROS). ROS are important signaling molecules produced inside live tissues and play important role in pathogen defense and programmed cell death [49,50]. Hence, imbalance between extracellular and intracellular Mg^{2+} levels can significantly influence ROS and indirectly to human or animals defense system against

pathogens [51]. In addition, magnesium is critically required for embryonic development in pregnant females [52,53]. A study in mice was conducted and it was found that the deficiency of magnesium during pregnancy resulted into growth retardation, abnormal fat metabolism, insulin resistance and diabetes in new born [54,55].

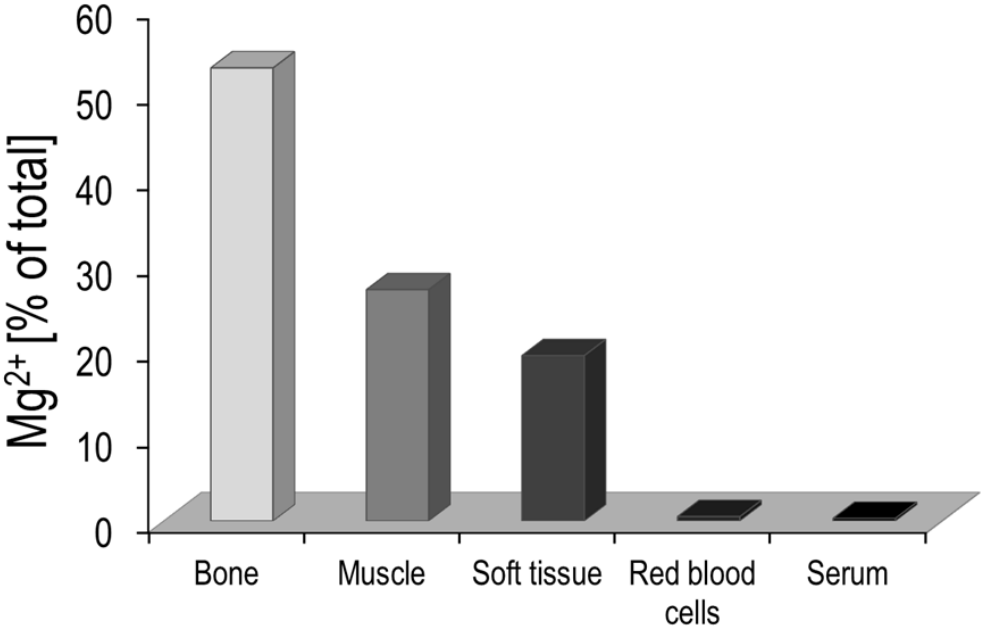

Figure 1: Distribution of magnesium in adult human body [56].

Table 1. **Importance of magnesium (Mg^{2+}) in human body**. Magnesium (Mg^{2+}) is actively involved in numerous activities of human body. Modified from [57].

Activities	Examples
Structural functions	Mitochondria Proteins Polyribosomes Nucleic acids Multiple enzyme complexes
Membrane functions	Cell adhesion Transmembrane electrolyte flux
Enzyme function	Enzyme Substrate (ATP-Mg, GTP-Mg) Kinases B Hexokinases Creatine Kinase Protein Kinase

	ATPases or GTPases Na^+/K^+-ATPase Ca^{2+}-ATPase Cyclases Adenylate cyclase Guanylate cyclase Direct enzyme activation Phosphofructokinase Adenylate cyclase Na^+/K^+-ATPase
Calcium antagonist	Muscle contraction/relaxation Neurotransmitter release Action potential conduction in nodal tissue

ATP, adenosine triphosphate; GTP, guanosine triphosphate; K, potassium; Mg, magnesium; Na, sodium; Ca, calcium.

1.1.3 Magnesium as biomedical implant

Magnesium has density 1.74 g/cm^3 and is the lightest of all commonly used metals. It is, therefore, implantable without putting much stress on the surrounding tissue [58]. For orthopedic applications, it has sufficient fracture toughness and its compressive yield strength as well as elastic modulus and Young's modulus values are close to natural bone [59,60]. After its application in the bone tissue in animal models, magnesium demonstrated excellent interaction with surrounding bone and stimulated the formation of new bone [37]. This means that magnesium would be the most appropriate candidate for repair of bone tissue as it could accelerate the process of new bone formation [37]. Hence, magnesium is a unique degradable metallic implant which can stimulate bone repair of fractured bones. Medical implants are always under the risk of being contaminated by resistant bacterial communities called biofilm [61]. Magnesium has demonstrated potential antibacterial properties *in vitro* against *Pseudomonas aeruginosa*, *Staphylococcus aureus* and *Escherichia coli* [62]. With inherent antibacterial properties, magnesium could overcome problems associated with device-related infections. Additional properties of magnesium are discussed further in detail below.

1.1.4 Cells and tissue response against magnesium

Implant materials act as “foreign body” for host tissue thus activating the immune system and recruiting host inflammatory cells [63]. If host immune reactions against implanted material are excessive, the material is not appropriate and it can have severe adverse effects on patient health [64]. Therefore, compatibility of biomaterial with host tissue is a fundamental requirement. A biocompatible implant material should be tissue friendly without provoking adverse effects like allergy and inflammation. Primarily, implant material candidates are first tested *in vitro* with different human or animal cell lines [65,66]. To this end, direct as well as indirect *in vitro* cell compatibility tests were conducted with magnesium as well as magnesium based alloys by using murine fibroblasts (NIH3T3 and L-929), osteoblasts (MC3T3-E1 and MG63) and blood vessels related cells (ECV304 and VSMC) and no cytotoxicity or reduced cells viability could be observed [67,68,65,69]. Fibroblasts were mainly employed because they are fundamental cells to establish tissue capsule around implants and remain in direct contact with implanted materials [70]. After exhibiting good compatibility with the individual cells, magnesium based implants have been evaluated *in vivo* in different animal models and were found compatible with the adjacent soft or hard tissues [37,71-73]. A comprehensive gene expression analysis of the tissue adjacent to magnesium after four weeks of implantation was also performed. It was found that gene expression pattern of the tissue surrounding magnesium was similar to standard materials titanium and polyglactin [74]. After showing promising compatibility with individual cells and animals, small screws made from magnesium were implanted into human being where they exhibited good compatibility and stability with the surrounding bone tissue without showing harmful effects on different body organs [73]. From this, it becomes quite evident that magnesium based implants show a promising compatibility with cells, in animals and in human tissue during preliminary clinical trials. Therefore, magnesium based implants can be proposed for clinical applications.

1.1.5 Major hindrances for clinical applications of magnesium

Despite having such advantageous properties, medical devices manufactured from magnesium have not been applied clinically so far due to certain limitations. Sometimes,

magnesium exhibits rapid degradation behavior in certain environments [75,76]. This may lead to pitting corrosion, cracks and cavities [77]. Associated with fast magnesium degradation is the production of hydrogen gas [78]. This gas release leads to the creation of gas cavities at implantation site (Figure 2) [79]. Although such gas bubbles have not been reported to pose toxic effects they may disrupt the contact between tissue and implant [80]. A strong tissue-implant interaction is necessary for fibrous tissue formation during the healing process and tissue repair that may be affected with such gas pouches. These gas cavities can also disturb the blood supply at the site of implantation thereby delaying healing process [81]. In some situations, gas cavities may result into cyst formation and tissue necrosis [82,83]. As alloy, magnesium is mixed with other metals and magnesium-based alloys are synthesized to overcome shortcomings [84,85]. However, some of the alloying elements have been found cytotoxic and must be avoided [86]. Biomedical surface coatings are another strategy to solve the problem of fast degradation [87,35]. Surface coatings are degradable and are replaced by a natural corrosion layer from the degradation of magnesium.

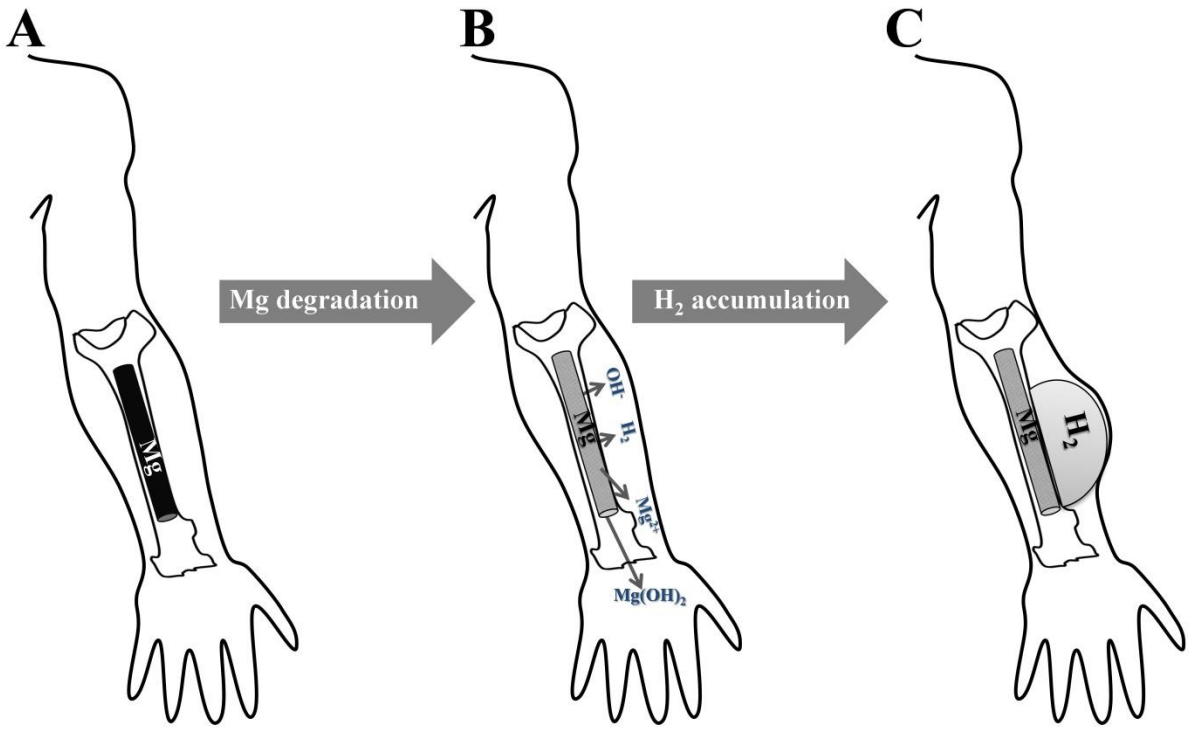

Figure 2: Corroding magnesium implants lead to the formation of gas cavities. Schematic diagram showing different stages after implantation of magnesium implants. A: Magnesium implant inserted in fractured radius bone. B: After sometime, magnesium starts to degrade into its corrosion products: hydroxide

ion (OH^-), hydrogen gas (H_2), magnesium ions (Mg^{2+}) and precipitation of magnesium hydroxide $Mg(OH)_2$ layer starts around magnesium. C: Hydrogen gas (H_2) starts to accumulate at the site of implantation leading to formation of gas bubbles.

1.2 Implant-associated infections

Bacteria thrive on medical implants [88-90]. Generally, surgical procedures for implantation are not completely sterile thus provide initial routes of entry for pathogens known as perioperative contamination [91]. Even if this implant insertion process is strictly hygienic, patients bearing fresh implants are inevitably hospitalized for short or long periods of time to support wound healing which is another threat for bacterial entry known as postoperative contamination or nosocomial infections [92]. Medical implants provide sites for initial microbial adherence [93]. Generally implant materials with rough surfaces augment bacterial adherence and therefore are more prone to infections [94]. Local immune system responses in the tissue adjacent to implant materials are also weak, such immune compromised zones provide an opportunity for bacterial colonization [95-97]. After *in vivo* implantation, medical device surfaces become a place of competition between host cells and bacteria. This competition has been phrased as "race for the surface" meaning that tissue cells and bacteria are in competition to make and initial attachment with implant surfaces [92]. Bacteria then undergo different stages to finally establish biofilms on the surface of medical implants. Biofilm is a structured consortium of surface attached bacteria surrounded by self-produced extracellular polymeric matrix [98]. Structurally, biofilms are constituted from well regulated release and amalgamation of polysaccharides, proteins, nucleic acids, lipids and DNA [99,100]. Diversity exists in the mechanisms of biofilm formation between different pathogens which varies from surface to surface. Generally biofilm formation can be divided into three different phases (A) Initial surface attachment (B) Proliferation and development of mature biofilm (C) Biofilm dispersal or detachment (Figure 3)[101]. Even though, under *in vivo* situations, molecular mechanisms involved in process of biofilm formation have not been well characterized and therefore little is known about them [102,103]. It has been reported that a conditioning film starts to develop on the surface of medical device after its exposure to body. This film facilitates subsequent bacterial adherence and is composed from different components from surrounding body fluids such as saliva, urine, blood and proteins such as fibrinogen,

collagen and fibronectin [104]. In addition, certain bacterial surface structures such as pili, fimbria and flagella help bacteria in the initial adherence and subsequent formation of micro colonies. Successful bacterial attachment is itself a shift into the second stage of biofilm maturation. During this stage, bacteria secrete certain proteins, exopolysaccharides, eDNA (extracellular DNA) and some other polymers and these components enable the formation of a multilayered extracellular matrix which provides protection from host defense [105]. Bacteria have cell-cell communication systems through diffusible chemical signaling molecules known as quorum sensing (QS) which plays an important role in biofilm maturation [106,107]. With the passage of time, nutrients deplete and waste products accumulate within biofilms. Therefore, bacteria trigger the release of certain factors such as D-amino acids leading towards biofilm disassembly so that they switch to the planktonic phase and may establish fresh biofilms at new sites [108]. This means that biofilms can have a finite life span depending on the availability of nutrients.

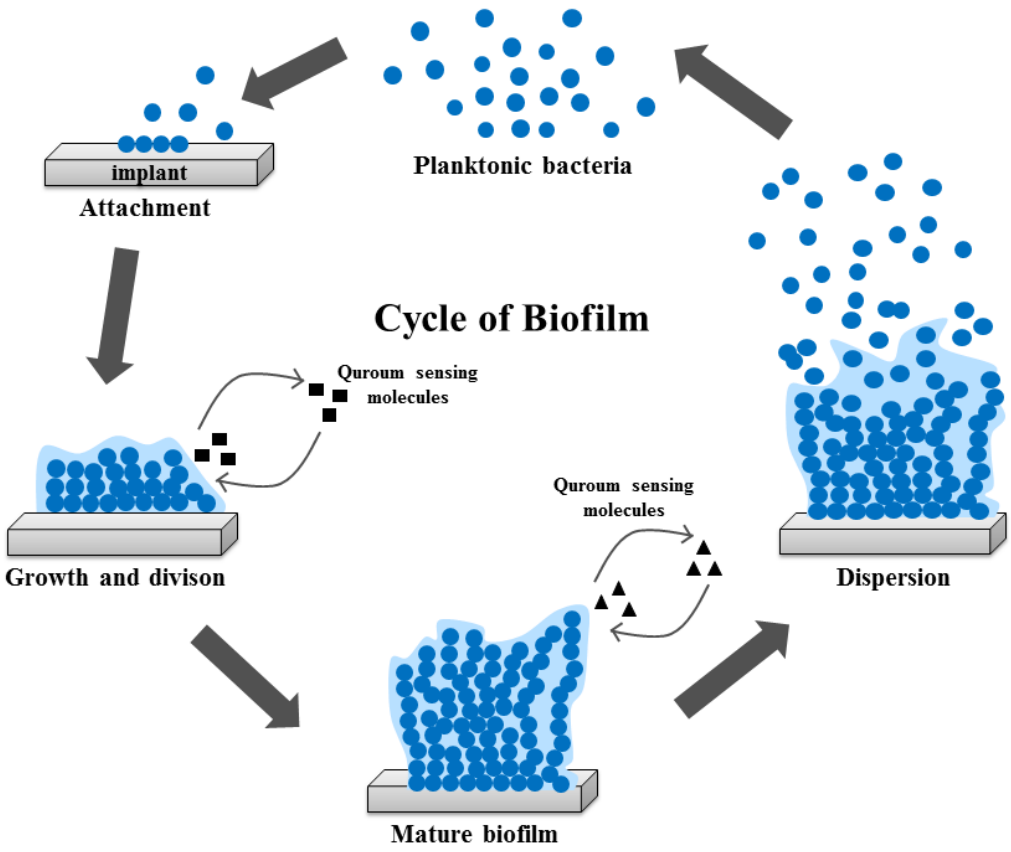

Figure 3: Schematic diagram demonstrating the process of biofilm formation on implant surfaces. Initially bacteria in their planktonic phase adhere on implant surfaces and start to make micro colonies.

Therewith, bacteria release certain quorum sensing molecules to attract other bacteria and side-by-side bacteria release mucous substances mainly composed from different proteins, sugar polymers and DNA which collectively lead to the formation of rigid Exopolysaccharide (EPS) matrix or mature biofilm. Within their respective biofilm matrix, bacteria show extremely low metabolic activities and therefore demonstrate resistance against antibiotics and host immune system. Due to nutrient depletion, bacteria release certain factors which lead to the biofilm disruption. Bacteria are then released from this self-produced matrix and switch back to their planktonic phase whereby they disperse to new appropriate surfaces to establish fresh biofilms.

1.2.1 Characteristics of bacteria within a biofilm matrix

Biofilm formation is a complex process. When bacteria transform to this distinct mode of living, they activate certain genes. Therefore, biofilm bacteria demonstrate different gene expression profiles as compared to their free-living (planktonic) counterparts. This is associated with phenotypic changes and therefore bacteria show different morphologies within both modes [109]. Bacteria in biofilms demonstrate strong resistance against conventional antibiotics and different antimicrobial agents (Figure 4) [90]. There are different factors responsible for the antibiotic resistance of biofilm bacteria. First, bacteria within biofilms are surrounded by a exopolymeric matrix structures which serve as diffusion barrier against antibiotics [110]. Second, growth rates, respiration rates and metabolic activities of biofilm bacteria are low and most antibiotics can only effectively target bacteria if they are actively growing. Third, higher cell densities and over-expression of protective molecules by bacteria within biofilms have been identified as important reason for antibiotic resistance [111]. Another serious concern of biofilms is their strong resistance against the host defense system. For this, bacteria release certain extracellular factors such as proteases, toxins and lipases that hinder the normal functions of immune cells (such as phagocytes, NK cells, T cells), inactivate certain cytokines (IL-1,IL-2), cause disruption of immunoglobulins and also inactivate the complement system [112]. Therefore, biofilms on biomedical implants are extremely difficult to eradicate. Such implant failures can result in severe implications for patient health and treatment costs [113].

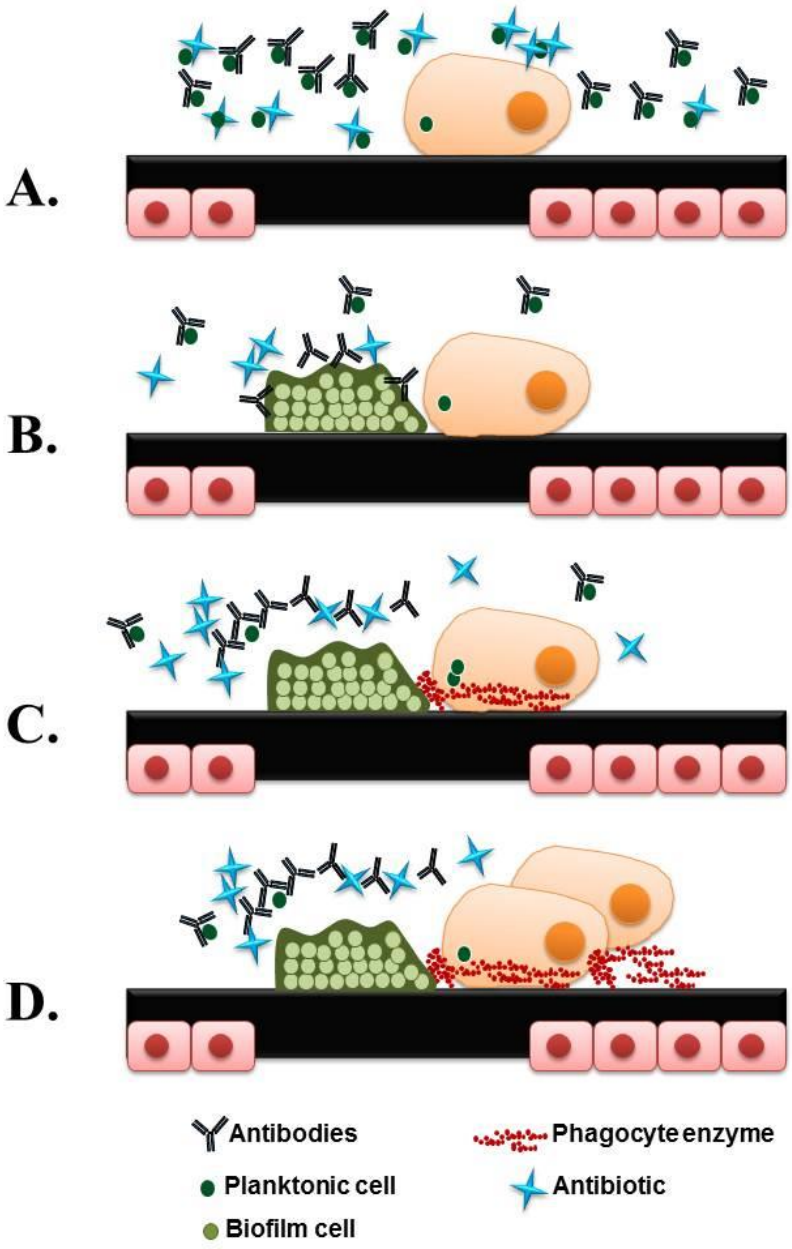

Figure 4: Biofilm resistance against host immune system and antibiotics. A: Planktonic bacterial cells are susceptible to conventional antibiotics and host defense system. B: bacteria attach with the surface of implant material and make biofilm which leads to the recruitment of antibodies, antibiotics and phagocytes. C: antibiotics, antibodies cannot penetrate inside biofilm matrix and phagocytes cannot engulf them. D: Inability of phagocytes to engulf biofilms leads to the massive release of phagocytic enzymes which may harm cells and tissue near implant surface.

1.2.2 Biofilm formation by major pathogens involved in implant-related infections

Staphylococcus aureus and *Pseudomonas aeruginosa* are major pathogens responsible for biomaterial-associated infections [114]. Normally, *Staphylococcus aureus* manage to infect

medical implant surfaces during surgical procedures or from transitory bacteremia. After attachment *S. aureus* proliferate and finally develop resistant biofilms on implant surfaces. Biofilm formation by *S. aureus* on medical implants can be divided into different stages; (1) primary bacterial attachment on implant surface (2) further proliferation to establish multiple layers and convert into micro colonies (3) finally, secretion of extracellular matrix and subsequent development of mature biofilm around bacteria (4) biofilm disassembly and conversion of bacteria into planktonic cultures. During the first stage of biofilm formation, *S. aureus* come into contact with abiotic implant surfaces and it is assumed that electrostatic and hydrophobic forces between material surfaces and bacteria accomplish the initial attachment. In addition, to augment stable attachment bacteria release specific proteins like autolysin and adhesins [91,92]. In the second stage, bacteria multiply and form micro colonies [84,115]. In the third stage, bacteria extend cell-cell adhesion by secreting polysaccharide intercellular adhesion (PIA) molecules and progressively move to subsequent biofilm formation on colonized surfaces [102]. This is most critical stage during which biofilm maturation and its persistence by *S. aureus* is regulated by a coordinated release of specific proteins such as Bap (Biofilm associated proteins), Aap (accumulation associated protein), FnBPs (fibronectin-binding proteins). *S. aureus* become completely encased within extracellular polymeric matrix which is constituted by exopolysaccharide, protein and extracellular DNA (eDNA)[103]. *S. aureus* also activate cell-cell communication system called quorum sensing (QS) which is encoded by *agr* (accessory gene regulator) locus and plays an important role in biofilm formation [94,104,116,101]. Biofilms in the maturation phase cannot last longer due to nutrient depletion and therefore enter into detachment phase. Auto inducing peptide (AIP) is released which trigger biofilm disassembly phase. With this, expression of RNAIII and production of extracellular proteases and phenol- soluble modulins is considerably increased which cause the lysis of biofilm [105]. *agr* (accessary gene regulator) mediated quorum-sensing system is also reactivated during dispersal stage and triggers biofilm detachment [117]. After biofilm disruption bacteria switch again to their planktonic phase and search for new surfaces to establish fresh biofilms.

Pseudomonas aeruginosa is an opportunistic pathogen and is the leading cause of morbidity and mortality in cystic fibrosis patients. Most commonly this pathogen colonizes

the lungs and air ways of patients and establishes mucoid biofilms [108]. In addition these bacteria can colonize on non-living surfaces like medical implants and can establish resistant biofilms [109]. Biofilm formation by *Pseudomonas aeruginosa* on medical implants involves three stages and is similar to *S. aureus*. In addition to proteins and exopolysaccharides, extracellular DNA (eDNA) is major constituent of the *P. aeruginosa* biofilm matrix [118]. Flagella and type IV pili facilitate the process of initial attachment [106,107]. Then, bacteria start to form micro-colonies. Attachment is a stimulus for the activation of genes such as algC, algD and algU::lacZ [110,111]. These genes are involved in the synthesis of extracellular matrix which is required for the formation of mature biofilms. In the next step, these surface attached micro colonies differentiate into a more complex architecture to form mature biofilms. During differentiation *P. aeruginosa* also activate the quorum sensing (QS) system and release signal molecules known as auto inducers (AI). The role of these AI in biofilm maturation has been evidenced after their isolation from infected catheters [112]. Usually, production and activation of AI is known to directly correlate with cell density. *P. aeruginosa* uses two well-known QS systems, *las* and *rhl* [119]. Both of these systems coordinate virulence gene products and are mandatory for biofilm maturation [120]. *las* and *rhl* mutant *P. aeruginosa* strains made thin biofilms which were lacking major biofilm components [119]. After sometime, bacteria start to detach and disperse to convert themselves into planktonic cells. The detachment process in *P. aeruginosa* is triggered by a self-produced process of local hydrolysis which digests extracellular polysaccharide matrix and converts sessile communities of bacteria into motile free living cells. A phenomenon of physical detachment was observed by which small biofilm micro colonies are disconnected from surfaces and carried by fluid to new places [121]. *P. aeruginosa* also activate anaerobic metabolism leading the production of nitric oxide (NO) which is involved in biofilm dispersal [122].

1.2.3 Strategies to combat biomaterial associated infections

Biofilms on implants can become life threatening. It is difficult to eradicate biofilms using conventional antibiotics or anti-biofilm compounds. The only effective treatment is revision surgery and prolonged antibiotic administration. Surgical procedures along with post-operative medication expenditures inflict serious consequences on patient health and

economy. Estimated medical expenses on the treatment of such infections are more than 3 billion dollars in USA alone [123]. Recently two important strategies have evolved (1) Establishment of antibacterial coatings on medical implants (2) antimicrobial and microbial adhesion resistant implant surfaces [124]. Controlled release of antibiotics directly from medical implants surfaces seems to be a suitable strategy to improve the efficacy of drugs against biofilms. Local drug delivery at the site of implantation has certain advantages. It allows the application of selected antibiotics against targeted pathogens. High drug concentration at the implantation site avoids the problem of systemic toxicity. Antibiotics such as amoxicillin, vancomycin, tobramycin, cefamendol, cephalothin, and gentamycin were coated on the surfaces of polymers which effectively prevented microbial adhesion [125,126]. Bacteria can develop resistance against antibiotics. To overcome this difficulty, local delivery of alternative antibacterial agents has been applied [127]. Silver nanoparticles (AgNPs) are reported as antibacterial and biocompatible agents [128]. Medical implants coated with silver nanoparticles do not induce resistance and synergistic antibacterial effects of silver and zinc coatings on implant surfaces have been reported [129]. Nitric oxide (NO) is reported as potent antibacterial agent and implant coatings with promising antibacterial and biofilm dispersal activities [130,131]. As another strategy, polymers with anti-adhesive surfaces demonstrate resistance against initial bacterial attachment. Due to their intrinsic properties, they facilitate mammalian cell attachment but pose significant resistance against bacterial attachment [132]. Similarly, broad-spectrum anti-biofilm peptides have been discovered which specifically target cellular stress responses and inhibit initial biofilm formation and disrupt existing ones [133]. Interference with biofilm formation using targeted molecules can be another strategy. Peptides have been discovered that inhibit quorum-sensing [134]. All these strategies established to overcome device related infections can significantly enhance the performance of medical implants. Still, there is great demand to investigate and establish new assays to protect medical implants surfaces from bacterial contamination.

1.2.4 Different animal models for biofilm formation

The majority of the molecular tactics used by bacteria to transform into biofilm mode have been discovered using *in vitro* assays. *In vitro* test systems are conducted in rather simple

conditions and therefore it is unpredictable if bacteria use similar strategies *in vivo.* Alternatively, animal models are established to verify *in vitro* results. Specifically, to understand biofilm formation on indwelling devices, different *in vivo* models representing device-related infections have been introduced. Urinary tract infection is the most frequent example of biomaterial-associated infections. Therefore, as a first attempt to establish an *in vivo* model, small catheter tubes infected with *Staphylococcus epidermidis* were subcutaneously implanted in mice [135]. In this foreign body mouse model, bacterial biofilms were evaluated by abscesses, adhesions, erythema and excessive slime productions. Further, intravascular venous catheter (IVC) and totally implantable venous access ports (TIVAP) rat models were introduced to study microbial colonization of medical implants [136]. For example, using such models the role of polysaccharide intercellular adhesion (PIA) and autolysin AtE in *S. epidermidis* biofilm formation was validated *in vivo* [137]. Later, this central venous catheter (CVC) model was successfully adopted and investigated in mice and rabbits [138,139]. After successful use of hollow structures to support artificial biofilm formation, stainless steel pins were inserted as foreign-body into rabbit tibia to support biofilm formation by *S. aureus* [140]. This model was successfully used to understand osteomyelitis and prosthetic joint infections (PJI) [141]. Endotracheal tubes were implanted into sheep, pigs or dogs as biofilm models for *P. aeruginosa* [142,143]. Tissue cages consisting of rigid tubes with holes were subcutaneously implanted into mice, rats, hamsters and guinea pigs to serve as foreign body biofilm animal models [144]. A vascular catheter animal model has been most frequently used for biofilm formation. In this model, vascular catheters were subcutaneously implanted into the animals [145]. With the advancement in imaging systems, bioluminescent bacterial strains have been used for the investigation of biofilms *in vivo*. It allowed a non-invasive *in vivo* imaging of biofilm formation [146]. Validation of staphylococcal accessory regulator (sarA) and ica in *S. aureus in vivo* biofilm formation was done using this mouse model [147]. Moreover, cardiac valves, vascular grafts, bone cement and surgical meshes have also been subcutaneously implanted in animal models as artificial devices to support biofilm formation [148-150]. Different animal models have significantly helped to understand *in vivo* biofilms. These models have been used to test

anti biofilm properties of different peptides [132]. There is still much to improve for animal models which mimic biofilm formation.

1.3 Aim

The present study was divided into different parts (Figure 5). Major aims of the this study were

(i) To establish suitable *in vitro* test systems to identify relevant parameters and suitable degradation conditions for metallic magnesium as medical implant material.

(ii) To establish biomechanical test systems to investigate interaction between magnesium for its application as orthopedic implant material with murine bones

(iii) To find novel strategies to overcome major problems associated with clinical application of magnesium as an implant material.

(iv) To identify underlying mechanisms responsible for *in vitro* antibacterial properties of magnesium.

(v) To establish a mouse model to study biomaterial-associated infections

(vi) To develop different strategies and animal models to combat biomaterial-associated infections.

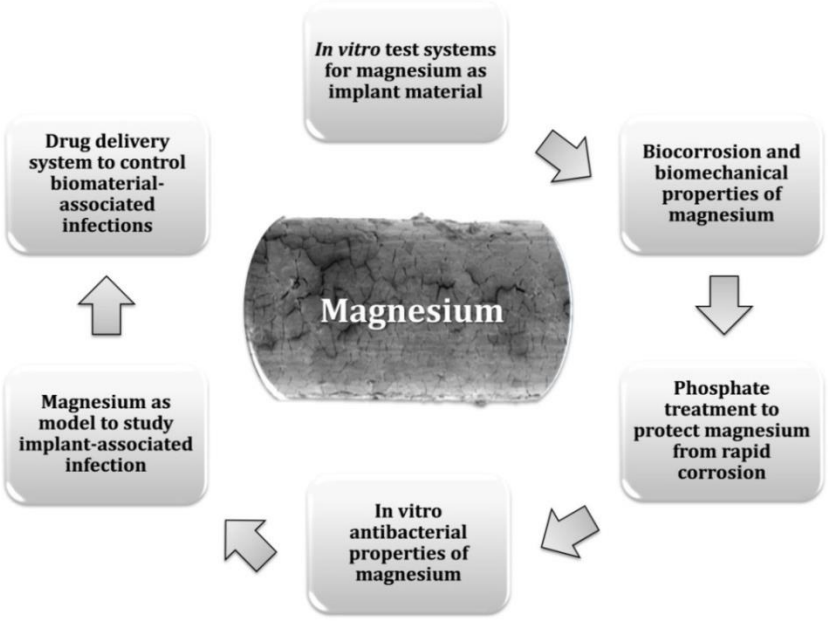

Figure 5: Schematic diagram representing the classification of current study into different projects. Magnesium was center of investigation and research during present study.

2 Material and Methods

2.1 Materials

2.1.1 Implant materials

Table 2: List of implant materials investigated during present study.

Implant material and their properties	Supplier
Magnesium discs with 99.99% purity and 5mm diameter and 2mm thickness	Institute of Materials Science, Leibniz University Hannover, Germany
Magnesium discs coated with fluoride (Shaped in discs with 5mm diameter and 2mm thickness)	Institute of Materials Science, Leibniz University Hannover, Germany
Magnesium wires (99.99% pure, 0.4 mm in diameter)	Good fellow Cambridge Ltd., Huntingdon
Magnesium granulates	Riedel-de Haen AG, Seelze, Germany
Magnesium silver alloy discs with 5mm diameter and 2mm thickness)	Helmholtz-Zentrum Geesthacht, Germany
Magnesium silver alloy wires (0.4mm in diameter)	Helmholtz-Zentrum Geesthacht, Germany
Plain titanium discs (Grade5 with 7mm diameter and 2mm thickness)	3di GmbH, Jena, Germany
Porous titanium discs (7mm diameter and 2mm thickness)	Department of Powder Technology, Helmholtz Center Geesthacht
Titanium wires (0.4 mm in diameter)	Good fellow Cambridge Ltd., Huntingdon
Mg,Fe-LDH pellets ($Mg_4Fe_2(OH)_{12}/(CO_3)\cdot 3H_2O$ with M(III) = Fe^{3+})	Fluka, Buchs, Switzerland
Mg,Al-LDH pellets ($Mg_4Al_2(OH)_{12}/(CO_3)\cdot 4H_2O$ with M(III) = Al^{3+}	Fluka, Buchs, Switzerland
Porous glass (4mm beads with 60µm pore size)	Robu, GmbH, Germany

Poly L lactic acid (PLLA) (5mm beads)	Good fellow Cambridge Ltd., Huntingdon
Magnesium granulates	Non ferrum, GmbH, Austria

2.1.2 Chemicals and antibiotics

Table 3: List of chemicals and antibiotics used in present work.

Chemical	Supplier
Potassium di-hydrogen phosphate	Carl Roth GmbH, Karlsruhe, Germany
Potassium mono-hydrogen phosphate	Merck, Darmstadt, Germany
Sodium di-hydrogen phosphate	Merck, Darmstadt, Germany
Magnesium chloride	Carl Roth GmbH, Karlsruhe, Germany
Magnesium hydroxide	Fluka Chemie GmbH, Deisenhofen, Germany
Magnesium powder	Riedel-de Haen AG, Seelze, Germany
Sodium hydroxide	Sigma Aldrich
Ciprofloxacin (Powder)	(Fluka Chemie GmbH, Deisenhofen, Germany)
Cipro HEXAL	Hexal, Germany
Hydrochloric acid	Roth
Layered double hydroxide micro particles ($Mg_4Al_2(OH)_{12}(SO_4)_2 \cdot 6H_2O$)	Fluka Chemie GmbH, Deisenhofen, Germany
Isofluran	Albrecht Gmbh, Germany
Luciferin	Caliper LS
Bepanthen eyes cream	Bayer

2.1.3 Buffers, media and reagents

Table 4: Overview of buffers, media and different reagents used in current study.

Buffers, media and reagents	Supplier
FCS (fetal calf serum)	Gibco/Life Technologies, Darmstadt, Germany
DMEM (Dulbecco's modified Eagle's medium)	Gibco/Life Technologies, Darmstadt, Germany
CFSE (Fluorescent cell proliferation dye), (5- and 6-Carboxyfluorescein diacetate succinimidyl ester)	eBioscience, Inc., San Diego, CA, USA
Xylidyl blue reagent	Magon, Pointe Scientific, Inc. USA
β-mercaptoethanol	Sigma Aldrich
DMSO	Sigma Aldrich
TRIzol reagent	Life Technologies, Darmstadt, Germany
DNA loading dye	Bioline

2.1.4 Cell lines

Table 5: List of cell lines mainly used to test biocompatibility of implants in present study.

Cell line	Supplier
Fibroblasts (NIH3T3)	ATCC CRL-1685; LGC Standards GmbH, Wesel, Germany
Osteosarcoma (MG63)	ATCC CRL-1427; LGC Standards GmbH, Wesel, Germany

2.1.5 Bacteria

Table 6: List of bacterial strains used in the present work.

Strain	Source
Pseudomonas aeruginosa (1 CTX::lux)	Laboratory strain which has been Genetically made bioluminescent by the insertion of the lux into the genomic DNA [151,152].
Pseudomonas aeruginosa (*pqsA*$^{-}$)	Bioluminescent by the insertion of the lux into the genomic DNA. This mutant strain is deficient in quorum sensing system [152].
Pseudomonas aeruginosa (1 WT)	Kindly donated by Dr. Susanne Häussler
Pseudomonas aeruginosa (PA14 WT)	Kindly donated by Dr. Susanne Häussler
Staphylococcus aureus (XEN29)	Bioluminescent by the insertion of the lux into the genomic DNA. (PerkinElmer, Massachusetts, USA)
Staphylococcus aureus (WT)	Kindly donated by Dr. Susanne Häussler
E. Coli (lux)	Bioluminescent by the insertion of the lux into the genomic DNA [153].
Salmonella (lux)	Laboratory strain genetically made bioluminescent by the insertion of the lux into the genomic DNA [154]

2.1.6 Kits

Table 7: List of kits employed during present study.

Kit	Supplier	Catalog No.
RNeasy mini kit(50)	QIAGEN	74104
Power Biofilm RNA isolation kit	MO BIO Lab, Germany	25000-50
DNase treatment kit	Life Technologies, Darmstadt, Germany	AM1906

RNase-free DNase	QIAGEN	79254
QIA shredder	QIAGEN	79656
MICROBE Enrich Kit	Life Technologies, Darmstadt, Germany	AM1901
MICROB *Express*™ Bacterial mRNA Enrichment Kit	Life Technologies, Darmstadt, Germany	AM1901
Script Seq™ (RNA-Seq Library Preparation Kit)	(HiSeq2500, Illumina, USA)	SSV21106 SSV21124

2.1.7 Equipment

Table 8: Overview of laboratory equipment used in current work.

Equipment	Manufacturer
Electron microscope	Zeiss, Oberkochen, Germany
EDX (Energy dispersive x-ray spectroscope)	Hitachi REM-S3400N
Diffractometer	STOE & Cie GmbH, Darmstadt
Microscopes	Zeiss, Jena, Germany
Fluorescent microscope	Zeiss, Jena, Germany
Autoclave	Belimed steam sterilizer 6-6-6 HS1 FD
Centrifuges	OMNILAB, GmbH, Germany, Thermo Fisher SCIENTIFIC
Binocular Microscope	Zeiss, Jena, Germany
Camera	CASIO, SAMSUNG
Nano drop	Peglab, Erlagen, Germany
-20°C freezer	Liebherr
-80°C freezer	Thermoforma

4°C refrigerator	Liebherr
CO_2 incubator for cell culture	Labotect
Hot plate	IKA®-Werke GmbH & Co. KG, Staufen, Germany
Deionized water setup	Millipore MilliQ
Micropipettes	Gilson
pH meter (microelectrode)	Mettler-Toledo GmbH, Giessen, Germany
Nanodrop ND-1000 UV-Vis Spectrophotometer	Nanodrop Technologies, Wilmington, USA
Weight measurement	Sartorius
Sterile work benches (Maxisafe 2020)	Thermoscientific
Vortex	Scientific industries Vortex Genie 2
Water bath	GFL
Microwave oven	Whirlpool
Pipette boy	Pipettboy IBS integra Biosciences
Pipettes	Gilson
Xenogen IVIS 200	Caliper Life Sciences
Surgical tools (forceps, scissors, scalpel)	Fine Science Tools GmbH, Germany
Tissue homogenizer	Milteryi biotec, Germany
Metal fixture	Rencast FC52/53 Isocyanate, FC53 Polyol, Füller DT 082; Gössl & Pfaff GmbH, Karlskron/Braulach, Germany
Vernier caliper	(Wisent tools, Germany)
Materials testing machine	Zwick/Roell 1445, Zwick GmbH & Co KG, Ulm, Germany
Hair trimmer	Aesculap suhl GmbH, Germany

2.1.8 Consumables

Table 9: List of consumables used in present study.

Material	Supplier
Multi well Cell culture plates (96wells, 96wells with black background, 48 wells, 24 wells, 12 wells and 6wells)	Nunc, Denmark
Petri dishes	Nunc, Denmark
Pipette tips (10µl,100µl,1000µl)	Star Lab
Falcon tubes (15ml and 50ml)	Griener bio-one
Eppendorf tubes (1.5ml and 2ml)	Sarstedt Labor
PCR tubes	Biozym
Syringe filters(0.2µM and 0.45µM)	Sartorius
Syringes (1ml, 3ml, 5ml,10ml and 20ml)	Omnifix
Needles(16gauge, 18gauge, 20gauge and 23 gauge)	B-Bern, Germany
Cell culture flasks ($25cm^2$, $175cm^2$ and $300cm^2$)	Nunc,TTP
Cryovials	Corning, Sigma Aldrich
Gloves	Microflex
Spectrophotometric cuvettes	Sarstedt Labor
Suture material	Vicryl Ethicon, Johnson and Johnson
Metal fixture (cold-curing resin)	Rencast FC52/53 Isocyanate, FC53 Polyol, Füller DT 082; Gössl & Pfaff GmbH, Karlskron/Braulach, Germany

2.1.9 Software

Table 10: Overview of software used in present study

Software	Manufacturer
Axiovision Rel. 4.5 software	Carl Zeiss MicroImaging Inc., Jena, Germany
Living Image software®, version 2.6	Xenogen, USA
Image J	National Institutes of Health, USA
GraphPad Prism (v5)	Statcon
MS office (2010)	Microsoft

2.1.10 Animals

Table 11: Mice employed for animal studies

Animal	Supplier
BALB/c mice	Harlan-Winkelmann, Borchen, Germany
C57Black/ 6 mice	Harlan-Winkelmann, Borchen, Germany
β-IFN-Luc mice	Luciferase reporter mice which allowed interferon-beta gene induction in response to bacterial infection [155].

2.2 Methods

2.2.1 *In vitro* and *in vivo* characterization of implant materials (Part A)

2.2.1.1 Sterilization

Plastic materials, bacterial culture, solutions for cell culture and corrosion study were autoclaved at 121°C before use. Implant materials were sterilized either by autoclave or immersion in 70% ethanol.

2.2.1.2 Properties and dimensions of tested implant materials

Magnesium discs were manufactured and processed in Institute of Materials Science, Leibniz University Hannover, Germany. Manufacturing was mainly done by gravity dicasting process. Pure magnesium (99.94% pure; Magnesium Elektron UK, Manchester) was melted at 750°C in a tilting crucible furnace. The melting was performed in a SF6 shielding gas atmosphere (volumetric flow rate of 21/min; Air Liquid, Dusseldorf) because of the high reactivity of liquid magnesium. Then, the melt was cast into a preheated steel die (450°C). Before extrusion billets were turned down to a diameter of 120mm to remove resulting cavities, pores and impurities from casting. Hot extrusion was carried out by a 10 MN extruder (SMS Meer, Moenchengladbach). For this, cast billets, the die (4x6.5mm) and the container of the extruder were heated to 350°C. The extrusion process was conducted with a pressure of 4.9MN and a profile velocity of 1.9 m/min. A 5 mm diameter cylindrical form with a height of 2 mm was selected as specimen morphology. All specimens were manufactured by using constant machining parameters, special fixation and a low feed. Specimens had an average mass of 68.6 mg ±0.25 and a calculated surface area of 19.63 mm^2. Porous titanium discs were prepared from Ti-6Al-4V micro beads grade 23 by metal injection molding (MIM) of 90%(w/w) beads with diameter from 125µm to 180 µm and 10% Ti-6Al-4V powder with a grain diameter of less than 45 µm. Whole mixture was sintered at 1100°C for 2h under high vacuum without further processing.

2.2.1.3 Corrosion media and in vitro incubation conditions

In vitro degradation properties of magnesium were investigated in cell culture media or in different salt chemical solutions. Corrosion media were as follows: (1) cell culture medium Dulbecco's modified Eagle's medium (DMEM) containing 10% FCS (Table 3). (2) A spent cell culture media was introduced in present study which was synthesized as a supernatant after the incubation of mice fibroblasts (NIH3T3) (ATCC CRL-1685) with DMEM. (3) Phosphate buffer saline (1x PBS) (Table 3) (4) Potassium phosphate (KH_2PO_4). Incubations of samples were done at room temperature, at 37°C and at 37°C with 5% CO_2 in a humidified cell culture incubator.

2.2.1.4 Determination of in vitro corrosion

The corrosion rate of magnesium in the shape of wires or discs was evaluated independently by monitoring (1) Changes in the weight after immersion (2) Changes in the pH of corrosion media (3) Determination of Mg^{2+} concentration in the incubation media (4) measurement of hydrogen gas released from magnesium.

2.2.1.4.1 Measurement of weight loss

Weight of magnesium samples (wires and discs) was measured by microbalance (Sartorius) then these specimens were left in their respective media for indicated time period at standard cell culture conditions. At the end of incubation, the samples were removed from the corrosion media. Before measuring final weight, corrosion layers from all samples were removed by cleaning with diluted chromic acid. Final weight loss was calculated in (mg/cm^2) which was then converted into corrosion rate (mm/year) according to ASTM-G31-72 as given below [156].

$$CR=KW/At\rho$$

CR is corrosion rate, coefficient $K=8.76x10^4$ W is weight loss (g), A is surface area of discs exposed to corrosion media, t is exposure time and ρ is magnesium density.

2.2.1.4.2 Measurement of magnesium ions (Mg^{2+}) concentration

Magnesium samples were immersed in their respective media at standard cell culture conditions for mentioned time period. Soluble magnesium ion concentrations were determined daily by mixing 10 µl of appropriately diluted magnesium corrosion supernatants with 1000 µl of Xylidyl blue reagent according to the manufacturer's instruction (Magon, Pointe Scientific, Inc. USA). In parallel, 2.05 mM Mg^{2+} standard solution provided with the kit was also mixed with 1000µl of Xylidyl blue. After 5-10 minutes incubation at room temperature, the OD_{546} of the reaction mixture was determined using a Nanodrop ND-1000 UV-Vis Spectrophotometer (Nanodrop Technologies, Wilmington, USA). Measured OD_{546} values were inserted into standard formula and Mg^{2+} concentration was determined in mg/dl.

2.2.1.4.3 Measurement of hydrogen gas evolution

Hydrogen gas evolution was measured using 1 or 10 ml syringes attached to needles (B. Braun, Germany) at 37°C in cell culture incubator. At the start of experiment, plunger was taken out of the syringe and test specimen was placed in it. The plunger was refixed and indicated amount of corrosion media was filled into the syringe. The syringe was then placed in glass jar already filled with corrosion media in a way that needle was completely dipped into media. This was done to inhibit environmental air penetration into the syringes from surrounding environment. Gas accumulation in syringes was recorded from scales of syringes and converted into units of ml/cm^2.

2.2.1.4.4 Monitoring changes in pH of corrosion media

Magnesium specimens were immersed in respective media and incubated at 37°C in cell culture incubator. The pH of media was measured using a micro electrode pH meter (Mettler-Toledo GmbH, Giessen, Germany).

2.2.1.5 Biomechanical pull out tests

Tibia bones were isolated from 6-8 weeks old BALB/c mice after euthanizing them with CO_2. Bones were incubated in formalin minimum for up to 1 week for fixation. Magnesium, magnesium silver alloy or titanium wires (15 mm length and 0.4mm diameter) were inserted into the medullary cavity of bones separately. These bones bearing wires were incubated in 1.5ml DMEM at 37°C in the presence of 5% CO_2 in a humidified cell culture incubator for 7, 15 or 30 days. In parallel, magnesium wires alone were inserted into bones and incubated in 1.5 ml either of 100 mM solution of KH_2PO_4, DMEM or in spent cell culture medium at 37°C in the presence of 5% CO_2 in a humidified cell culture incubator for 3, 7, 15 or 30 days. To exclude the effect of bones, magnesium wires (10 mm) were also directly incubated in 100 mM solution of KH_2PO_4, DMEM or spent cell culture medium at 37°C in the presence of 5% CO_2 in a humidified cell culture incubator for 7 days. After incubation, tibia bones containing wires were removed from their solutions. The wire pull out force from tibia bones was determined in Newton (N). For this, bones were embedded into a metal fixture using a cold-curing resin containing the three components (Rencast FC52/53

Isocyanate, FC53 Polyol and Füller DT 082 (Gössl & Pfaff GmbH, Karlskron/Braulach, Germany). The maximum pull-out force was determined with a materials testing machine. The mechanical testing was conducted with a pre-load force of 0 N and a velocity of 0.5 mm/min. The fixation strength between the wires and bones without any incubation was measured as control.

2.2.1.6 Phosphate coating procedure

Functional salt solutions for potassium di-hydrogen phosphate (Carl Roth GmbH, Karlsruhe, Germany), potassium mono-hydrogen phosphate (Merck, Darmstadt, Germany) sodium di-hydrogen phosphate (Merck, Darmstadt, Germany) and magnesium hydroxide (Fluka Chemie GmbH, Deisenhofen, Germany) described in table 12 were prepared with deionized water. Magnesium implants were incubated for three days in individual wells 24-well cell culture plate (Nunc, Denmark) containing 2ml coating solutions. Two separate sets of these plates were incubated at two different environmental conditions (i) 37°C in the presence of 5% CO_2 in a humidified cell culture incubator (ii) and at 37°C. During incubation, the discs were flipped every 24 h to ensure vigorous corrosion layer formation. Following incubations, magnesium discs were removed and then placed on tissue papers so that small drops sticking with them were absorbed. Further, these discs were dried at room temperature for 48 h. Surfaces of magnesium were observed using a binocular microscope (Stemi SV11, Carl Zeiss Microscopy Gmbh, Germany). The weight of all discs was recorded before and after incubation and drying. For each immersion solution, magnesium discs were used in triplicates and data points correspond to mean value with standard deviation represented by error bars.

2.2.1.7 Fluoride coating on magnesium

For magnesium fluoride coating, specimens were boiled in NaOH (200 g/L) for 120 minutes and subsequently placed in hydrofluoric acid (40 %). After a 96 hours immersion, the specimens were rinsed with distilled water and ethanol to remove the acid remains from the MgF_2 layer. The chemicals used to achieve MgF_2- coating were acquired from Carl Roth GmbH & Co. KG, Karlsruhe, Germany.

2.2.1.8 In vitro cell culture assays and conditions

To test cell compatibility of implant materials, immortalized murine fibroblasts (NIH3T3) and bone cells (MG63) were used (Table.4). Cells were grown in Dulbecco's Modified Eagle's Medium at 37°C in a humidified cell culture incubator with 5% CO_2. Medical implants in the form of discs were sterilized using 70% ethanol and then placed individually into the wells of 24 well plates. Cells were directly seeded on the surfaces of these implants. Blank polystyrene wells of plates and titanium discs were used as control. After cell seeding, plates were incubated at 37°C in a humidified incubator with 5% CO_2 until the cells got confluence in control wells. Then, cells were stained using a cell proliferation fluorescent dye. For this purpose, spent cell culture media and non-adherent cells were removed and adherent cells on implant surfaces were washed off with 1x phosphate-buffered saline (PBS). Cells were then treated with 4µM of cell proliferation dye CFSE prepared from 10 mM stock solution for 15 minutes. Afterwards, cell adhesion, spreading, and proliferation were observed by capturing green fluorescence from cells using Axio Observer A-1 microscope. While, fluorescent images of cells were taken using the Axiovision software, release 4.5 and cells from images were counted using Image J software.

2.2.2 Implantation procedure in small animal model

2.2.2.1 Animal permission

All animal experiments were conducted in accordance with the regulations and approval from the local authorities Lower Saxony State Office for Consumer Protection and Food Safety (*LAVES*) under permission number 33.42502/07-10.5.

2.2.2.2 Animal housing

Wild type female BALB/c mice and transgenic β-IFN luciferase positive mice [157] (HZI breeding) of 8-10 weeks age with average weight 22-25 mg were considered for animal experiments (Table 10). Healthy β-IFN mice were bred in T2 facility while BALB/c mice were ordered from Harlan laboratory and then kept in cages under controlled

environmental conditions with standard diet and water ad libitum in the animal facility of Helmholtz center for infection research (HZI), Braunschweig.

2.2.2.3 Surgical process for implantation

In vivo implantations were carried either subcutaneously on the dorsum or into the tail artery of mice. Sterilized magnesium and titanium implants, in the shape of discs were preferably implanted subcutaneously while these implants in the shape of wires were inserted into tail artery. Before surgery, mice were anesthetized using intraperitoneal injection of ketamine (10 mg/kg) and Xylazine (4 mg/kg). Mice fur on the dorsum was removed using a hair trimmer. Mice were then shifted under the clean bench. First of all, Three incisions were made using surgical scissors to create small subcutaneous pockets on both right and left sides of hindquarter and one close to neck. With the help of tissue forceps, implants were inserted into these subcutaneous pouches. Then, openings of these subcutaneous pockets were closed by simple interrupted wound sutures with the help of surgical needle. For implantations into tail artery, small openings were made at three positions into the tail artery using 18 gauge needles. 1 cm long pieces of wires were directly inserted into the tail artery through these openings. After surgical intervention, mice were shifted back into their respective cages and their general health conditions and physical parameters were carefully observed after implantations.

2.2.2.4 Measurement of hydrogen gas around subcutaneously implanted discs

After implantation, mice were shifted back into their respective cages. Gas accumulation as primary degradation product around subcutaneously implanted magnesium was measured by establishing a novel method. For this, height and diameter of subcutaneously implanted discs were measured immediately after implantation using Vernier caliper (Wisent tools, Germany). Later, additional increases in diameter and height around implanted discs due to gas accumulation were measured on daily basis during the first week and on weekly basis for 8 weeks. Subcutaneously implanted discs after gas accumulation were considered showing a close similarity to half sphere therefore formula used to calculate volume (v in mm^3) of a partial sphere was applied to get quantitative values for gas formation.

$$V = \pi h^2 r - \frac{\pi h^3}{3}$$

While “r” is radius of the partial sphere and “h” is height.

2.2.2.5 Histology of tissue surrounding implants

For histological analysis, mice were sacrificed by CO_2 asphyxiation followed by cervical dislocation. Disc implants sandwiched between 2 mm thick layer of skin on the upper side and skeletal tissue layer on the lower side were removed from mice. In the case of tail implants the whole tail piece containing the implant was placed in histology cassettes and fixed in 4% formalin for 48 hrs. Following fixation, tissues were dehydrated in 70% ethanol and then embedded in paraffin. Tissues embedded in paraffin were cut into 5 µm sections and then stained with hematoxylin and eosin (H&E).

2.2.2.6 Energy Dispersive X-ray (EDX) spectroscopy

Elemental compositions and surface properties of implant materials were analyzed in institute for Multiphase Processes, Leibniz University of Hannover, Germany using energy dispersive x-ray spectroscopy (EDX), a fully automated variable pressure Hitachi REM-S3400N. For this purpose, samples were fully dried and then fixed with the help of conducting glue foil. 10 KeV was selected as acceleration voltage and the distance was adjusted to 10mm. Images were captured at a magnification of 200-fold at a working distance of 21-22 mm with emission current of 80-110 IA. Quantifications were performed in accordance with the standard less ZAF method (Z, atomic number effect; A, absorption correction; F, fluorescence correction). Different energy peaks represent respective electron transmissions to the K-shell, except for titanium where energies for both L- and K-shell were detected.

2.2.2.7 X-ray diffraction analysis of implant materials

To determine crystalline properties of coated and uncoated implants, XRD analysis was also performed in Institute for Inorganic Chemistry, Leibniz University of Hannover, Germany. LDH coatings on titanium and phosphate coatings on magnesium were characterized using the STOE Theta/theta Diffractometer (STOE & Cie GmbH, Darmstadt)

which was operated at 40 kV and 30 mA. Disc samples were scanned in reflection geometry at a step width of 0.02° with 2.0 s counting time per step, employing monochromatized CuKα 1 radiation at a wavelength of 1.54060 Å.

2.2.2.8 Scanning electron microscopy (SEM)

Detailed analysis of the surface morphologies of all implants before as well as after their incubation or implantation was done using a Merlin field emission scanning electron microscope using an acceleration voltage of 5 kV with the Everhart-Thornley SE-detector and Inlens SE-detector ratio set to 25:75.

2.2.3 Implant associated-infections (Part B)

2.2.3.1 Bacterial strains and their cultivation

For biomaterial associated-infections and to test antibacterial properties of implants, bioluminescent strains of *P. aeruginosa* (1 CTX::lux), *P. aeruginosa pqs*A (quorum sensing mutant), *Staphylococcus aureus,* wild type *P. aeruginosa,* Bioluminescent *E. Coli*, Bioluminescent *Salmonella* were employed (Table. 5). Bacteria were grown in LB medium (composition given below) in sterile glass flasks with loose caps to allow air penetration. For solid media growth, frozen cultures were first aerobically overnight grown at 37°C on LB agar plates (composition given below in table). Bacterial cultures were grown at 37°C on shaking speed of 150 rpm to desired optical cell density (OD_{600}=0.1; approximately $1x10^8$ CFU/ml). For long term storage, planktonic cultures of all strains were stored in LB medium containing 25% glycerol at -80^{o}C.

2.2.3.2 Initial inoculum to infect implant surfaces

For *in vivo* establishment of biofilm on implant surfaces, immediately or 24h after implantation 5 µl of bacteria in LB suspension at (OD_{600}=0.1; approximately $5.45x10^6$ CFUs/5µl) were directly injected on the surfaces of implants.

2.2.3.3 Determination of minimum bacterial inoculum capable of biofilm formation

To estimate minimum number of bacteria that could lead to biofilm formation, *P. aeruginosa* (PAO1 CTX::lux) were grown to an OD_{600}=0.1 in LB suspension by conditions as mentioned previously. Initial inoculum (OD_{600}=0.1; approximately $5.45x10^6$ CFUs/5 µl) was further 1:3 diluted in LB suspension. Magnesium discs were subcutaneously implanted into eight BALB/c mice. Minimum three discs were implanted per mice. Soon after implantation, infection was done directly on the surface of each implanted discs. Implant infection was done separately in each mouse from different bacterial dilution. After infection, all animals were regularly observed under *in vivo* imaging system.

2.2.3.4 Non-invasive in vivo imaging of biofilm on implant surfaces

Bioluminescent activity of bacteria was detected using IVIS®-200 *in vivo* imaging systems (Xenogen, USA). This allowed non-invasive direct monitoring of implant infection without killing animals. Photons produced by luminescent bacteria diffuse through animal skin and were captured by a sensitive photon charged-coupled device (CCD) camera. For bioluminescent imaging, mice were initially anesthetized using 2% Isofluran (gaseous anesthesia) with the help of XGI-8 anesthesia unit (Calipers). Mice were then shifted inside IVIS with constant supply of Isofluran and *in vivo* imaging was done. Transgenic mice expressing β-IFN under luciferase promoter were also observed under the same system. For imaging, β-IFN luciferase mice were first injected intraperitoneally (i.p) with 150 mg/Kg of luciferin in 1x PBS. After 10-15 minutes of injection, bioluminescent images were captured from mice. The luminescence intensity was determined using the Living Image software® Version 2.6 (Xenogen) and given as average radiance ($p \cdot sr^{-1} \cdot m^{-2}$).

2.2.3.5 Bioluminescent imaging of E. coli on implant surfaces

To investigate if *E. coli* could establish prolonged infections on implant surface, magnesium, plain titanium and porous glass discs were separately implanted subcutaneously into BALB/c mice. After implantation, bioluminescent *E. coli* were injected directly on the surface of discs. Soon after infection, bacterial luminescence from the surfaces infected discs was captured using the IVIS®-200 *in vivo* imaging system (Xenogen, USA).

2.2.3.6 Bioluminescent imaging of Salmonella on implant surfaces

For infection, magnesium, plain titanium and porous glass discs were implanted subcutaneously in BALB/c mice. Bioluminescent *Salmonella typhimurium* were injected directly on the surface of each of the discs. Luminescence from infected implants was measured daily with an IVIS®-200 *in vivo* imaging system (Xenogen, USA).

2.2.3.7 In vivo infection pattern by planktonic and biofilm cultures of P. aeruginosa

Plain titanium discs were subcutaneously implanted each on right side in the region of fore and hind limbs of female BALB/c mice. Magnesium discs each on left side of the region of fore and hind limbs were implanted in same animal. Both titanium and magnesium implanted on upper limbs were infected with bioluminescent 5 µl *P. aeruginosa* (approximately $5.45x10^6$ CFUs). While, same discs implanted on lower limbs were infected with 5 µl of bioluminescent *P. aeruginosa* in LB medium, isolated from a 12 days old biofilm established on magnesium discs in a separate mouse. These bacteria were prepared by taking small amount of pus from biofilm and then mixing it in LB shortly before infection. After infection, mice were observed under IVIS®-200 (Xenogen, USA).

2.2.3.8 Time-dependent antibiotic administration against P. aeruginosa biofilms

To test biofilm responses against antibiotics administered at different time points after initial infection, mice bearing magnesium implants were infected with bioluminescent *P. aeruginosa* directly on the surfaces discs. Then, 100 µl of ciprofloxacin (2mg/ml) was injected intravenously in first mouse. Second mouse was injected with ciprofloxacin (same dose and route) after 6h, 3rd mouse after 24h and 4th mouse after 48h post-infection. One mouse was kept as control where 100 µl of 1x PBS was injected intravenously post implantation and infection. Later antibiotic administrations at constant dose and route were continued on daily basis for two weeks. Antibiotic sensitivity of biofilms was imaged using IVIS®-200 (Xenogen, USA).

2.2.3.9 Dose-dependent antibiotic administration against P. aeruginosa biofilms

To test biofilm response to different concentrations of antibiotics, four independent groups (4 mice /group) of mice were organized. In individual mice of all groups, subcutaneous

implantation of magnesium and subsequent infection with bioluminescent *P. aeruginosa* was done. Ciprofloxacin (2mg/ml) and PBS in control mice was injected immediately after infection and then daily. Luminescence from all groups was captured daily.

2.2.3.10 RNA isolation from in vitro cultures of P. aeruginosa

Planktonic cultures of *P. aeruginosa* (PAO1 CTX:lux) grown at ambient conditions (mentioned previously) at OD_{600}=0.4 were used for RNA isolation. In parallel, stationary bacterial cultures grown under same conditions at OD_{600}=1.00 were also used for RNA. RNA isolation was done separately either using TRIzol reagent or using RNeasy mini kit (QIAGEN). Under both options, RNA isolation was done by following manufacturer's protocol. The amount of RNA was determined using NanoDrop. RNA quality (RIN number) was checked by Bio analyzer. Isolated RNA was stored at -80°C.

2.2.3.11 Electron microscopy of biofilm

2.2.3.11.1 Field emission scanning electron microscopy

Mice bearing biofilm were euthanized and infected magnesium along with tissue were removed and fixed with 5% formaldehyde and 2% glutaraldehyde in HEPES buffer (100 mM HEPES, 90 mM sucrose, 10 mM $MgCl_2$, 10 mM $CaCl_2$, pH 6.9) washed twice in TE buffer (10 mM TRIS, 2mMEDTA, pH 6.9), dehydrated with a graded series of acetone (10, 30, 50, 70, 90, 100%) for 15 min on ice and further dehydrated in 100% acetone at room temperature. After critical-point drying with liquid CO_2 (CPD300, Leica or CPD030 Bal-Tec) samples were sputter coated with palladium-gold (SCD500, Bal-Tec) and imaged in a Zeiss Merlin field emission scanning electron microscope with an acceleration voltage of 5 kV. Images were taken with the Zeiss Smart SEM software version 5.05. For imaging discs alone and porous glass beads samples were sputter coated with palladium-gold before examination in the Zeiss Merlin as above.

2.2.3.11.2 Transmission electron microscopy

Samples were fixed with 2.5% glutaraldehyde and 5% formaldehyde in HEPES-buffer on ice for 1 hour and then kept at 5°C. After washing with HEPES buffer samples were further fixed with 1% aqueous osmium for 1 hour at room temperature. Dehydration was achieved

with a graded series of acetone (10%, 30% and 50%) while on ice. After dehydration with 70% acetone samples were incubated overnight in 70% acetone containing 2% uranyl acetate at 4°C. The following day samples were dehydrated further with 90% and 100% acetone on ice and finally with 100% acetone at room temperature. Samples were then embedded in the epoxy resin according to previously described procedures[158]. Ultrathin sections were cut with a diamond knife, picked up with butvar-coated grids, counterstained with uranyl acetate and lead citrate and examined in a TEM910 transmission electron microscope (Carl Zeiss, Oberkochen) set to an acceleration voltage of 80 kV. Images were digitally recorded at calibrated magnifications with a Slow-Scan CCD-Camera (ProScan, 1024x1024, Scheuring, Germany) using the ITEM-Software (Olympus Soft Imaging Solutions, Münster, Germany). Contrast and brightness were adjusted with Adobe Photoshop version CS3 (Adobe).

2.2.3.12 Histology of biofilm

Peri-implant tissue was fixed with 3.6% neutrally buffered formaldehyde, dehydrated in 70% ethanol, embedded in paraffin and then histological sections of 3µm thickness were prepared with a cryostat microtome (HM550,Thermoscientific, Germany). The sections were stained with Hematoxylin/Eosin (H&E) and Periodic Acid Schiff (PAS) staining according to standard procedures[159,160]. Anti-*Pseudomonas* antibody (Biotrend, AP086 at dilution 1:400) staining was performed after heat-mediated-antigen retrieval of the samples. The slides were evaluated histo-pathologically using a light-microscope (Axioscope.A1, Zeiss, Germany) accompanied by camera (AxioCam ICc1, Zeiss, Germany), .Images from the slides were taken using Axiovision software, release 4.5 (Carl Zeiss Micro Imaging Inc., Germany) randomized and blinded to the experimental groups. Contrast and brightness were adjusted using Adobe Photoshop version Cs5.

2.2.3.13 In vivo imaging of IFN-beta response against biofilm

Interferon-β expression against *P. aeruginosa* biofilm on the surface of magnesium discs was monitored using transgenic Interferon-β luciferase positive mice. In each transgenic mouse two magnesium discs were subcutaneously implanted and side by side one sham surgical pouch was created. Wild type *P. aeruginosa* (PAO1) were injected separately on the

surface of magnesium disc and into sham pouch. One magnesium disc was left without infection in each mouse. Soon after infection, 150 µl (30 mg/ml) of luciferin was injected intravenously into each mouse. 15 minutes after injection, mice were placed under IVIS system supplied by gaseous anesthesia and luminescence images were daily for two weeks.

2.2.3.14 Colony forming unit (CFU) of P. aeruginosa in biofilm and different organs

P. aeruginosa made slimy biofilms in the present animal model with pus formation. 50 µl of this liquid biofilm was taken and mixed into 450 µl of 1x PBS. This mixture was mixed and vortexed well and 10 fold dilution series in 1x PBS was made till 10^{-9}. Later 10 µl drop from each of dilution was taken and dropped directly on LB agar plates three times at separate places. These plates were overnight incubated at 37°C. Freshly grown single colonies were counted from countable dilution. Then CFU/ml was achieved by multiplying number of colonies with dilution factor and dividing it by the volume. To calculate CFU from the organs of mice bearing *P. aeruginosa* biofilm, animals were sacrificed and liver and gut were isolated from them. Weight of these organs was measured and then they were shifted separately into homogenizing tubes containing 2 ml of 0.1% triton in 1x PBS for liver and 5-6 ml of 0.1% triton for gut. Tissues were homogenized for 86 seconds. After homogenization, 100 µl from each tube was taken and mixed with 900 µl of PBS. Then a 10 fold serial dilution series was made till 10^{-6} dilution. 100 µl from each dilution was taken either from liver or gut samples and streaked on LB agar plates. Plates were overnight incubated at 37°C. Fresh colonies were counted from plates in case of liver or gut and finally CFU/grams of bacteria were calculated.

2.2.3.15 RNA extraction from in vivo grown P. aeruginosa biofilm

RNA was isolated from *in vivo* established *P. aeruginosa* biofilms using a Power Biofilm RNA isolation kit or TRIzol reagent following manufacturer's protocol. RNA isolation was done using RNAse free tubes and water. Briefly, mice bearing *P. aeruginosa* were killed with CO_2 and shifted in cold room to maintain RNA integrity during isolation process. Whole biofilm matrix from the back of mice was removed and shifted into RNAse free Power Biofilm bead tubes containing beads. These tubes are equipped with beads which can efficiently break biofilm structures during homogenization process. Power tubes were

fixed on a tissue homogenizer and shaking was set at full speed for 15 minutes. Then homogenized supernatant was collected and mixed with chloroform and centrifuged. After centrifugation, RNA is mainly concentrated in aqueous phase. RNA precipitation was done by mixing this aqueous phase with 100% isopropanol. After centrifugation, RNA pelleted at the side and bottom of tubes. The supernatant was removed and the pellet was washed with ethanol. Finally, RNA was resuspended using RNAse free water. RNA concentrations were determined on NanoDrop and RNA was stored at -80°C for further use.

2.2.3.16 RNA clean up using DNase digestion kit

100 µg of RNA in 100 µl of RNA free water was taken for cleaning process. DNase treatment was given using (DNA-free DNA removal Kit, Life technologies, Germany) following manufacturer's instructions.

2.2.3.17 Agarose gel electrophoresis

Agarose gels were prepared by adding 0.3 grams of agarose into 30 ml of 1x TAE buffer into cassette. 5µl of Midori green was added into this mixture and slowly mixed to avoid bubble formation. The cassette was placed at room temperature for up to 20 minutes so that the agarose did get solidified. The cassette was fixed in electrophoresis chamber and was filled with 1x TAE buffer. 1.5 µl of DNA loading dye was mixed with 8.5 µl of isolated RNA and this total of 10 µl was loaded into gel. After RNA loading, the chamber was connected with positive and negative electrodes and electrophoreses of the samples was done at 70 V for 30 minutes. The gel was removed from the chamber and placed under a UV trans-illuminator.

2.2.3.18 RNA sequencing

RNA isolated from a *P. aeruginosa in vivo* biofilm was subjected to sequencing. To remove host RNA contamination, bacterial RNA enrichment was done using MICROBE Enrich kit as per manufacturer's protocol. Then bacterial mRNA enrichment was done with MICROB Express kit as per manufacturer's protocol. Library preparation was done using ScriptSeq (Illumina, USA). Small amount of the library was sequenced to evaluate the libraries (Table 6).

2.2.3.19 General composition of media used

DMEM (Dulbecco's Modified Eagle's Medium)

Na^+ 127.3 mM/L K^+ 5.3 mM/L Mg^{2+} 0.8 mM/L Ca^{2+} 1.8 mM/L Cl^- 90.8 mM/L 1% (v/v) glutamine, 1% (v/v) penicillin and streptomycin (100U/ml penicillin G and 100µg/ml streptomycin) and 10% (v/v) fetal calf serum.

PBS (Phosphate buffer saline)

NaCl 140, 27 mM KCl, 7.2 mM NaH_2PO_4 pH 7.0-7.4.

r-SBF (Simulated body fluid)

Na^+ 142 mM/L, K^+ 5.0 mM/L, Ca^{2+} 2.5 mM/L, Mg^{2+} 1.5 mM/L, Cl^- 103 mM/L, HCO_3- 27.0 mM/L, HPO_4^{-2} 1.0 mM/L, SO_4^{-2} 0.5 mM/L at pH 7.4.

Plasma

The plasma was obtained after the centrifugation of blood of several pigs and stored at a temperature of -80° C. After thawing, in a water bath, 1 vol. % of penicillin was added to plasma to prevent bacterial growth during the incubation period. Na^+ 142 mM/L, K^+ 5.0 mM/L, Ca^{2+} 2.5 mM/L, Mg^{2+} 1.5 mM/L, Cl^- 103 mM/L, HCO_3- 27.0 mM/L, HPO_4^{-2} 1.0 mM/L, SO_4^{-2} 0.5 mM/L at pH 7.4

LB (Lysogeny broth)

10g/l bactotrypton, 5g/l yeast extract, 10g/l NaCl

LB agar

10g/l bactotypton, 5g/l yeast extract, 10g/l NaCl and 15g/l agar

3 Results

3.1 Characterization of implant materials (Part A)

3.1.1 Effect of corrosion media on the weight of magnesium samples

To identify relevant parameters and suitable degradation conditions, magnesium implants were incubated in immersion media with variable compositions and various biological conditions were evaluated. Weight loss is assumed as simple and fast method to determine degradation of metals thereby changes in weight of magnesium pins were measured over the time. A significant weight loss was observed for pins incubated in spent cell culture medium at 37°C in the presence of 5% CO_2 in a humidified cell culture incubator (Figure 6B filled rhombi). At room temperature as well as at 37°C the weight of pins in same medium remained constant (Figure 6A, B filled rhombi). Magnesium pins incubated in potassium phosphate solution showed significant increases in weight after all incubations (Figure 6 A, B, C, black squares). However, no change in weight of these pins could be observed when incubated in DMEM (Figure 6A, B, C, black circles). The weight of pins incubated with DMEM in the presence of live fibroblasts (NIH3T3) also remained unchanged during first 6 days, however at later time points; it started to decrease slowly (Figure 6B empty rhombi). Magnesium pins incubated with PBS also showed a slight weight gain at tested environmental settings (Figure 6A, B and C blank squares). It seemed spent cell culture medium containing cellular excretion products was highly corrosive medium particularly at 37°C with 5% CO_2 at standard cell culture conditions. Independent of environmental conditions, potassium phosphate solution was a highly corrosive medium for magnesium enhancing corrosion layer formation and the subsequent sample weight gain was highest for magnesium pins incubated. Overall, these results show that weight of magnesium is greatly influenced by the variation in composition of incubation media and surrounding conditions.

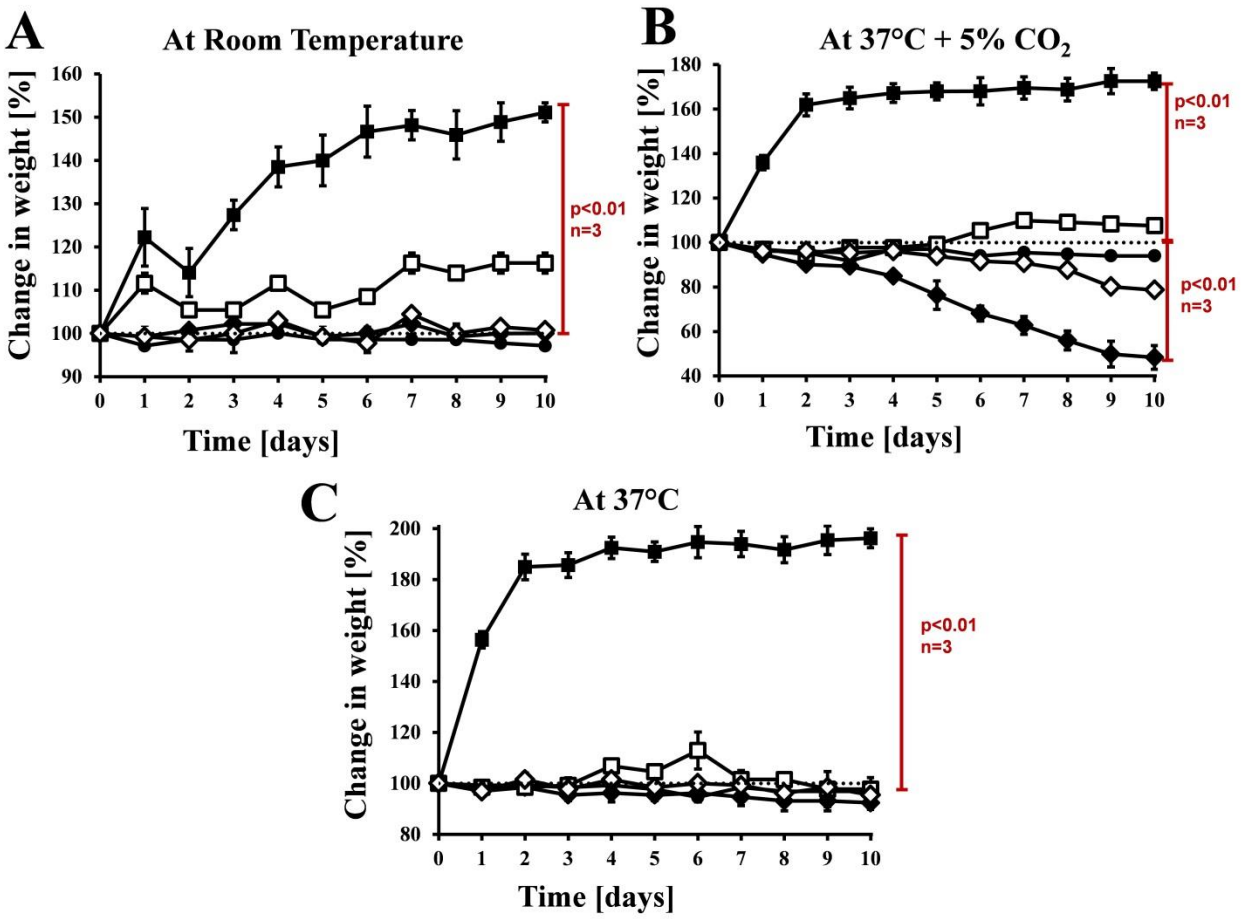

Figure 6: Weight of magnesium pins is influenced by variation in incubation settings. Magnesium pins with 10 mm length and 0.4 mm diameter were incubated in DMEM (filled circles), used DMEM (filled rhombi), fibroblasts (empty rhombi), KH_2PO_4 (filled squares) and PBS (empty squares) at room temperature, at 37°C with 5% CO_2 under standard cell culture conditions and at 37°C and then changes in weight of individual pins were measured daily over the time. Percent change in the weight of magnesium pins incubated in DMEM (filled circles), used DMEM (filled rhombi), fibroblasts (empty rhombi), KH_2PO_4 (filled squares) and PBS (empty squares) at room temperature (A), at 37°C plus 5% CO_2 in a humidified cell culture incubator (B) and at 37°C (C). Magnesium pins without immersion in physiological solutions served as control (dotted line). Statistical analysis was done using Student's T-Test.

3.1.2 Effect of magnesium degradation on local pH of corrosion media

During the degradation of magnesium, hydroxide ions (OH^-) are released as corrosion product which leads to the rise in pH of the surrounding medium. Therefore, a change in pH of the immersion media containing magnesium implants is another criterion to estimate the degradation rate. For monitoring pH values, magnesium wires were cut into pins with 5mm in length and incubated in 250 µl of test solutions. pH values of all media containing magnesium pins increased after 24h incubation (Figure 7A-C). Rises in pH of test solutions

due to degradation of magnesium were higher in media incubated at 37°C or room temperature as compared to the solutions that were incubated at 37°C with 5% CO_2 under standard cell culture conditions. However, at later time points, pH values of all media became stable. This could be explained by the influence of the pH, whereby CO_2 decreases the pH and increases the initial degradation rate. The corrosion product $Mg(OH)_2$ increases the pH and decreases the degradation rate.

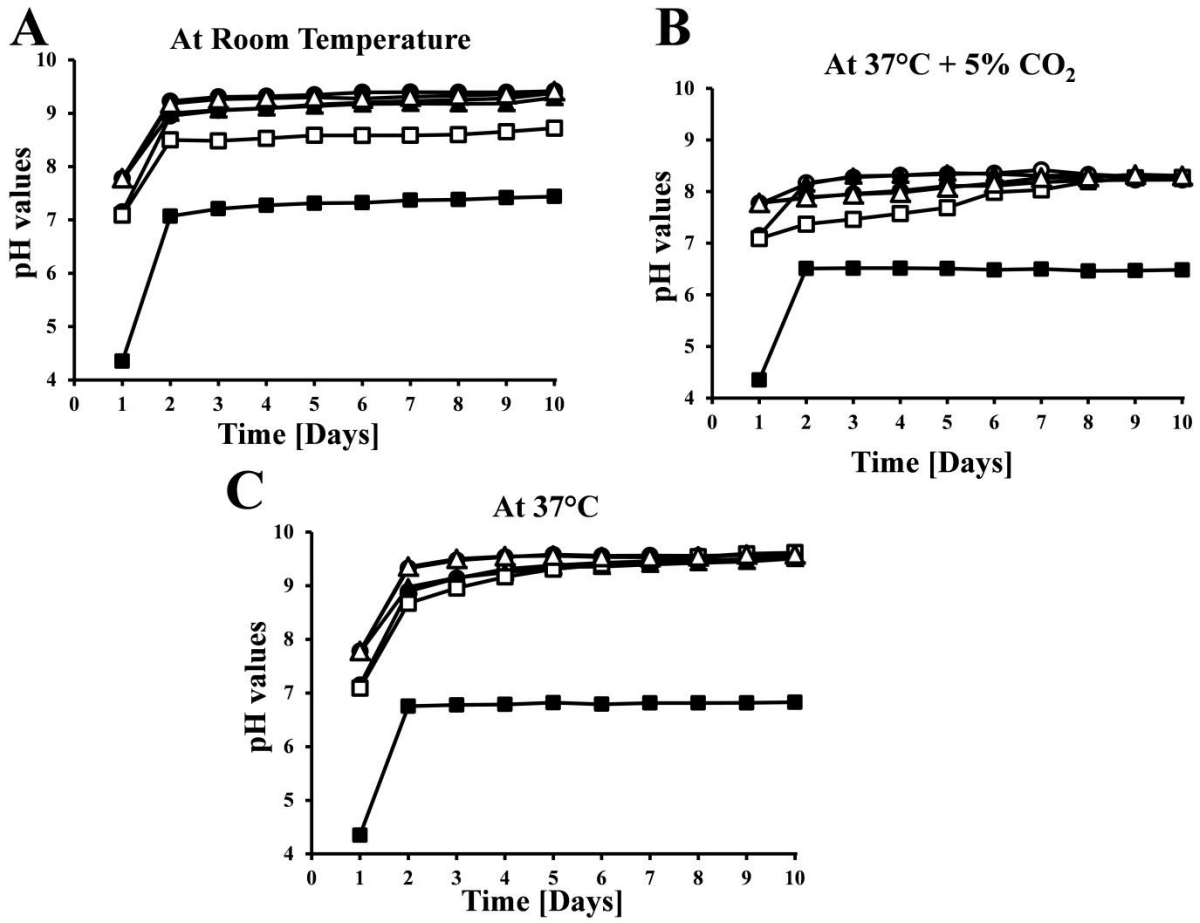

Figure 7: Magnesium degradation increases pH of corrosion media. Magnesium pins with 5 mm length and 0.4 mm diameter were immersed in 250 µl of DMEM (filled circles), used DMEM (empty circles), used DMEM with pH adjusted to 7.5 (filled triangles), fibroblasts (empty triangles), KH_2PO_4 (filled squares) and PBS (empty squares) and then incubated at three variable environmental setting (A-C). Changes in pH of DMEM (filled circles), used DMEM (empty circles), used DMEM with pH adjusted to 7.5 (filled triangles), fibroblasts (empty triangles), KH_2PO_4 (filled squares) and PBS (empty squares) containing magnesium pins incubated at room temperature (A), at 37°C plus 5% CO_2 in cell culture incubator(B) and at 37°C (C) were recorded over the time.

3.1.3 Measurement of hydrogen generation

Hydrogen gas is generated as a result of magnesium degradation. The measurement of hydrogen gas is considered another criterion to determine the degradation rate of magnesium implants. It is also known that degradation of one gram magnesium leads to the generation of one ml of hydrogen gas. Hence, this method is too simple and direct way to determine corrosion of magnesium. Due to the small dimensions of magnesium pins and fast escape of hydrogen gas, it was difficult to measure the exact amount of hydrogen. However, due to rapid corrosion properties, it was possible to measure hydrogen production from magnesium incubated in used DMEM and to compare it with fresh DMEM. To measure hydrogen gas, samples were incubated under standard cell culture conditions (Figure 8). Amount of hydrogen produced was significantly higher for wires dipped in spent cell culture medium (Figure 8 empty circles) as compared to DMEM (filled circles).

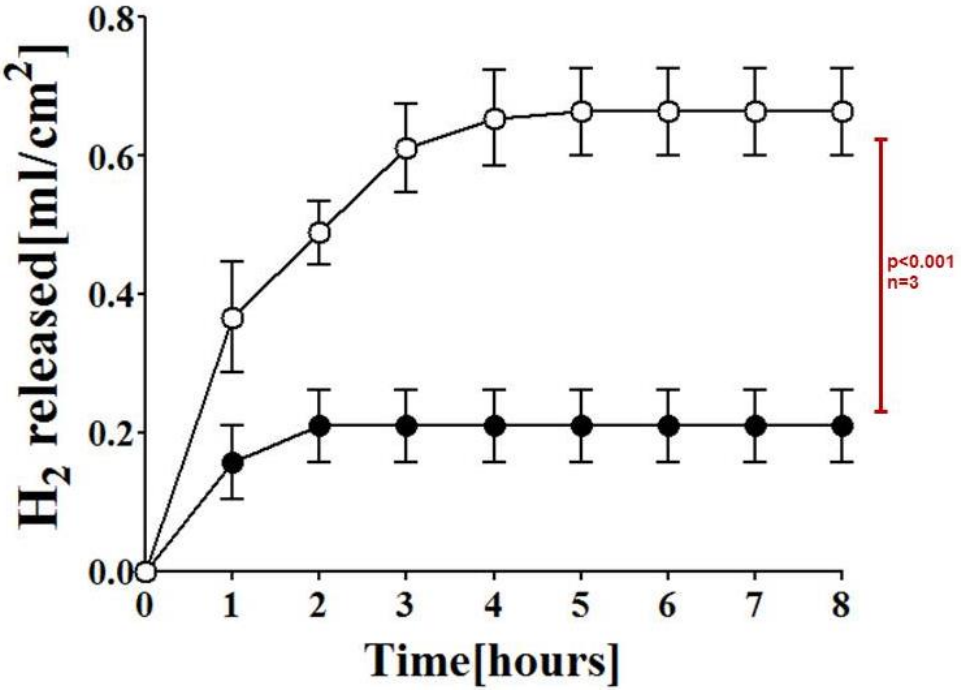

Figure 8: High release of hydrogen is produced form magnesium implants. Magnesium pins with 15 mm length and 0.4 mm diameter were individually placed into 1ml syringes each filled with fresh cell culture medium DMEM or used cell culture medium. Syringes were incubated at 37°C with 5% CO_2 under optimum cell growth conditions and hydrogen gas as degradation product was measured from the scale of each syringe at indicated time points. Hydrogen volume produced by magnesium incubated in used DMEM (empty circles) as compared to magnesium incubated in DMEM (black circles). (Statistical analysis was done using Students's T-Test (paired) and p-value was calculated)

3.1.4 Surface properties of magnesium implants

To reveal surface properties of magnesium implants incubated in fresh DMEM and spent DMEM, magnesium pins were incubated for the indicated time points at optimum cell culture conditions. After incubations, corrosion layers on magnesium implants were observed by scanning electron microscopy. Magnesium implants incubated in fresh DMEM corroded slowly therewith remained intact for 8 weeks and evidenced the formation of corrosion layer (Figure 9A-C). In comparison, used cell culture medium led to rapid degradation of magnesium pins and completely dissociated into small corrosion fragments within 2 weeks of immersion (Figure 9D-E). This confirmed that used cell culture medium containing cellular excretion products had more aggressive corrosion potential.

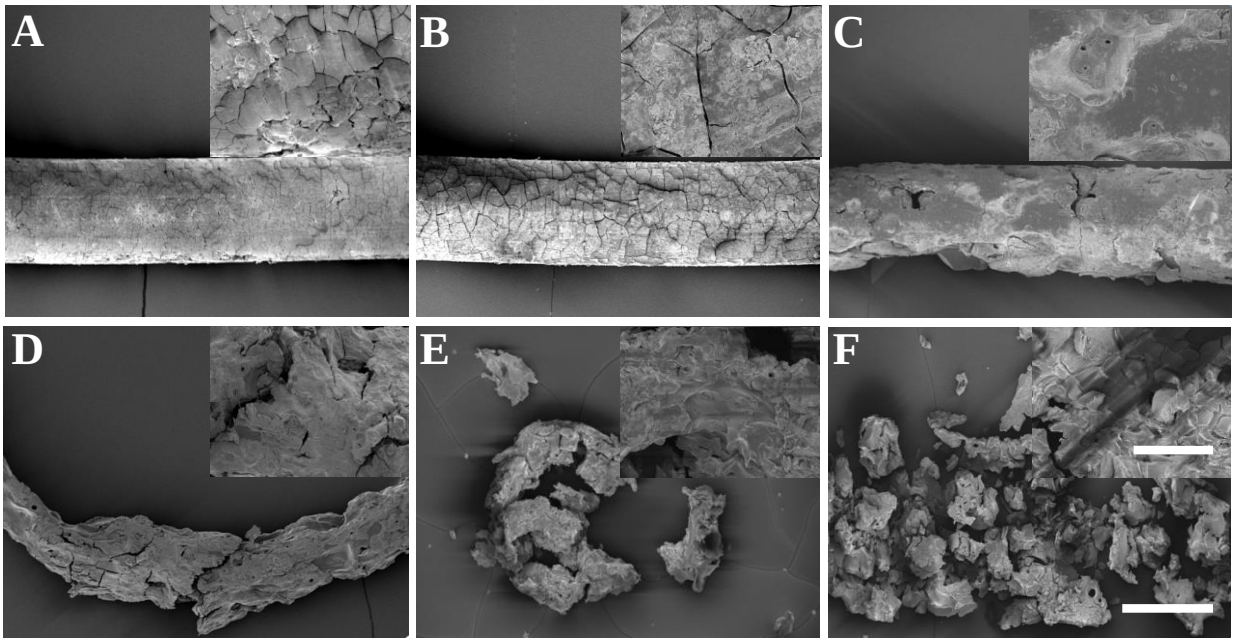

Figure 9: Magnesium corrodes more rapidly in spent cell culture medium. Magnesium pins with 15 mm length and 0.4 mm diameter were immersed in DMEM and used DMEM for 2, 4 and 8 weeks at 37°C with 5% CO_2 in a cell culture incubator. Then these pins were observed by SEM after 2 (A), 4 (B) and 8 weeks (C) of incubation in fresh DMEM and after 2 (D), 4 (E) and 8 weeks (F) of incubation in used cell culture medium. Small picture (A-F) indicates detailed morphology of corrosion layer in each case. Scale bar in each large image corresponds to 100 µm and 20 µm to each small image. (SEM images courtesy by Manfred Rohde, HZI)

3.1.5 *In vivo* implantation of wires in mouse model

To compare *in vitro* degradation with *in vivo*, magnesium pins were implanted subcutaneously and in tail artery of mice as described [27]. To see if difference in site of implantation and tail movement had any apparent effect on the degradation of magnesium,

magnesium pins were implanted either under the skin (subcutaneously) or into tail artery for indicated time. After implantation, surfaces of magnesium were observed with SEM (Figure 10). The surfaces of magnesium implants after residing in subcutaneous tissue seemed more closely to specimens which were incubated in DMEM. However, surfaces of implants explanted either from subcutaneous region or from tail artery seemed similar and remained intact after 8 weeks of implantation (Figure 10A-F). Over all, changes in site of implantation as well as tail movement did not seem to lead to differences in the degradation and formation of corrosion layer on the surface of magnesium. *In vitro* degradation and the degradation rate in vitro seemed

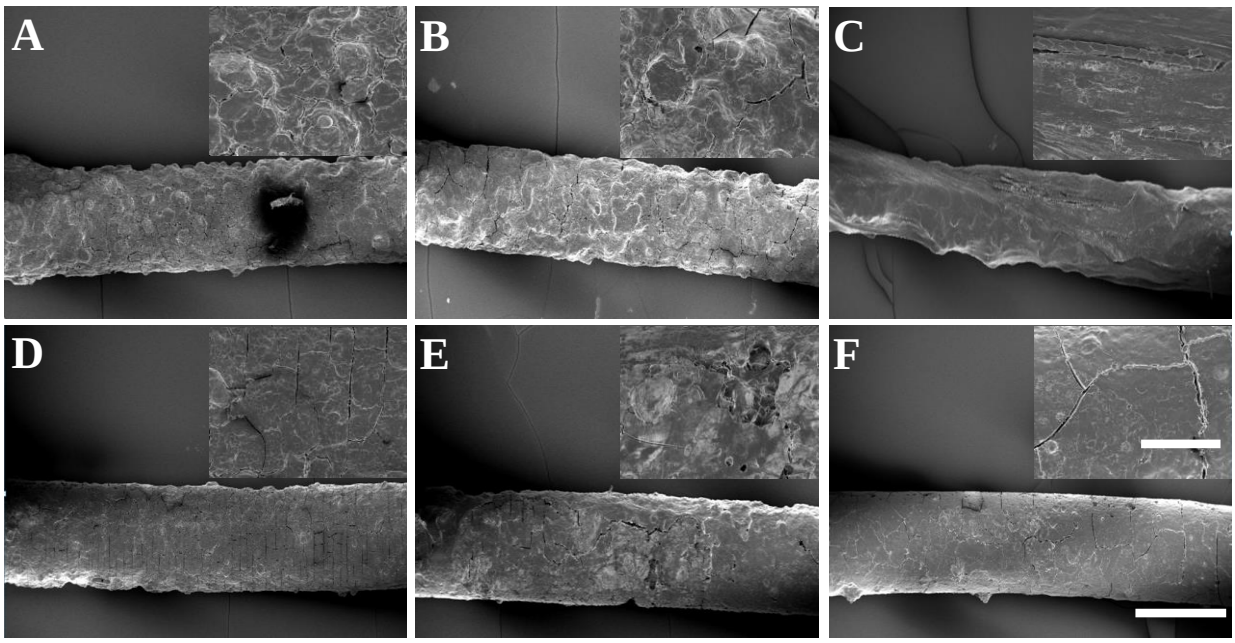

Figure 10: Changes in site of implantation shows no apparent effects on degradation of magnesium. Magnesium implants with 10 mm length and 0.4 mm diameter were surgically inserted into the tail artery and under the skin of BALB/c mice. Implants were then removed from the body of animals after 2, 4 and 8 weeks of implantation and their surfaces were observed by scanning electron microscopy (A-F). Surface morphology of magnesium pins after residing for 2 (A), 4 (B) and 8 weeks (C) under the skin of mice. Surfaces of magnesium implants after staying for 2 (D), 4 (E) and 8 weeks (F) in tail artery. Small picture (A-F) indicates detailed morphology of corrosion layer in each case. Scale bar in each large image corresponds to 100 µm and 20 µm to each small image. (SEM images courtesy by Manfred Rohde, HZI)

3.1.6 *In vivo* compatibility of magnesium pins with the adjacent tissue

To determine the host reaction against magnesium pins, histology of the respective tissue sections was performed. It was found for magnesium pins implanted in subcutaneous

region that they were enclosed in connective tissue and isolated from skin and skeletal tissue fibers due to their small dimensions. Thereby, histological evaluations of tail tissue containing magnesium pins were performed only. For comparison, tail tissues implanted with standard titanium and magnesium silver alloy pins as well as mice without implantations were used as controls. No gross pathological changes as well as recruitment of high number of inflammatory cells could be seen in tissues around magnesium, magnesium silver alloy or titanium implants (Figure 11A-D). However, a fibrous tissue layer was visible around each of the tested implant (Figure 11B-D; i). The connective tissue seemed thicker around magnesium silver pins (Figure 11C; i). This analysis showed that degrading magnesium implants were as tissue compatible as titanium.

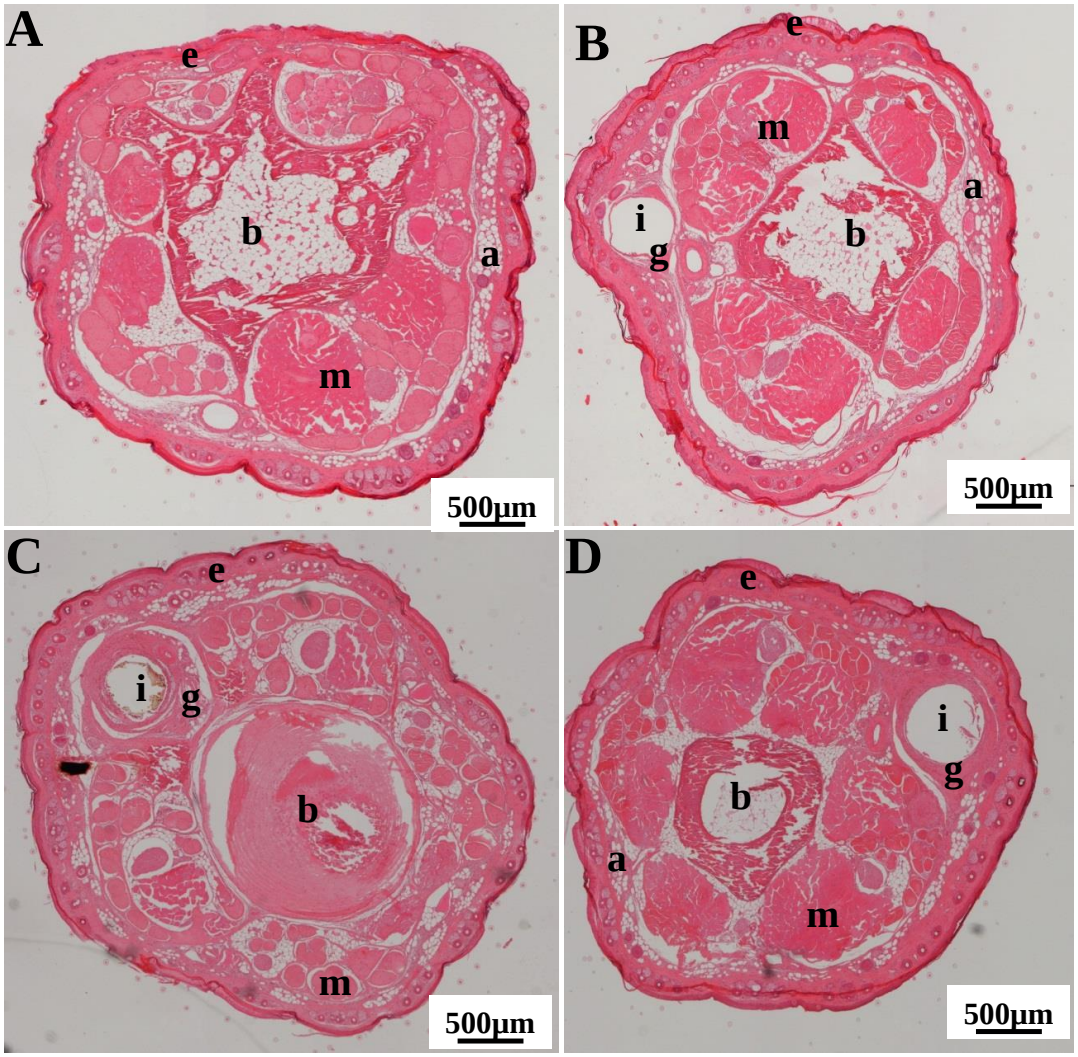

Figure 11: Magnesium implants are compatible with tail tissue similar like titanium. Magnesium, magnesium silver alloy and titanium pins with 10 mm length and 0.4 mm diameter were taken after 8 weeks

of implantation in tail artery of mice, formalin fixed, paraffin embedded and hematoxylin and eosin-stained. Tail implants (i) were removed before tissue sectioning. Mouse tail tissue without any implantation was stained for comparison (A), tail tissue adjacent to magnesium implant (B), magnesium silver alloy (C) and titanium (D). The labelled structures shown are as follows: site of implantation (i); adipose cells (a); granular tissue (g); muscle fiber (m); tail bone with marrow (b) and epidermis (e). (Histology courtesy by Andreas Weizbauer and Elmar Willbold from MHH, Hannover)

3.2 Interlocking strength between magnesium and tibia bones

3.2.1 Determination of interlocking force between magnesium and tibia bones

To investigate if magnesium can establish strong bonding with surrounding hard tissue, magnesium pins were inserted into tibia bones and incubated in DMEM under standard cell culture conditions. For comparison magnesium silver alloy and non-degradable titanium pins were inserted in tibia bones and subsequently incubated under same conditions. To completely eliminate the contribution of live tissue, tibia bones isolated from mice were immersed in formalin solution for one week so that osteocytes are dead. To determine strength of bone-implant interaction a biomechanical pull-out test was performed by employing material testing machine. Pure magnesium as well as magnesium silver pins evidenced significantly higher pull out force as compared to titanium at all tested time points (Figure 12A). To confirm if increase in binding force between magnesium and tibia bones were purely due to corrosion process, magnesium pins were inserted in tibia bones and incubated in three different immersion solutions as described. Pull out force between magnesium wires and tibia bones in effect to different incubation media (Figure 12B) also increased. However, this pull out force was significantly higher when specimens were incubated in fast corroding medium which led to the formation of robust corrosion layer. Hence, it was confirmed that development of strong interlocking at magnesium-bone interface was mainly due to formation of corrosion layer around degrading magnesium and not dependent on new bone formation. This indicates that pull-out experiments cannot be used as parameters for bone healing or bone conductive effects of magnesium implants.

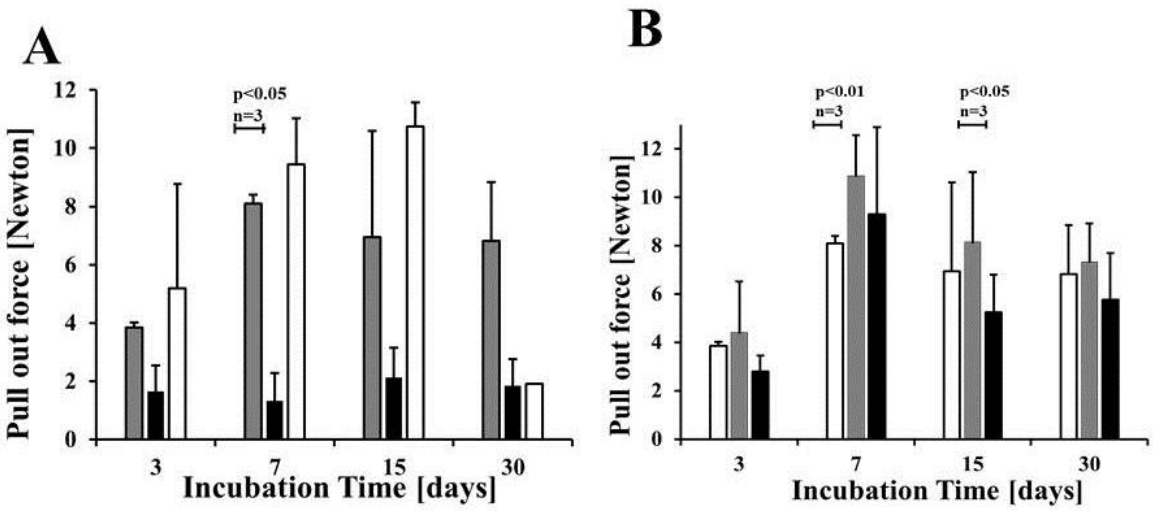

Figure 12: Interlocking at magnesium-bones interface is increased even in the absence of cells. Magnesium (Mg), magnesium silver alloy (Mg2Ag) and titanium pins (Ti) with 15 mm length and 0.4 mm diameter were inserted into tibia bones isolated from BALB/C mice which were then treated with formalin to eliminate live cells. Tibia bones inserted with implants were immersed in corrosion media and incubated at 37°C with 5% CO_2 under standard cell culture conditions for indicated time points. At each of the indicated time points, interlocking strength between implants and bones was determined by applying mechanical pull out test setup. A: The bars indicate average values of pull out force measured between magnesium and tibia bones (grey bars), magnesium silver alloy and tibia bones (empty bars) and titanium and tibia bones (black bars). In parallel, magnesium implants inserted in tibia bones were incubated in fresh DMEM containing 10% serum, used DMEM and 100 mM KH_2PO_4 under the same conditions. Pull out force in effect to different corrosion media was measured at indicated time points. The bars represent average of pull out force determined between magnesium and tibia bones after incubations in DMEM (empty bars), KH_2PO_4 (grey bars) and used DMEM (black bars). (Statistical analysis was done using Students's T-Test (paired) and p-value was calculated. (Pull out measurements courtesy by Andreas Weizbauer from MHH, Hannover)

3.2.2 Surface morphology of corrosion layers on magnesium

Formation of corrosion layer around magnesium seemed a major player to stimulate strengthening of bone-implant interlocking. Therefore, to reveal its morphology, magnesium pins were directly incubated in DMEM, used DMEM and KH_2PO_4 under standard cell culture conditions for seven days and then observed under scanning electron microscope (Figure 13A-D). Scanning electron microscopy of magnesium wires was done to see morphologies of corrosion layers after incubations in DMEM, spent cell culture medium and KH_2PO_4. As compared to magnesium pins without incubation (Figure 13A), a thick corrosion layer developed over the time around the corroding magnesium in effect to immersion solutions (Figure 13B-D). However, this layer was variable in shape with the composition of corrosion media and probably this might be the reason for variation in pull

out force. Thus, corroding magnesium implants develop a corrosion layer and the elements of this layer interact with bone tissue and develop strong bonding showing that the increase in the implant pull out force occur independent of bone growth. This technique therefore appears not appropriate to demonstrate bone- growth stimulating effects of magnesium implants [161].

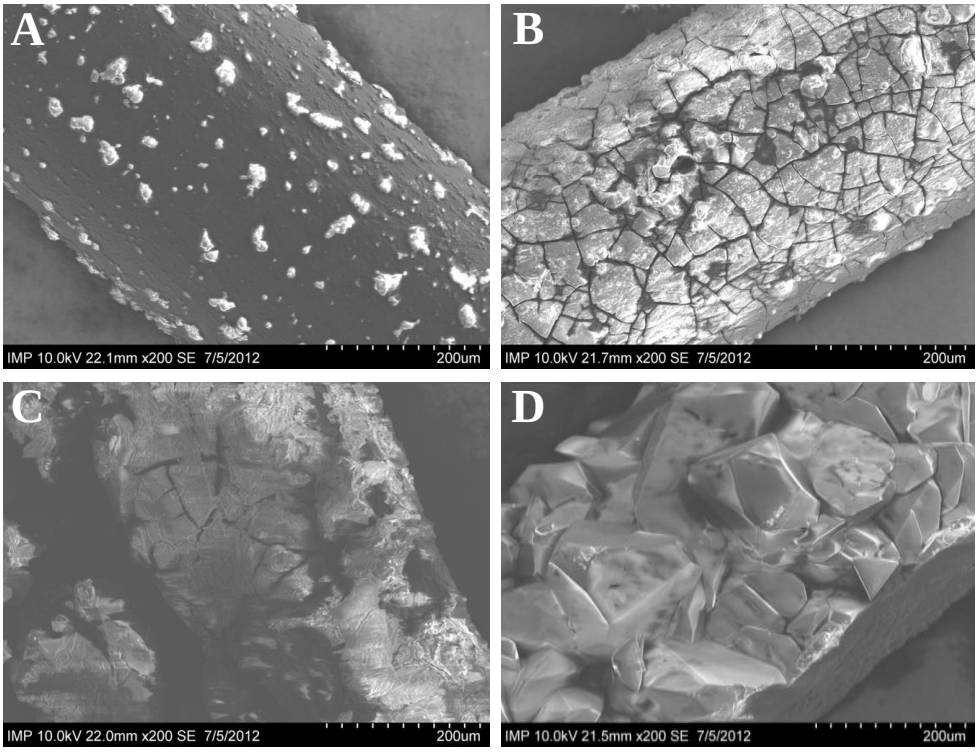

Figure 13: Corroding magnesium implants develop a corrosion layer over the time. Magnesium pins with 15mm length and 0.4 mm diameter were incubated for 7 days under standard cell culture conditions. Samples were then removed and the corrosion layer on each was visualized by employing SEM. Surface of magnesium pins before incubation as control (A) and after incubation in fresh DMEM (B), in spent DMEM (C) and in 100 mM KH_2PO_4 (D) attracted the formation of corrosion layer. (SEM courtesy by Florian Evertz from Leibniz University, Hannover)

3.2.3 Surface analysis of pulled out wires from tibia bones

To know the elemental composition of corrosion layer and factors responsible for the increase in pull out force, magnesium pins incubated directly or those removed from bones by pull out setup were subjected to Energy dispersive X-ray spectroscopy (EDX). EDX analysis of magnesium wires before incubation showed elements of magnesium (Mg), some amount of oxygen and also carbon (Figure 14A). After corroding for seven days, a corrosion layer mainly composed from additional elements of carbon, oxygen, sodium, magnesium,

calcium and phosphorus was detected (Figure 14B-D). However, calcium was detected only on the surfaces of implants which were incubated in DMEM and in spent cell culture medium (Figure 14B, C). The cavity of tibia bones analyzed for comparison and the elements of carbon as a major element and additionally oxygen, phosphorus and calcium were detected (Figure 14E). Then EDX analysis of pulled-out magnesium implants indicated the presence of carbon, oxygen, sodium and magnesium (Figure 14F-H). In addition, potassium was detected only from the surfaces of wires incubated in KH_2PO_4 (Figure 14H). This indicated that elemental compositions of magnesium pins remained same if implants were incubated directly or after insertion in bones into their respective media. Increase in the amount of carbon on each of the pulled-out wire also did not seem to be from bone as the samples were incubated in the presence of carbon dioxide and therefore carbon was also detected from the samples incubated directly into the media (Figure 14B-D compare with F-H). This confirmed that the strong interlocking between magnesium and adjacent bone tissue is solely due to the formation of a corrosion layer.

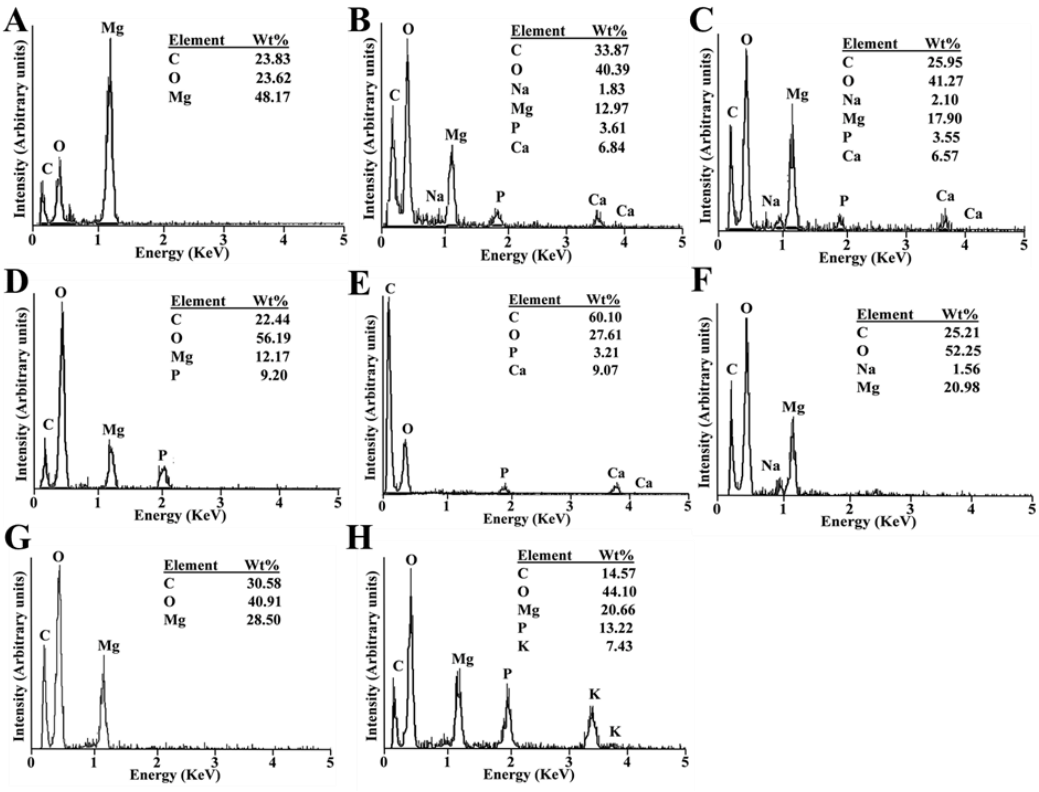

Figure 14: EDX analysis of magnesium implants. Magnesium pins with 15mm length and 0.4 mm diameter were directly incubated for seven days in physiological solutions and incorporation of corrosion layer

elements was determined by employing EDX. EDX analysis and percent elemental composition of magnesium pins without incubation as control (A), after 7 days of incubation in DMEM (B), in spent cell culture medium (C) and in 100 Mm KH_2PO_4 solution(D). Magnesium pins which were pulled out from tibia bones after incubations in indicated media were also subjected to EDX. For comparison, EDX of the internal cavity of tibia bones isolated from mice (E). EDX of pulled-out magnesium pins after 15 days of incubation in DMEM (F), spent cell culture medium (G) and100 mM KH_2PO_4 solution (H). (EDX analysis courtesy by Florian Evertz from Leibniz University, Hannover)

3.3 A protective coating for magnesium to limit fast degradation and hydrogen generation

3.3.1 The selection of suitable phosphate solution as coating medium

Phosphorus is essential component of natural corrosion layer deposited on the surface of corroding magnesium implants. To see the feasibility of phosphate coatings, magnesium discs were incubated in three phosphate compounds (Table 12) at 37°C and 37°C with 5% CO_2 under cell culture conditions. A bulky crystalline phosphate coating adhering around magnesium formed when samples were incubated under cell culture conditions with CO_2. In comparison, at 37°C coatings with similar morphologies formed but to a minor extent (Table12, Figure 15). Out of tested phosphate solutions, KH_2PO_4 led to the accumulation of maximum coating mass around magnesium implants (Table 12).

Table 12: Properties of coating solutions

Coating solutions	KH_2PO_4	K_2HPO_4	NaH_2PO_4	$Mg(OH)_2$	MgF2
Concentrations	100mM	100mM	100mM	1M	NaOH 200 g/l HF 40 %
pH	4.62±0.02	9.23±0.005	4.65±0.03	9.92±0.005	-
Coating mass (mg/cm^2) at 37°C+CO_2	14.23±0.29	3.72±0.78	11.62±0.59	16.06±0.51	-1.6±0.5
Coating mass (mg/cm^2) at 37°C	9.14±0.40	1.63±0.56	8.88±0.68	14.10±0.83	-

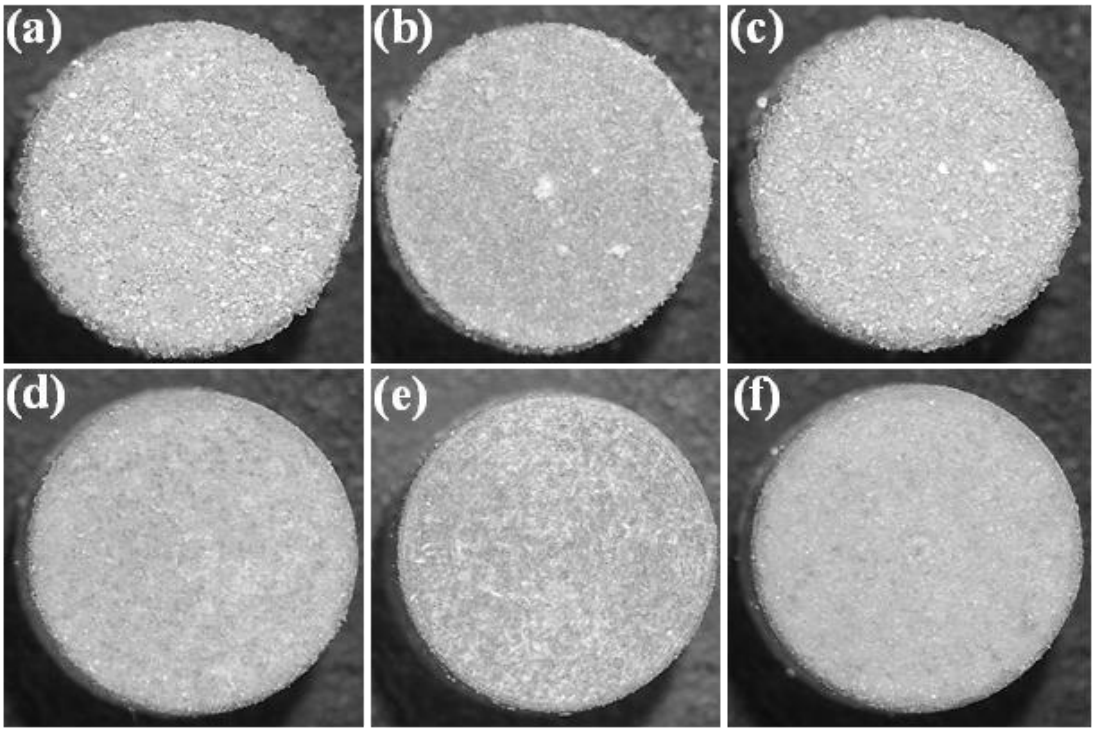

Figure 15: Di-hydrogen phosphate (H_2PO_4) forms a coating on metallic magnesium in the presence of CO_2. Magnesium discs with 5 mm diameter and 2 mm height were incubated individually in 100 mM of KH_2PO_4, K_2HPO_4 and NaH_2PO_4 solutions for three days either at 37°C with 5%CO_2 under standard cell culture conditions (a-c) or at 37°C alone (d-f). After 3 days, discs were removed and images were taken using a bimolecular microscope. Magnesium coated with KH_2PO_4 (a, d), K_2HPO_4 (b, e) and NaH_2PO_4(c, f).

3.3.2 Performance of phosphate coated implants in cell culture medium

In vitro immersion assay by using DMEM was performed to select best phosphate compound as coating solution. Corrosion resistant properties of magnesium discs coated with or without indicated phosphate solutions were tested by measuring weight loss, hydrogen evolution and pH elevation at standard cell culture settings. All phosphate based coatings degraded slowly as compared to magnesium discs without coating during the tested time period (Figure 16A). No measureable hydrogen gas production from both KH_2PO_4 and NaH_2PO_4 coated discs was found. However, plain magnesium as well as K_2HPO_4 coated magnesium led to H_2 production (Figure 16B). Also, pH values of the corrosion medium for KH_2PO_4 and NaH_2PO_4 coated discs remained stable like control medium without discs. However, in case of plain magnesium as well as magnesium coated with K_2HPO_4 pH of the medium increased gradually (Figure 16C). On the basis of these data,

from three coating solutions, potassium dihydrogen phosphate was selected as best coating media because it led to the formation of degradable corrosion resistant stable coating around magnesium. For further studies, OH^- ion formation as by-product of magnesium degradation that can promote precipitation of magnesium hydroxide Mg $(OH)_2$ on the surface of magnesium was selected as coating solution. Fluoride coatings have been reported as corrosion resistant; therefore, fluoride coated magnesium discs (MgF_2) were used as reference coating.

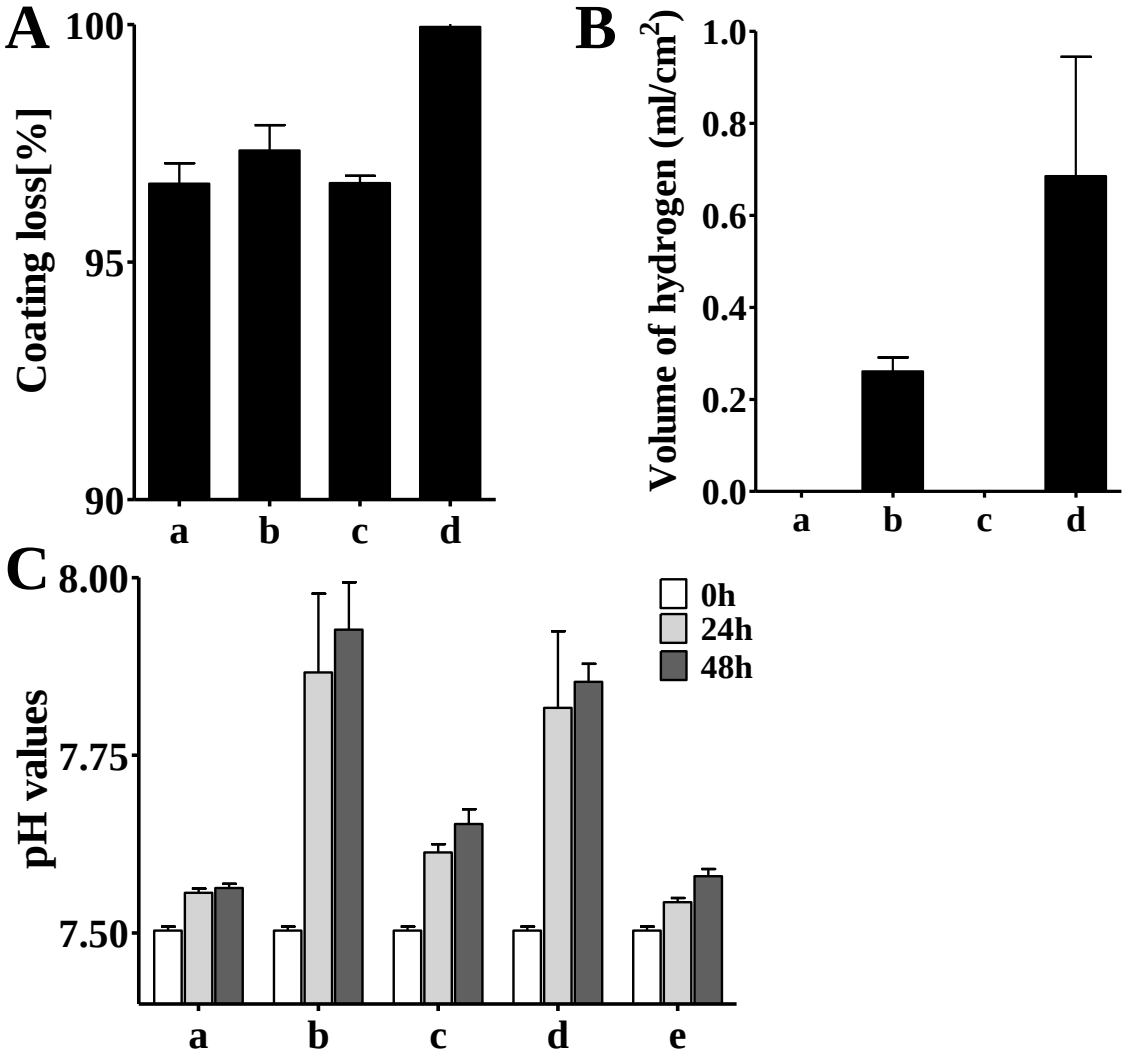

Figure 16: KH_2PO_4 is preferred coating solution. Magnesium discs coated with phosphate salts were immersed in 10 ml of DMEM and incubated for 2 days at 37°C with 5% CO_2 under standard cell culture conditions. After 48h of incubations, the decrease in mass was determined. **A:** Decreases in the weight of KH_2PO_4 coated (a), K_2HPO_4 coated (b) and NaH_2PO_4 coated (c) magnesium discs after 48h of incubations. Magnesium without coating served as control (d). **B:** Discs were incubated in syringes containing 10 ml of DMEM at conditions as described previously. Hydrogen gas measured from KH_2PO_4 coated (a), K_2HPO_4 coated (b) and NaH_2PO_4 coated (c) magnesium discs after 48h of incubation. **C:** Test specimens were immersed in 10

ml of DMEM and changes in pH of test solution containing KH_2PO_4 coated magnesium (a), K_2HPO_4 coated magnesium (b) and NaH_2PO_4 coated magnesium (c) plain magnesium discs after 48h of incubations.

3.3.3 Determination of appropriate time required for KH_2PO_4 coatings

To select a suitable time required for the formation of phosphate coatings, magnesium discs were incubated in KH_2PO_4 solutions at standard cell culture conditions and the resulting coatings mass was measured at indicated time points. In parallel, the pH of KH_2PO_4 in the presence of magnesium samples was measured. The degradation process of magnesium provokes a slow phosphate coating, a process that took a minimum of 3 days. Immersion in KH_2PO_4 at standard cell culture conditions led to gradual increase in the weight of these discs (Figure 17A). After immersion for 24h up to two weeks, no further addition in weight of magnesium discs incubated in KH_2PO_4 could be observed, indicating that 3 days was an optimum time period required for coating. Similarly, changes in pH of KH_2PO_4 solution containing discs showed an initial burst increase however at later stages pH of the phosphate solution became stable (Figure 17B). This experiment confirmed that in the presence of potassium phosphate, magnesium discs develop a coating within three days.

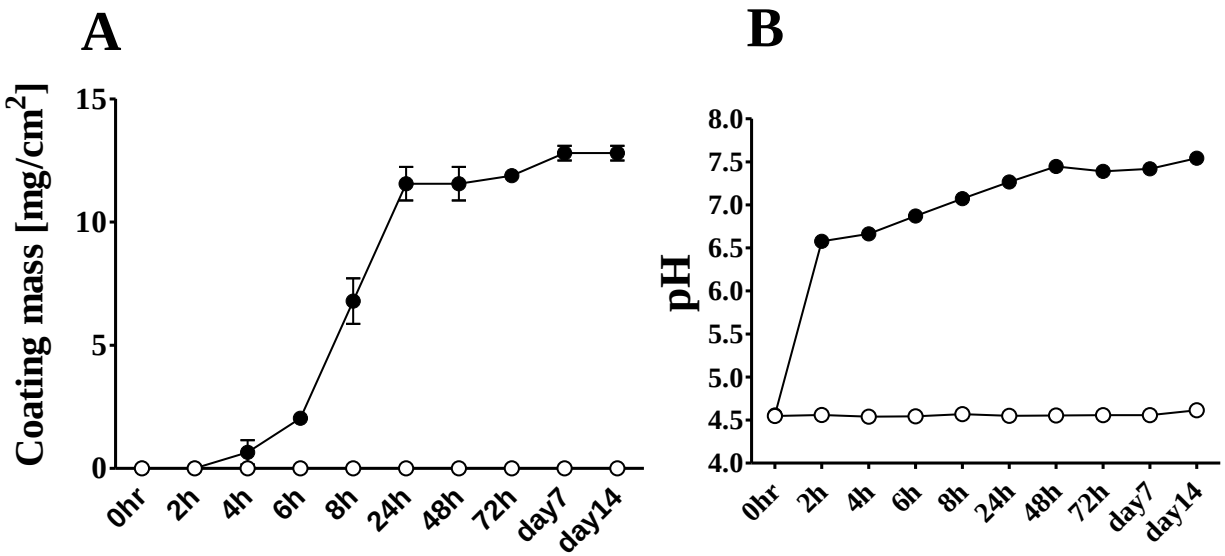

Figure 17: **Process of phosphate coating on magnesium takes 3 days of incubation.** Magnesium discs were incubated in 100 mM KH_2PO_4 solution to estimate minimum time required for coating process. **A**: Gradual increases in weight of coating mass on the surface of magnesium discs incubated in KH_2PO_4 due to accumulation of potassium phosphate crystals (filled circles) as compared to control (empty circles). **B**: changes in the pH of 100 mM KH_2PO_4 solution containing magnesium discs (filled circles) as compared to solution without discs.

3.3.4 Detailed analysis of KH_2PO_4 coated magnesium discs

To reveal detailed morphology and elemental composition of phosphate coatings, SEM, EDX and XRD analyses were performed. Electron microscopy of phosphate coated magnesium discs showed the presence of white crystalline coating on magnesium implants (Figure 18A). The EDX pattern of these coatings specifies that they were constituted mainly from oxygen, magnesium and phosphorus (Figure 18B). Further, XRD diffraction pattern at angles 2θ from plain magnesium and phosphate coated magnesium discs was also recorded. The diffraction peaks recorded from magnesium without coating were typical for pure magnesium surfaces. However, after the development of phosphate coatings, some additional peaks emerged most of which were corresponding to Newberyite ($MgHPO_4.3H_2O$) (Figure 18C right). Thereby, indicating that Newberyite ($MgHPO_4.3H_2O$) is most likely the dominant crystalline compound of the coating.

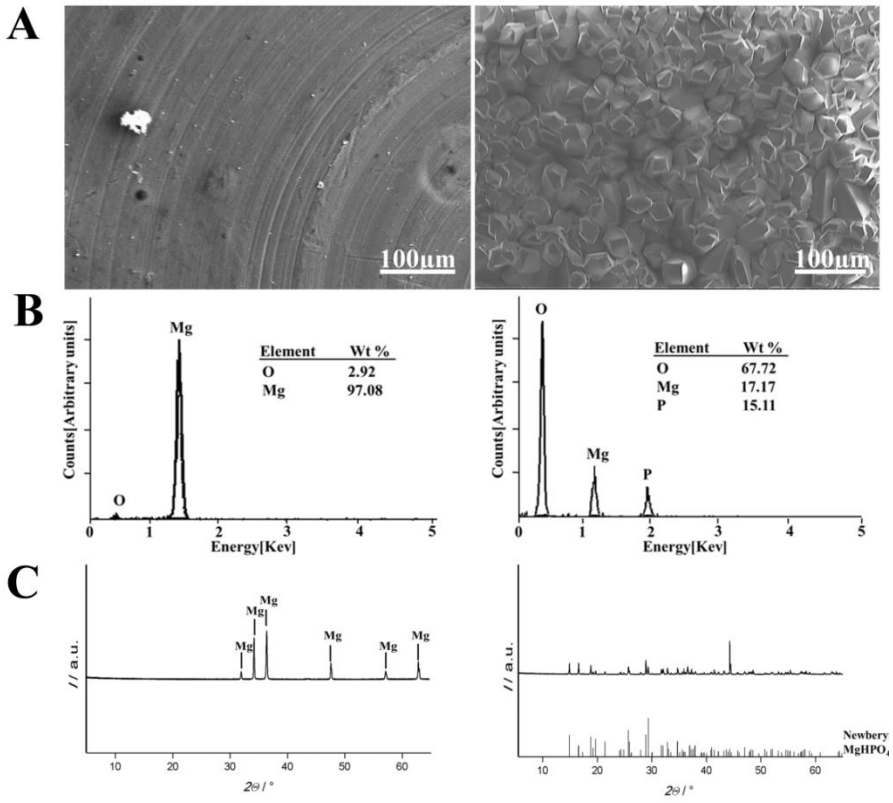

Figure 18: Newberyite coating develops around magnesium after incubation in KH_2PO_4. Magnesium implants were incubated in 100 mM KH_2PO_4 solution for three days at 37°C with 5% CO_2 under standard cell culture conditions. After indicated incubation time, magnesium discs were removed and to identify final coating these samples were subjected to SEM, EDX and XRD analyses. **(A)** SEM images of magnesium before phosphate treatment (left) and after treatment with KH_2PO_4 (left). Scale bar 100µm. **(B)** EDX of plain

magnesium (left) and after the development of phosphate coating. Corrosion elements correspond to the emitted X-ray energy and are shown above the particular peaks. Within corresponding inset tables, the percentage of elements is also given. O, oxygen; Mg, magnesium; P, phosphorus. **(C)** X-ray diffraction (XRD) analysis of magnesium discs without coating (left), and after coating with phosphate (right B)**.** *I*, relative X-ray reflection intensity, *2θ*, diffraction angle (SEM and EDX analysis courtesy by Florian Evertz and XRD analysis courtesy by Marc Kieke from Leibniz University, Hannover)

3.3.5 *In vitro* immersion tests for phosphate treated magnesium implants

To determine if phosphate coatings were protective, immersion tests were performed by employing DMEM cell culture medium containing proteins. Specimens were incubated in media for short and long time under standard cell culture conditions. Degradation after short exposure time was determined by measuring hydrogen (H_2^{evo}) and the pH. The mass loss was minute and could only be determined after prolonged incubation. Magnesium without coating (Mg) and magnesium hydroxide coated [$Mg(OH)_2$] samples exhibited rapid corrosion and led to the generation of hydrogen gas and a rise in the pH of surrounding solution (Figure 19A). Contrary to it, phosphate coated specimens did not show any signs of gas production similar to fluoride coated magnesium and titanium (Figure 19B). This was also consistent with the weight change which was measured after removing corrosion products with chromic acid. Minimal weight loss was observed for phosphate coated (MgP) discs as compared to other coatings (Figure 19C and Table 3)

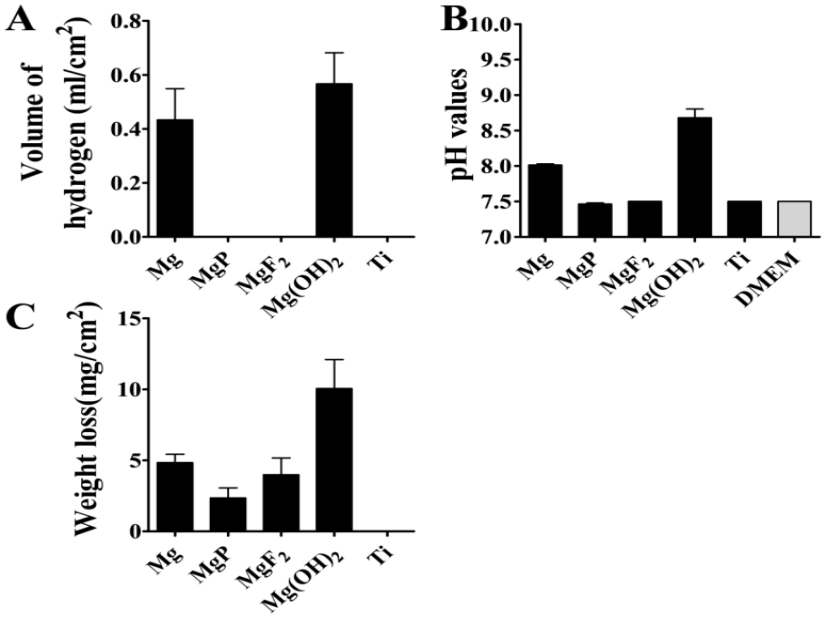

Figure 19: Corrosion rate in magnesium is reduced after phosphate treatment. Magnesium implants before or after phosphate (MgP), fluoride (MgF_2) or magnesium hydroxide $Mg(OH)_2$ coatings were incubated

in individual setups containing 10ml of DMEM at standard cell culture environment. Early corrosion was assessed either by measuring hydrogen generation or pH elevation after 48h of incubation. However, overall corrosion rate was estimated after 8 weeks of incubation in DMEM by measuring weight loss after treating samples with diluted chromic acid. A: Amount of hydrogen gas produced in DMEM due to corrosion of plain magnesium (Mg), magnesium coated with potassium phosphate (MgP), magnesium coated with fluoride (MgF_2), magnesium coated with magnesium hydroxide ($Mg(OH)_2$ and titanium after 48 h incubation. B: Variations in pH as an indicator of corrosion process measured after 48h in DMEM containing plain magnesium (Mg), phosphate coated magnesium (MgP), fluoride coated magnesium (MgF_2), magnesium hydroxide coated magnesium $Mg(OH)_2$ and titanium (Ti). DMEM without implants served as a control. C: Cumulative mass loss after 8 weeks of immersion.

Table 13: *In vitro* and *in vivo* comparison of degradation rates of coated magnesium implants

Implant	*In vitro* degradation (mm/year)*	*In vivo* degradation(mm/year)**
Mg	0.17±0.02	1.01±0.33
MgP	0.08±0.025	0.55±0.029
MgF_2	0.14±0.042	0.52±0.007
$Mg.Mg(OH)_2$	0.37±0.073	0.67±0.066
Ti	0.00	0.00

Mg, magnesium without coatings; MgP, phosphate coated magnesium; MgF_2, fluoride coated magnesium; $Mg.Mg(OH)_2$, magnesium hydroxide coated magnesium; Ti, titanium.
*Test specimens as indicated were immersed in DMEM for 8 weeks
**Indicated surfaces were implanted subcutaneously in mice for 8 weeks

3.3.6 Elemental composition of coated discs after short and long-term incubation

Magnesium corrosion layer components particularly calcium and phosphorus are known to be involved in new bone formation. To characterize the composition of the corrosion layer, specimens were subjected to SEM and EDX analyses after short term and long term incubations in cell culture medium (Figure 20A- D). Within 48h, white corrosion precipitates composed of the elements of magnesium, calcium and phosphorus emerged on the surface of magnesium (Figure 20A and B left to right). After this period, all coated implants had largely maintained the original coating composition (Figure 20A and B left to right). However, even though magnesium hydroxide coating did not completely disappear they appeared fragile and did not eliminate hydrogen evolution nor rise in pH. Titanium (Ti) surfaces remained unchanged (Figure 20A and B right). On all discs small amounts of

carbon emerged. After prolonged incubation in cell culture medium, surfaces of magnesium with as well as without coating were covered by thick corrosion layer containing the elements of magnesium, oxygen, calcium, phosphorus and traces of carbon (Figure 20C and D). However, internal features typical for original phosphate coatings were still apparent (Figure 20C and D). After corroding, the elemental compositions detected on phosphate coatings were highly similar to those on magnesium without coating or magnesium coated with fluoride and magnesium hydroxide coated magnesium. In comparison, phosphate coatings avoided the rapid initial corrosion of magnesium without disturbing the subsequent precipitation of corrosion products. In comparison, changes in the structure as well as composition of titanium discs could be detected (Figure 20C and D).

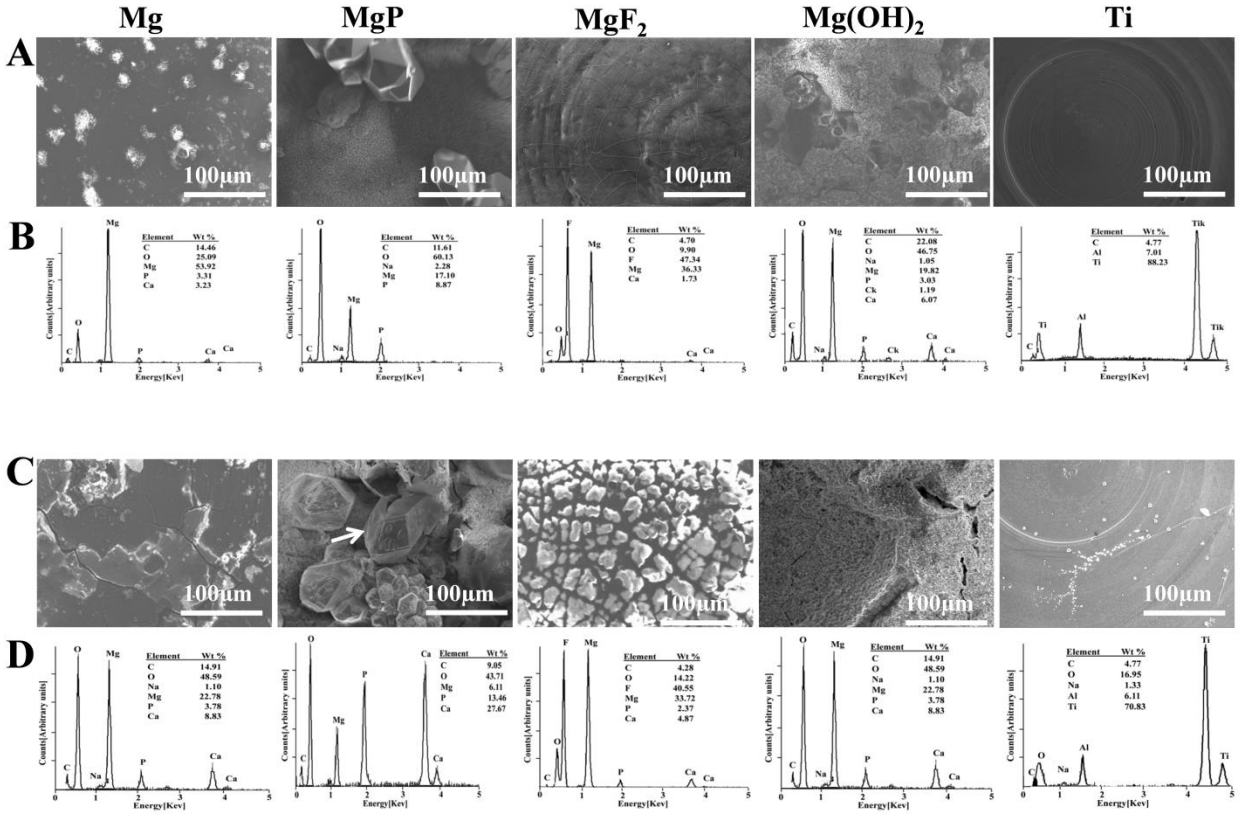

Figure 20: Phosphate coatings preserve desirable properties of magnesium implants. Magnesium discs with and without coatings were immersed in DMEM for 48h and 8 weeks at 37˚C with 5% CO_2 in a humidified cell culture incubator A: SEM images of implants after 48 h of incubation from left to right magnesium without coatings, phosphate coated, fluoride coated, magnesium hydroxide coated and titanium. B: EDX pattern of indicated surfaces. C: SEM images of discs after 8 weeks of incubations. D: EDX pattern same of same discs. Corrosion elements correspond to the emitted X-ray energy and are shown above the particular peaks. Within corresponding inset tables, the percentage of elements is also given. C, carbon; O, oxygen; Mg,

magnesium; Na, sodium; F, fluoride; P, phosphorus; Ca, calcium; Al, aluminum; Ti, titanium. (SEM and EDX analysis courtesy by Florian Evertz from Leibniz University Hannover)

3.3.7 Degradation kinetics of KH_2PO_4 treated magnesium in plasma and r-SBF

To confirm the initial corrosion resistance provided of magnesium phosphate coatings, immersion tests were performed in blood plasma and simulated body fluid (SBF) by measuring magnesium ions concentration under standard cell culture conditions. Small concentrations of magnesium ions were detected in plasma supernatant of both magnesium implants with and without phosphate coatings (Figure 21A). However, lesser magnesium ion concentrations were measured in plasma containing phosphate coated magnesium as compared to magnesium without coating (Figure 21A). Simulated body fluid resulted in higher release of Mg^{2+} ions from magnesium implants. Even then, phosphate coated magnesium implants were more resistant against degradation particularly during the initial time period (Figure 21B). As listed in Table 14, the corrosion rate as calculated from the weight loss was slow in phosphate coated magnesium as compared to magnesium without coating. An examination of the corrosion layer composition by SEM and EDX after immersion in plasma and SBF showed presence of oxygen, carbon, calcium, magnesium, phosphorus and traces of sodium (Figure 21C-F). Hence, phosphate coatings proved efficient protective barrier against fast initial corrosion and also led to the formation a of corrosion layer closely resembling to a pure magnesium in composition.

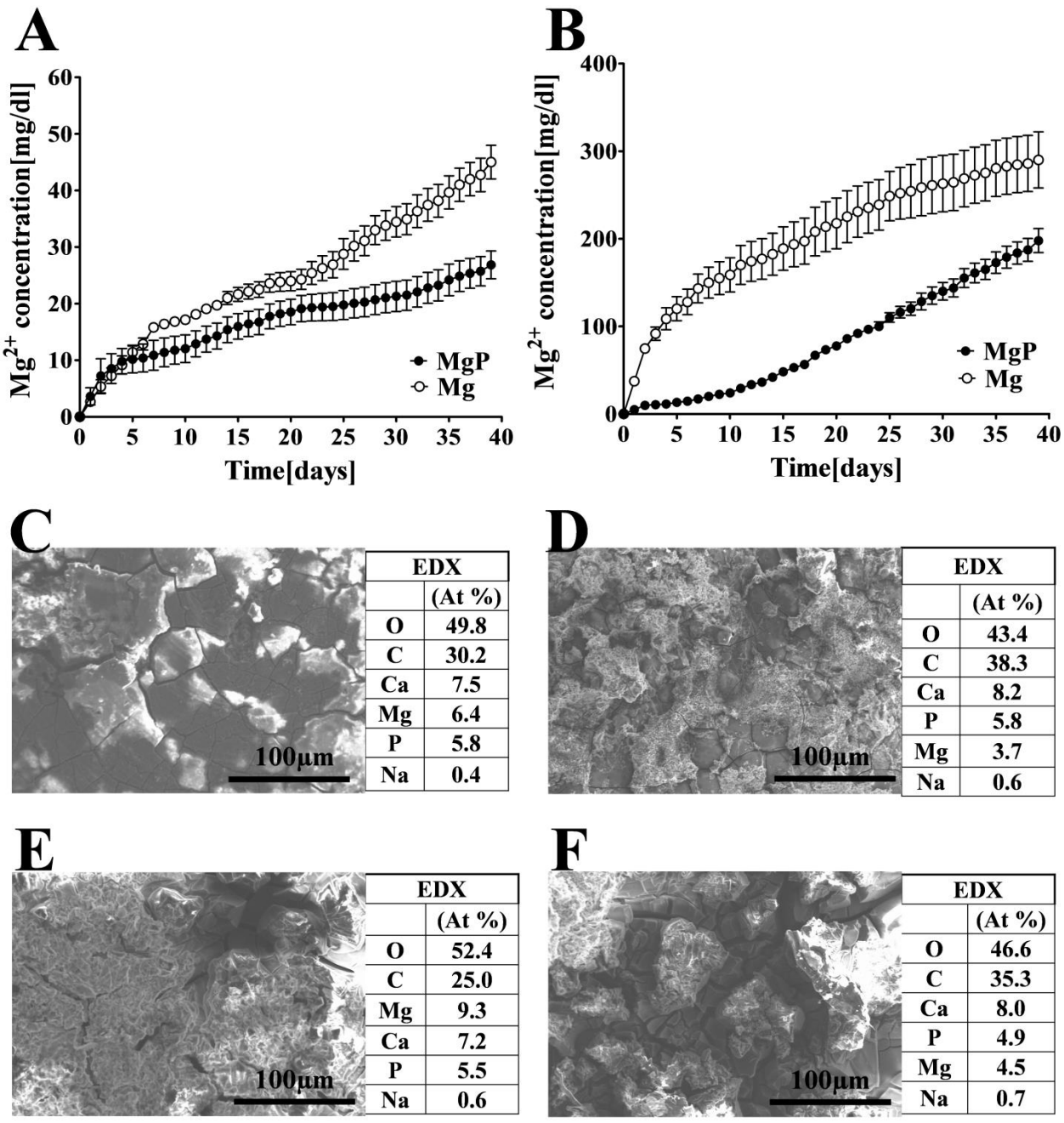

Figure 21: Phosphate treated magnesium resistance to initial corrosion burst. Phosphate coated and plain magnesium discs were individually incubated in plasma and SFB under standard cell culture conditions for 6 weeks. Corrosion supernatants were collected on daily basis and magnesium ions concentrations were determined after mixing it with magnesium binding reagent. After 6 weeks, test specimens were subjected to SEM and EDX analysis and then treated with diluted chromic acid to determine mass loss. Measurement of magnesium concentration from plasma or rSFB corrosion supernatants containing plain or phosphate treated discs (A and B). Magnesium concentration determined at indicated time points from plasma containing discs without coatings (white circles) and after phosphate coating (black circles) (A). Magnesium concentration determined at indicated time points from plasma containing discs without coatings (white circles) and after phosphate coating (black circles) (B). Surface analysis of discs (C-F). SEM and corresponding EDX of magnesium without coating (C) and phosphate coated (D) after 6 weeks incubation in plasma. SEM and EDX

of magnesium without coating (E) and phosphate coated (F) after 6 weeks incubation in r-SBF. (SEM, EDX and corrosion measurement courtesy by Ana Silva from Leibniz University, Hannover)

Table 14: Corrosion rates of plain magnesium and phosphate coated magnesium determined by immersion tests

Implants	Plasma (mm/year)	r-SBF (mm/year)
Mg*	0.41±0.04	2.78±0.25
MgP	0.35±0.04	1.80± 0.19

Mg*, magnesium without coatings; MgP, phosphate coated magnesium were incubated in the indicated media at 37°C with 5% CO_2 under standard cell culture conditions for 6 weeks. Samples were removed treated with chromic acid and corrosion rate was determined by weight loss method.

3.3.8 Compatibility of phosphate coatings with mammalian cells

A cell culture assay was established by employing mouse fibroblasts (NIH3T3) to evaluate biocompatible properties of phosphate coated surfaces and compared with plain magnesium and standard titanium as controls. Cells were directly seeded on the surfaces of plain as well as coated magnesium implants. Selection of fibroblasts was done on the basis of the fact that these are abundant tissue cells that *in vivo* contact the implant surfaces. Fluorescent staining and microscopy was applied to observe cell adherence and proliferation. After 3 days of cultivation at standard cell culture conditions, few cells were visible on the surface of magnesium without coating (Figure 22A). However, phosphate coatings promoted efficient adhering of cells exhibiting similar morphologies as on fluoride coated magnesium, standard titanium or on tissue culture plastic (Figure 22A; compared MgP with others). As presumed, magnesium hydroxide coatings did not support cells attachment and cell proliferation (Figure 22A; $Mg(OH)_2$). Cells density on phosphate coated magnesium was similar to the controls (Figure 22B; MgP compare MgF_2, Ti and CTR). Over all, phosphate coatings supported adhesion and proliferation of murine fibroblast thereby indicting excellent cell compatibility

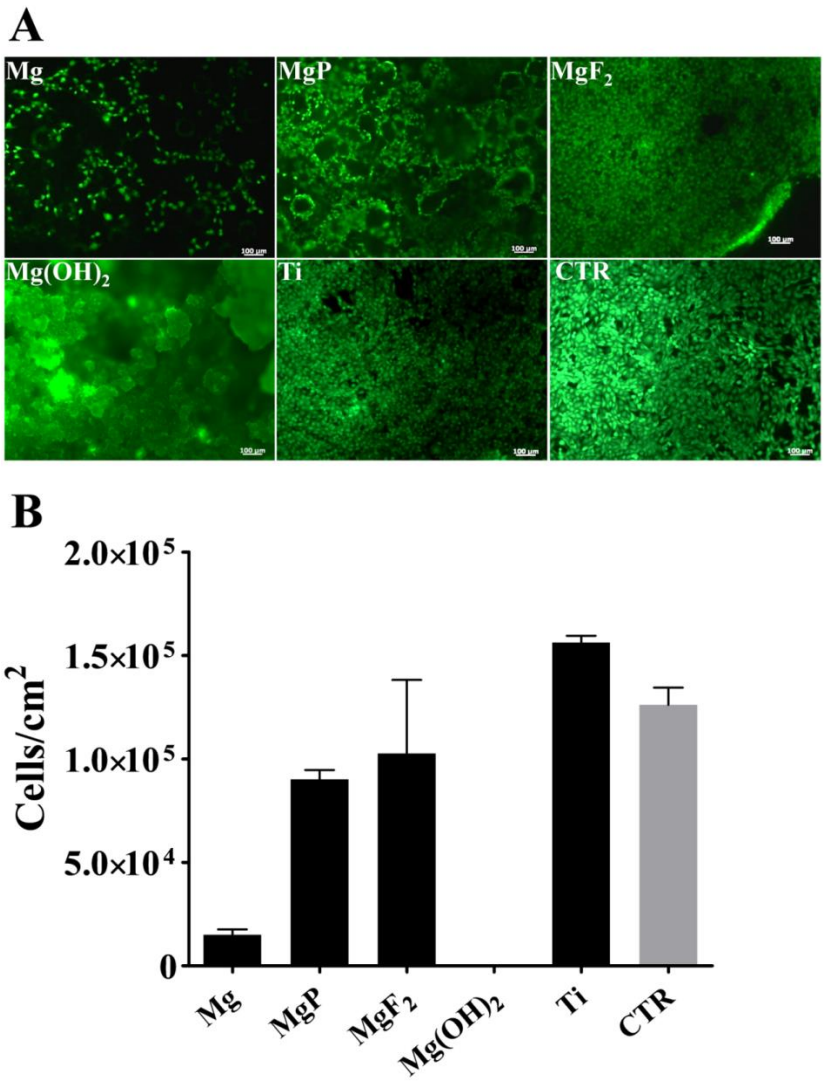

Figure 22: Phosphate coated magnesium are compatible with murine fibroblast. Fibroblasts (NIH3T3) were seeded on indicated surfaces and incubated for three days under optimum cell culture conditions and then then stained with fluorescent cell proliferation dye (CFSE) **A:** Fluorescent microscopy of cells on the materials used as well as adhesion substrates were as follows: magnesium without coatings (Mg), KH_2PO_4 coated (MgP), fluoride coated (MgF_2), magnesium hydroxide coated discs ($Mg(OH)_2$) and titanium (Ti) polystyrene surface (CTR) (Scale bar 100 µm). **B:** Quantitative determination of adherent cells counted from mentioned surfaces.

3.3.9 Cell viability and interleukin 8 (IL-8) response

To validate biocompatibility of phosphate coatings for various biomedical applications magnesium implants coated with or without phosphate were incubated with porcine nasal epithelial cells (PNEC). Metabolic activity of these cells after incubation with implants was determined as indicator of cells viability. Metabolic activity of these cells significantly decreased in the presence of magnesium samples without coatings (Figure 23A; Mg).

However, on phosphate coatings metabolic activity of cells remained normal similar like cells which were incubated without any implant (Figure 23A; MgP compare with CTR). In agreement with this finding, a gradual rise in magnesium concentration was determined from culture medium containing magnesium without coating as compared to phosphate coated magnesium at indicated time points (Figure 23B). Phosphate coated implants increased corrosion resistance and reduced the release of magnesium ions thereby promoting cells metabolic activity (Figure 23B; MgP). To determine potential inflammatory responses of cells to implants, magnesium implant with and without phosphate coatings were incubated with PNEC and IL-8 secretion as a pro-inflammatory marker was measured in the culture medium. IL-8 secretion increased significantly from cells containing magnesium implants without coatings (Figure 23C; Mg). In contrast to this, subtle increase in IL-8 production was measured from cells containing phosphate coated magnesium (Figure 23C; MgP). However, after 48h of incubation IL-8 release from PNEC increased even in the presence of phosphate coated magnesium samples (Figure 23D). Overall, it seemed phosphate coatings increased the corrosion resistance of magnesium and also improved the cell compatibility in cell culture assays.

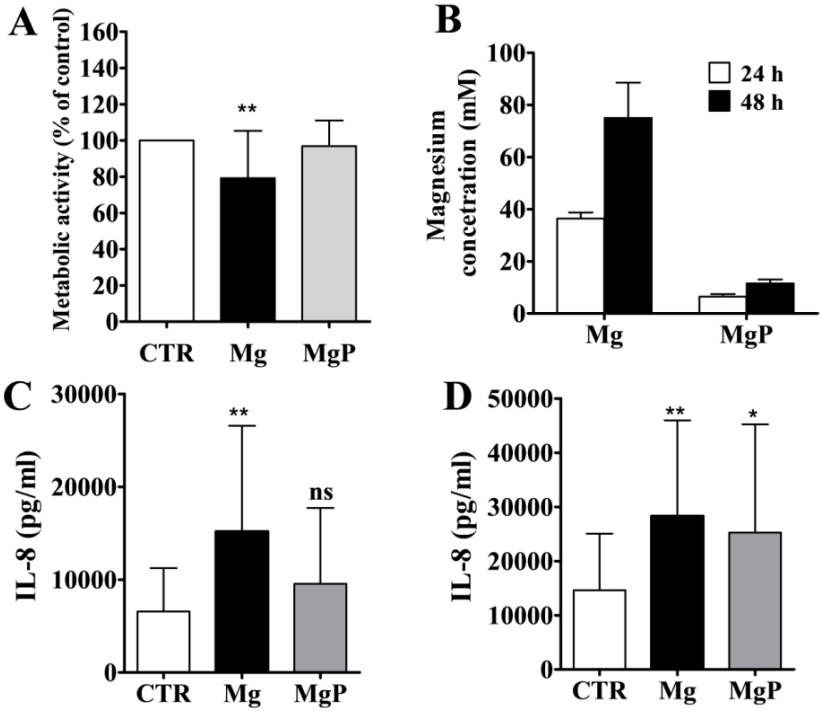

Figure 23: Phosphate treatment reduces corrosion and enhance viability of epithelial cells. Porcine nasal epithelial cells (PNEC) were cultivated for 48h with plain magnesium or phosphate coated magnesium discs under optimum cell culture conditions and then their metabolic activity was determined by employing

CellTiter 96 Aqueous One solution test. In parallel, concentration of magnesium released from the corroding implants into surrounding cell medium was also determined calorimetrically using commercial kit. **A:** Metabolic activity of cells without implants as control (CTR), after incubation with plain magnesium (Mg) and phosphate coated magnesium (MgP) B: Concentration of magnesium determined from the supernatant cell culture medium (AECGM) containing plain or phosphate coated magnesium discs. After 24(C) or 48h (D) of incubation, the culture medium containing each of the mentioned implants was collected and interleukin-8 (IL-8) concentration was determined by commercially available ELISA Kits. (Cell viability as well as IL-8 assays performed by Stephan Schumacher from TiHo, Hannover)

3.3.10 Observation of gas cavities around subcutaneously implanted magnesium discs

As an effort to investigate if phosphate coated magnesium were resisting fast corrosion *in vivo*, a novel strategy by employing a murine model (Figure 24). To facilitate the localization, implants were inserted subcutaneously at the back of mice (Figure 25A). Measurement of height and diameter of subcutaneous gas pouches around corroding implants was used to assess *in vivo* degradation kinetics. After a day of implantation, subcutaneous gas pockets started to develop around magnesium implants without coatings and magnesium hydroxide coated magnesium (Figure 25A; Mg and $Mg(OH)_2$). In contrast to this, no signs of gas formation could be visualized around phosphate coated and fluoride coated magnesium discs (Figure 25A; MgP and MgF_2). However, on day 7 post-implantation, small gas bubbles emerged around fluoride coated magnesium discs (Figure 25A; MgF_2) which disappeared gradually. Gas pouches were always visible around magnesium hydroxide coated discs. This indicated that these coatings were not corrosion protective (Figure 25A; $Mg(OH)_2$). Gas bubbles could be seen around magnesium discs without coatings during early weeks but they disappeared with time this confirmed that degradation rate of magnesium diminishes with the formation of a corrosion layer and suggests that modest gas volumes were diffusing through the tissue without leading to bubbles. The phosphate coated magnesium implants completely abrogate gas cavities while magnesium without coating and magnesium hydroxide coating led to gas burst shortly after implantation (Figure 25B).

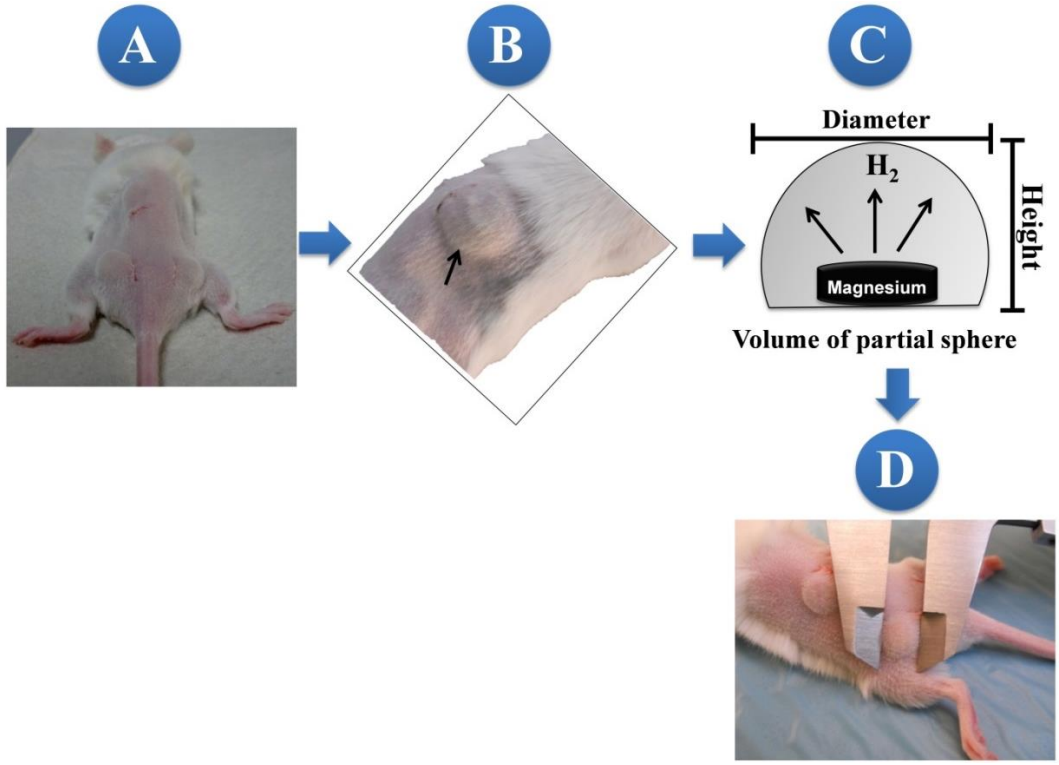

Figure 24: Establishment of murine model for measurement of gas cavities around corroding magnesium discs. **A**: Magnesium discs were subcutaneously implanted into mouse. **B**: After implantation gas cavities are generated around the magnesium discs and this subcutaneous air bubble looks like partial sphere. **C**: Height and diameter of this partial sphere were measured with help of Vernier caliper as mention and then volume of gas was calculated **D**.

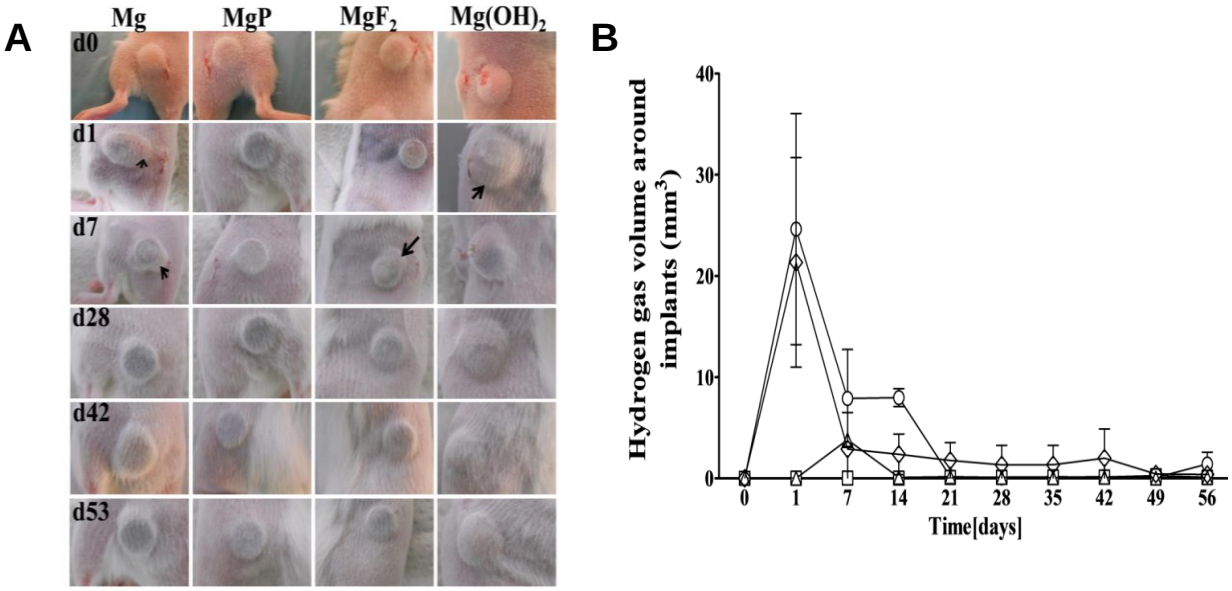

Figure 25: Potassium phosphate treatment eliminates gas accumulation from magnesium implants. Magnesium without coatings (Mg), phosphate coated magnesium (MgP), fluoride coated magnesium (MgF_2) and magnesium hydroxide coated magnesium were surgically implanted subcutaneously in Balb/C mice and

then mice were observed for 8 weeks post-implantation. Gas accumulation around implanted discs was imaged using camera and their dimensions were measured with Vernier caliper at the indicated time points after transplantation. A: from left to right magnesium without coatings, phosphate coated, fluoride coated and magnesium hydroxide coated magnesium implants after subcutaneous implantation on the dorsum of mice. B: Volume of gas accumulation around implanted discs, plain magnesium (circles), KH_2PO_4 coated magnesium (squares), fluoride coated magnesium (triangles) and magnesium hydroxide coated magnesium (rhombi).

3.3.11 Surface properties of discs after implantation

The corrosion process of magnesium is greatly influenced by the environment. To investigate changes in the elemental distribution and corrosion morphology, all implants were explanted and subjected to EDX and SEM analyses. Two days after implantation, a corrosion layer consisting of carbon, oxygen, magnesium, phosphorus, calcium and traces of sodium could be detected on plain magnesium implants (Figure 26A). Interestingly, after two days incubation in DMEM, a compact corrosion layer was not established on plain magnesium. Accordingly, this corrosion of magnesium appeared rapid in the soft tissue as compared to cell culture medium. Phosphate coated magnesium implants maintained their original morphology and composition after short time of implantation (Figure 26A; MgP). No major changes in the structure of fluoride and magnesium hydroxide coated implants could be observed. However, phosphorus and calcium from tissue had accumulated on these implants (Figure 26A; MgF_2 and $Mg(OH)_2$). There were no detectable changes of titanium implants except accumulation of carbon which may consist of tissue remnants (Figure 26A;Ti). After residing for prolonged time in soft tissue, surfaces of magnesium implants with and without coatings were surrounded by clearly visible corrosion layer (Figure 26C). This layer was composed from carbon, oxygen, magnesium, phosphorus and calcium in case for plain or coated magnesium implants (Figure 26D). These experiments confirmed that phosphate based coatings while inhibiting initial hydrogen generation allow the formation of corrosion layer that is closely resembling in morphology and elemental composition to the layer formed with time on the surface of magnesium without coating. Carbon on titanium discs was remnant of fibrous tissue capsule (Figure 26D; Ti).

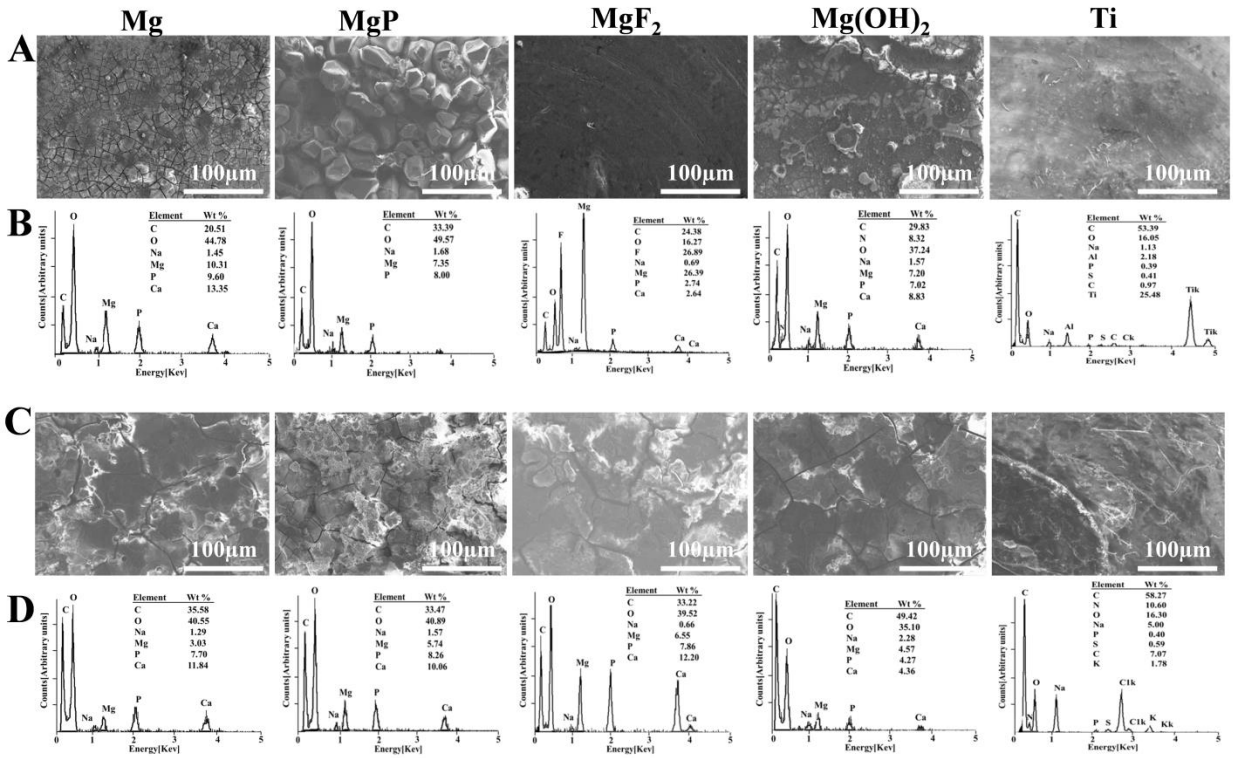

Figure 26: Structure and elemental composition of corrosion layers at early and later stages post-implantation. Magnesium discs with or without coatings were surgically implanted subcutaneously in Balb/C mice and then after 48h and 8 weeks post-implantation, implants were removed and subjected to SEM and EDX analyses. The materials used were as follows: Magnesium without coatings (Mg), phosphate coated magnesium (MgP), fluoride coated magnesium (MgF_2) and magnesium hydroxide coated magnesium. SEM and corresponding EDX of indicated surfaces after residing 48h in soft tissues (A, B). SEM and EDX of indicated surfaces after 8 weeks of residing in soft tissue. Corrosion elements correspond to the emitted X-ray energy and are shown above the particular peaks. Within corresponding inset tables, the percentage of elements is also given. C, carbon; O, oxygen; Mg, magnesium; Na, sodium; F, fluoride; P, phosphorus; Ca, calcium; Al, aluminum; Ti, titanium.(SEM and analysis courtesy by Florian Evertz from Leibniz University, Hannover)

3.3.12 *In vivo* corrosion rate determined by weight loss

In vivo corrosion of phosphate coated magnesium was estimated by the weight loss. As expected, magnesium discs without coatings showed the highest weight loss (Figure 27A and B). In addition, deep corrosion pits were observed (Figure 27A; Mg). Interestingly, phosphate coated magnesium appeared corrosion resistant under the identical conditions and minor weight loss similar to fluoride coated magnesium was observed. Surfaces of phosphate coated and fluoride coated discs were intact (Figure 27A; MgP and MgF_2). In comparison, magnesium hydroxide coated magnesium samples showed a high weight loss and substantial gas generation (Figure 27B). Deep corrosion cracks was present on the

surface of $Mg(OH)_2$ coated discs (Figure 27A). The corrosion rate of phosphate coated magnesium showed a modest corrosion compared to magnesium implants without coating Table 14. Hence, in addition to the elimination of gas cavities, phosphate coatings reduced weight loss and corrosion rate of magnesium.

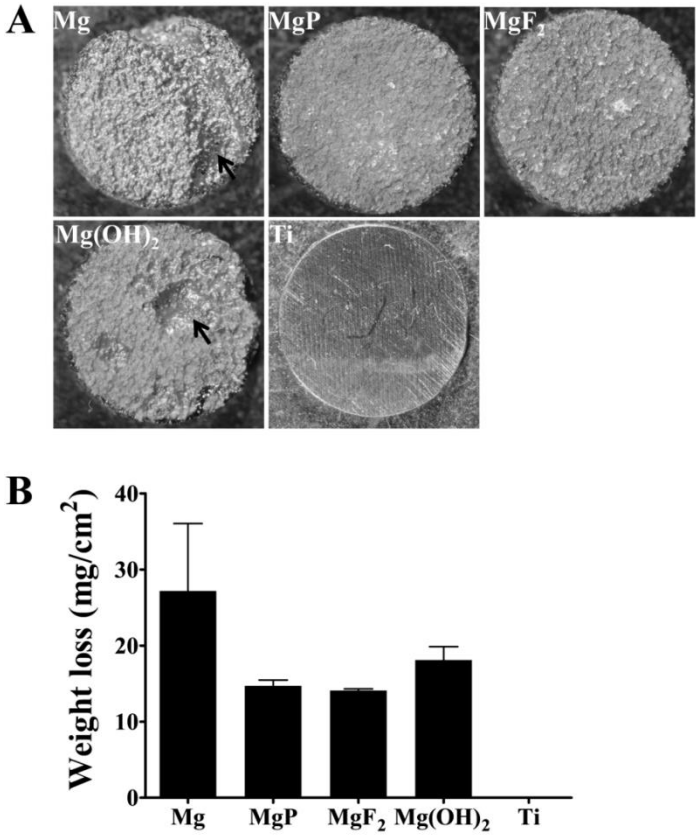

Figure 27: Phosphate treatment results in the reduction of mass loss after *in vivo* implantation. Tested implants were left in soft tissue for 8 weeks and then treated with diluted chromic acid to remove tissue debris and corrosion layer. A: Surfaces of magnesium without coating (Mg), phosphate coated (MgP), fluoride coated (MgF_2), magnesium hydroxide coated $Mg(OH)_2$ and titanium implants. B: Mass loss from indicated implants after 8 weeks of implantation.

3.3.13 Modest inflammatory response against implanted discs

Implants may trigger immune reactions and accumulation of inflammatory cells at tissue-implant interfaces. To test the biocompatibility and to evaluate the reaction of living tissue to coated magnesium implants, tissue samples were stained with hematoxylin and eosin. A layer of fibrous tissue with infiltration of some giant cells and granulocytes was observed around magnesium discs without coating and titanium discs (Figure 28A and B). In addition, a focal infiltration of inflammatory cells including some foreign body giant cells, mostly granulocytes was visible (Figure 28D). Some foreign body giant cells could also be

detected in the vicinity of the site of implantation of the magnesium discs (Figure 28 D). All of the coated magnesium discs elicited an adequate host response (Figure 29). Fibrous tissue was observed to encapsulate the coated implants. The infiltration of inflammatory cells, mostly granulocytes, with some macrophages was slightly more pronounced in samples containing discs coated with fluoride (Figure 29 B, D). A small accumulation of gas could be observed around the implants surrounding degradable samples. Additionally, a substantial corrosion layer was visible on the surface of all of the implants. The tissue surrounding the magnesium implants coated with potassium phosphate indicated that this coating provides superior soft tissue compatibility.

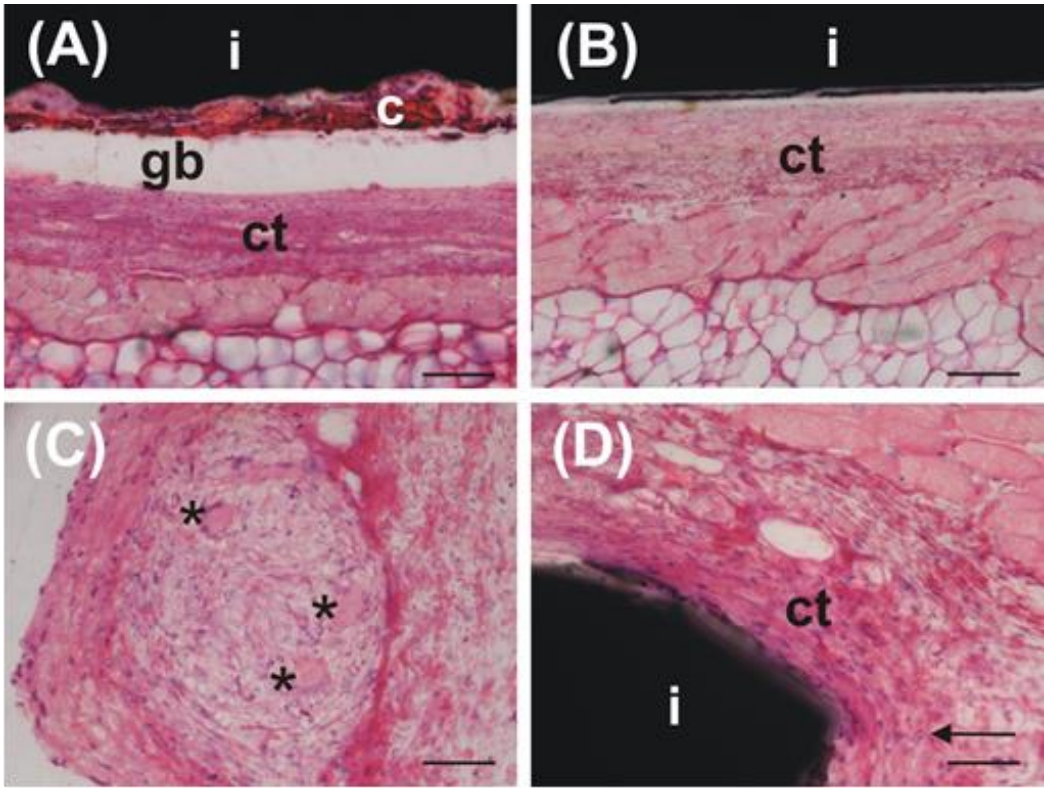

Figure 28: Non-inflammatory tissue-implant interface after implantation. Magnesium implants were inserted in mice and then after 8 weeks, implants with the adjacent tissue were removed and fixed in ethanol, paraffin embedded and stained with hematoxylin and eosin. (A) A magnesium disc without coating. (B) A titanium disc. (C) Few giant cells (∗) at the magnesium disc interface. (D) Focal infiltration of inflammatory cells (mostly granulocytes) around the titanium implant (black arrows). Features are noted as follows: 'i' = implant, 'c' = corrosion layer, 'ct' = connective tissue, 'gb' = gas bubble, '*' = giant cells, 'black arrow' = granulocytes. Scale bar = 100 μm in parts a and b; scale bar = 50 μm in parts c and d. (Histology courtesy by Andreas Weizbauer and Elmar Willbold from MHH, Hannover)

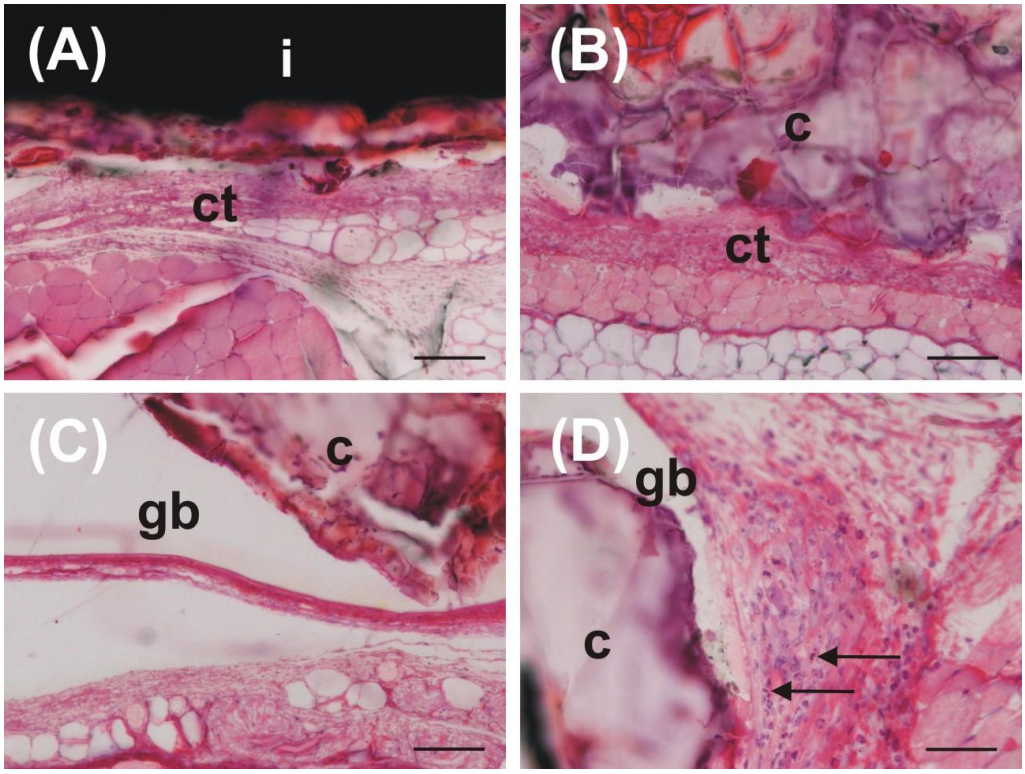

Figure 29: After phosphate treatment magnesium implants show compatibility with the soft tissue. (A) A magnesium disc with phosphate coating. B) A magnesium disc with fluoride coating. C) A magnesium disc with magnesium hydroxide coating. D) Inflammatory cells (mostly granulocytes) around the implant with fluoride coating. Features are noted as follows: 'i' = implant, 'c' = corrosion layer, 'ct' = connective tissue, 'gb' = gas bubble, 'black arrow' = granulocytes. Scale bar = 100 µm in parts a, b, and c; scale bar = 50 µm in part D. (Histology courtesy by Andreas Weizbauer and Elmar Willbold from MHH, Hannover)

3.4 Mouse model to understand implant-associated infections (Part B)

3.4.1 Prolonged survival of *P. aeruginosa* on magnesium implants

Metallic magnesium shows antibacterial properties under *in vitro* conditions[62]. To see if such inherent properties could also be achieved under *in vivo* situations, magnesium discs were implanted subcutaneously on the back side in mice (Figure 30). For side by side comparison, titanium and porous glass beads were implanted. Planktonic cultures of bioluminescent *pseudomonas aeruginosa* were directly injected on the surfaces of implants either immediately or 24h after implantation. *P. aeruginosa* could be seen soon after infection on the surfaces of subcutaneously implanted magnesium (Mg), titanium (Ti) discs and porous glass (PG) beads (Figure 31A; d0) which started to disappear from the surfaces of all implants. Surprisingly, on day1, bacteria resurfaced on magnesium discs alone and continued to exist for more than two weeks (Figure 31; Mg mice). However, bacteria did

not reemerge on titanium discs and porous glass beads (Figure 31; Ti and PG). In case when *P. aeruginosa* were injected locally on the surfaces of indicated implants after one day post- implantation, bacteria established prolonged infections on magnesium discs alone (Figure 32; Mg). To investigate if magnesium implants are susceptible to systemic infection, *P. aeruginosa* were injected intravenously into mice either immediately after implantation of magnesium, titanium and porous glass beads or after 24h of implantation. In this case, bacteria did not reappear on any of the implants (Figure 33A and B). Overall, it seemed magnesium implants were prone to locally injected *P. aeruginosa in vivo* as compared to titanium or porous glass beads. Bacteria were persisting on magnesium implants for a prolonged period of time. Hence, antibacterial properties of magnesium were limited to *in vitro* situations.

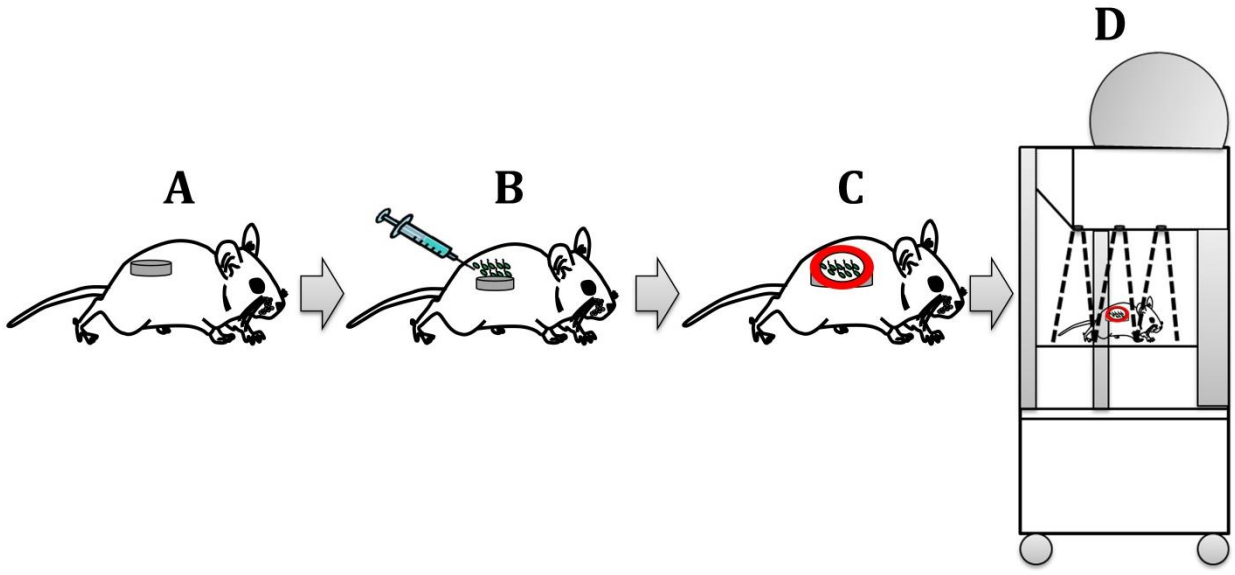

Figure 30: Establishment of biofilm on implant surfaces. **A:** Magnesium discs were implanted subcutaneously on the back of BALB/c mice. B: Soon after implantation, bioluminescent bacteria were directly injected on the surface of these discs. C: with the course of time, bacteria switch into biofilm mode of life. D: Bioluminescence of bacteria embedded within biofilm matrix was measured using a non-invasive *in vivo* imaging system

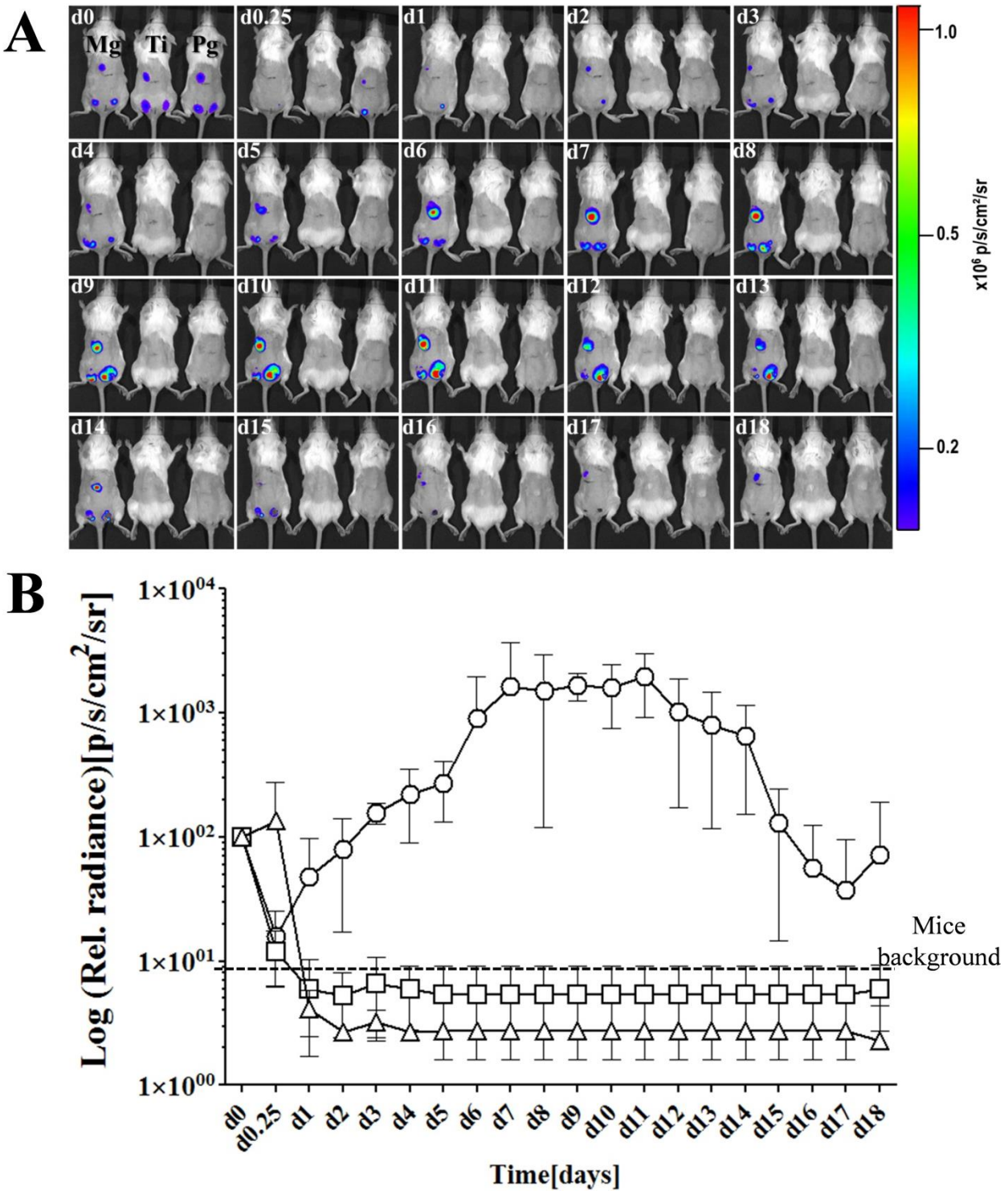

Figure 31: Magnesium implants are prone to *P. aeruginosa* infections. In each mouse implantations were done surgically subcutaneously on the back of mice as follows: Mg, magnesium; Ti, titanium; PG, porous glass. Immediately after implantation, 5µl of freshly grown bioluminescent *P. aeruginosa* at OD_{600}=0.1 in LB suspension were directly injected on the indicated implants. Bacterial luminescence was measured by putting mice under *in vivo* imaging system at indicated time points. The bacterial luminosity was recorded shortly after infection (d0) later after 6h (d0.25) and then daily for two weeks (A). The relative average luminescence

associated with magnesium (circles), with titanium (squares) and porous glass beads (triangles) was determined at indicated time points. Average tissue luminescence values calculated from mice without infection are indicated with background line.

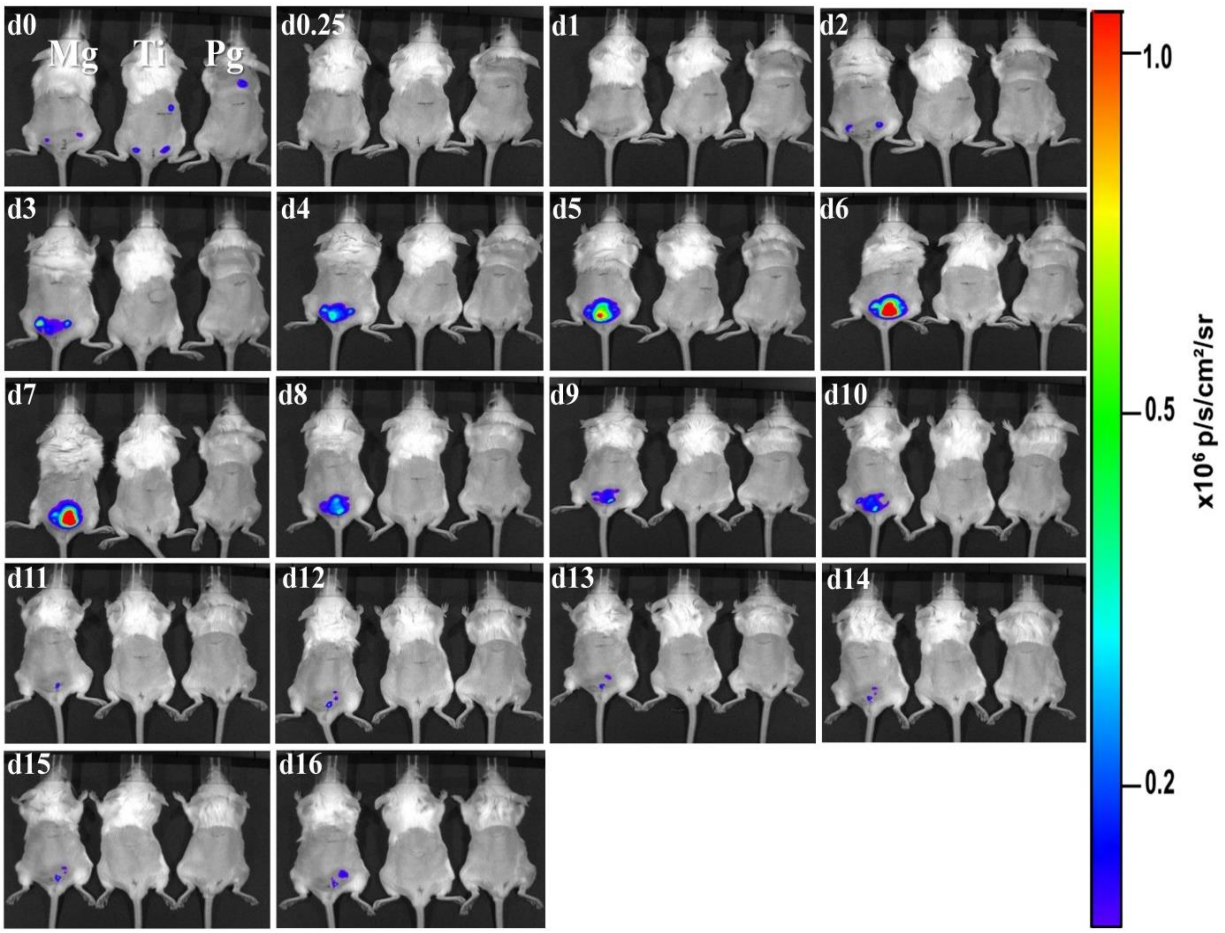

Figure 32: Magnesium implants are susceptible to *P. aeruginosa* colonization 24h after implantation.

In each mouse implantations were done surgically subcutaneously on the back as follows: Mg, magnesium; Ti, titanium; Pg, porous glass. 24h after implantation, 5µl of freshly grown bioluminescent *P. aeruginosa* at OD_{600}=0.1 in LB suspension were directly injected on the indicated implants. Bacterial luminescence was measured by putting mice under *in vivo* imaging system at indicated time points. The bacterial luminosity was recorded shortly after infection (d0) later after 6h (d0.25) and then daily at indicated time points.

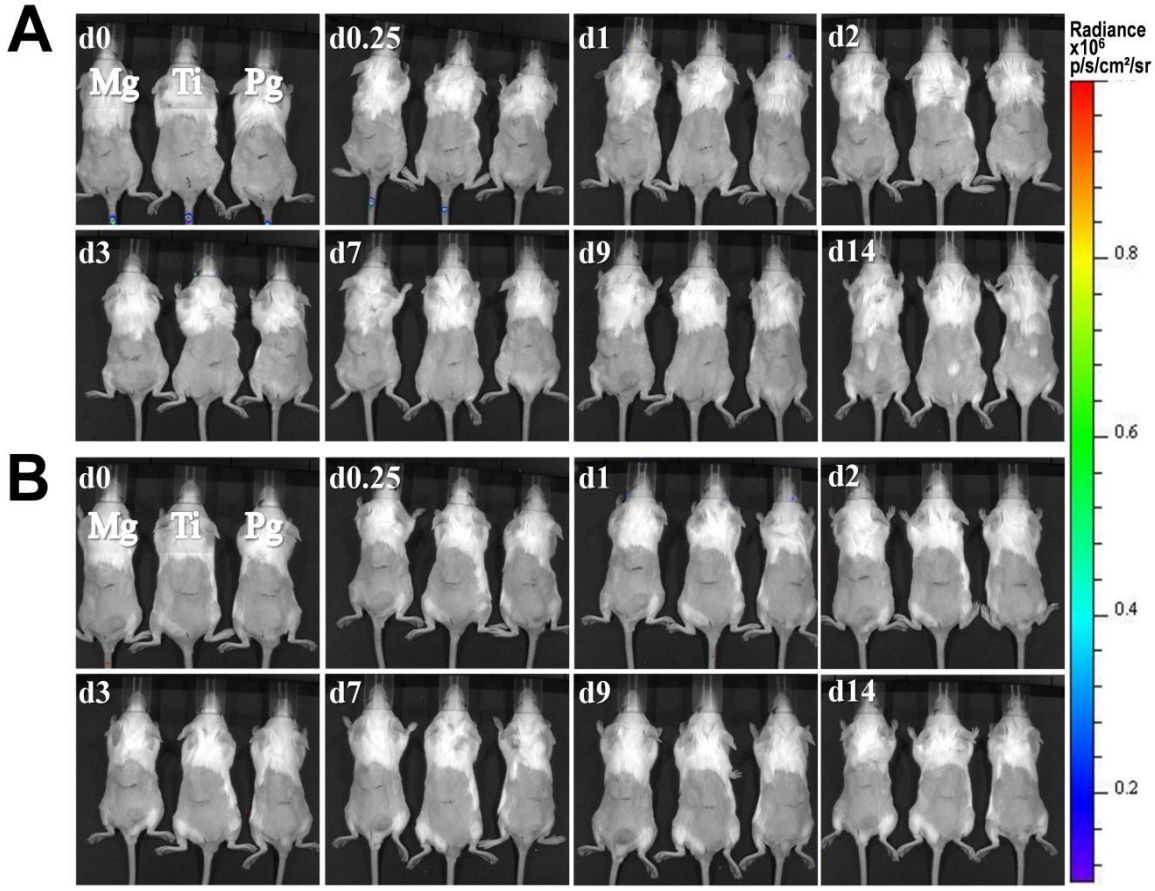

Figure 33: Magnesium implants are not systemically infected. In each mouse implantations were done surgically subcutaneously on the back of mice. Implant materials were as follows: Mg, magnesium; Ti, titanium; Pg, porous glass. 5µl of freshly grown bioluminescent *P. aeruginosa* at OD_{600}=0.1 in LB suspension were injected into the tail vein of each mice either immediately or 24 h after implantation. Bacterial luminescence was measured from mice which were infected immediately after implantation (A) or 24h after implantation (B).

3.4.2 Estimation of *P. aeruginosa* numbers required for infection

To examine the possibility that prolonged infection might be due to high bacterial load present in the initial inoculum, infections were done with smaller bacterial numbers. Different colony forming units of bacteria were injected on the surfaces of magnesium discs implanted subcutaneously in individually mice. Minimum of 100 colony forming units (CFUs) of *P. aeruginosa* were capable to establish an infection on magnesium discs (Figure 34; 74). This experiment proved that magnesium implants were highly susceptible even to low bacterial numbers.

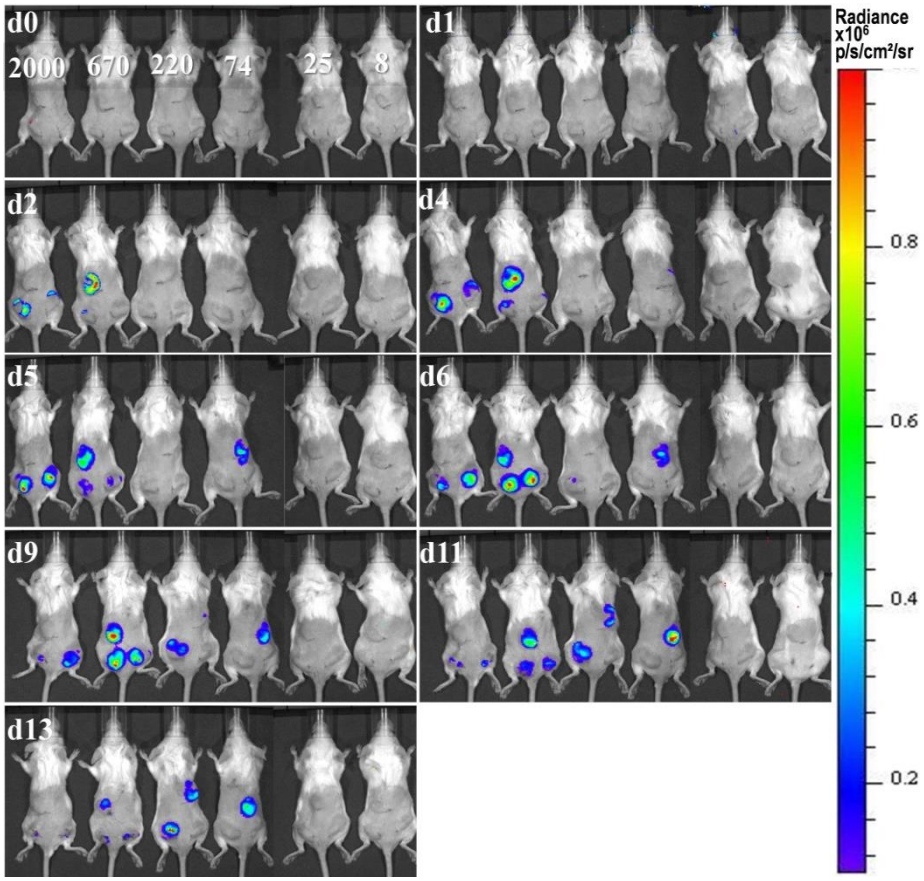

Figure 34: Prolonged infection threshold inocula of *P. aeruginosa.* Magnesium discs were surgically implanted in mice and then 10 µl of indicated in d0 bacterial CFUs were injected locally on magnesium implants into individual mice. Bacterial luminescence was detected at indicated time points from all infected animals.

3.4.3 Characterization of persistent bacterial infections

3.4.3.1 P. aeruginosa exhibit strong antibiotic resistance

To determine if bacteria were surviving on magnesium for extended time period by establishing biofilm a detailed characterization was performed. It is known that bacteria exhibit strong antibiotic resistance within biofilm matrix. Initially to see if bacteria are sensitive to antibiotic, *P. aeruginosa* were subcutaneously injected locally in the tissue of mice and then these mice were treated with intravenous injection of either antibiotics or PBS as control. Bacteria disappeared from the mice which were treated with antibiotic as compared to PBS treated 4h after administration (Figure 35; CFX). However at later time

points, bacterial luminosity decreased from the control mice because of the immune cells invasion at the site of infection. It confirmed that *P. aeruginosa* injected in the absence of implants were sensitive to antibiotic. To see the sensitivity of bacteria in the presence of implants, magnesium discs were implanted in mice. Immediately after implantation, *P. aeruginosa* were injected on the surface of subcutaneously implanted magnesium discs. Intravenous antibiotic administration in these mice was started at variable times after infection as indicated (Figure 36). Despite antibiotic administration, bacterial luminosity remained higher on magnesium implants comparable to PBS treated mice (Figure 36). Antibiotic administration started at early or late post-infection had no influence on bacteria. This indicated that bacteria adopt resistance against systemic antibiotic treatments if they are present on magnesium implants. For verification, mice were implanted with magnesium implants and then immediately after implantation, different numbers of *P. aeruginosa* were injected locally in individual mice. These mice were then intravenously treated with different concentrations of antibiotics daily for two weeks. PBS treated mice served as control. Groups of mice infected with varying inoculums of *P. aeruginosa* on magnesium implants showed a strong resistance against high concentrations of antibiotics (Figure 37 and 38).

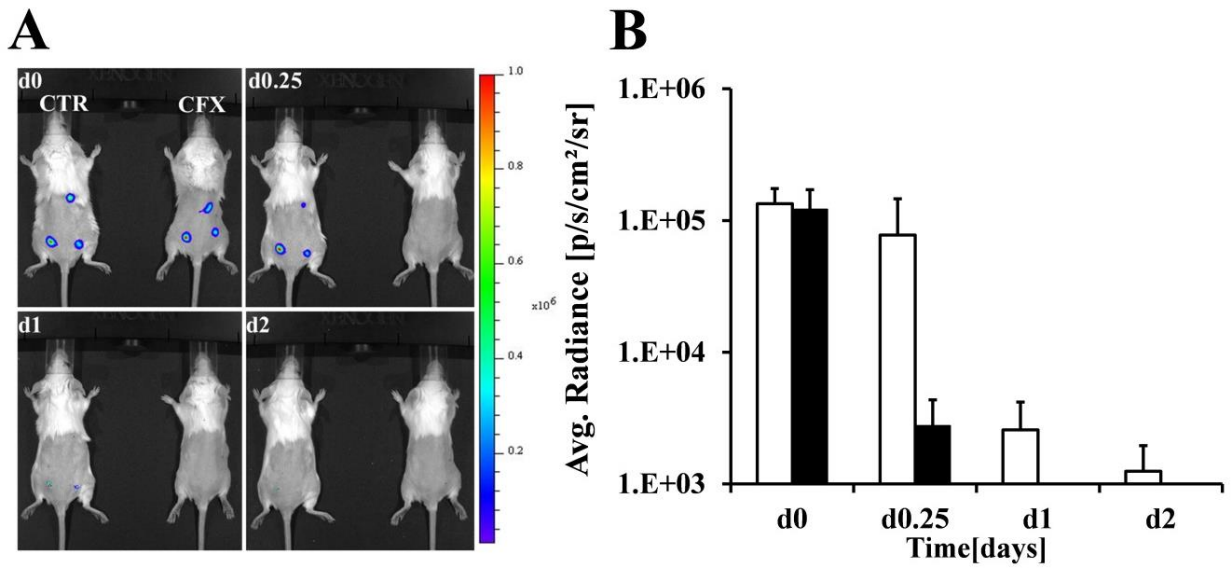

Figure 35: *P. aeruginosa* are susceptible to antibiotics in the absence of magnesium. 5 µl luminescent *P. aeruginosa* cultures were with an OD_{600} of 0.1 were injected subcutaneously without any implantation in mice. 100 µl ciprofloxacin 2 mg/ml was injected into tail vein of mouse (CFX) and PBS (CTR) in other. Bacterial luminosity was measured at indicated time points shortly after infection and subsequent antibiotic

administration (A). Average radiance (B) associated with ciprofloxacin treated mice (black bars) and control mice (white bars).

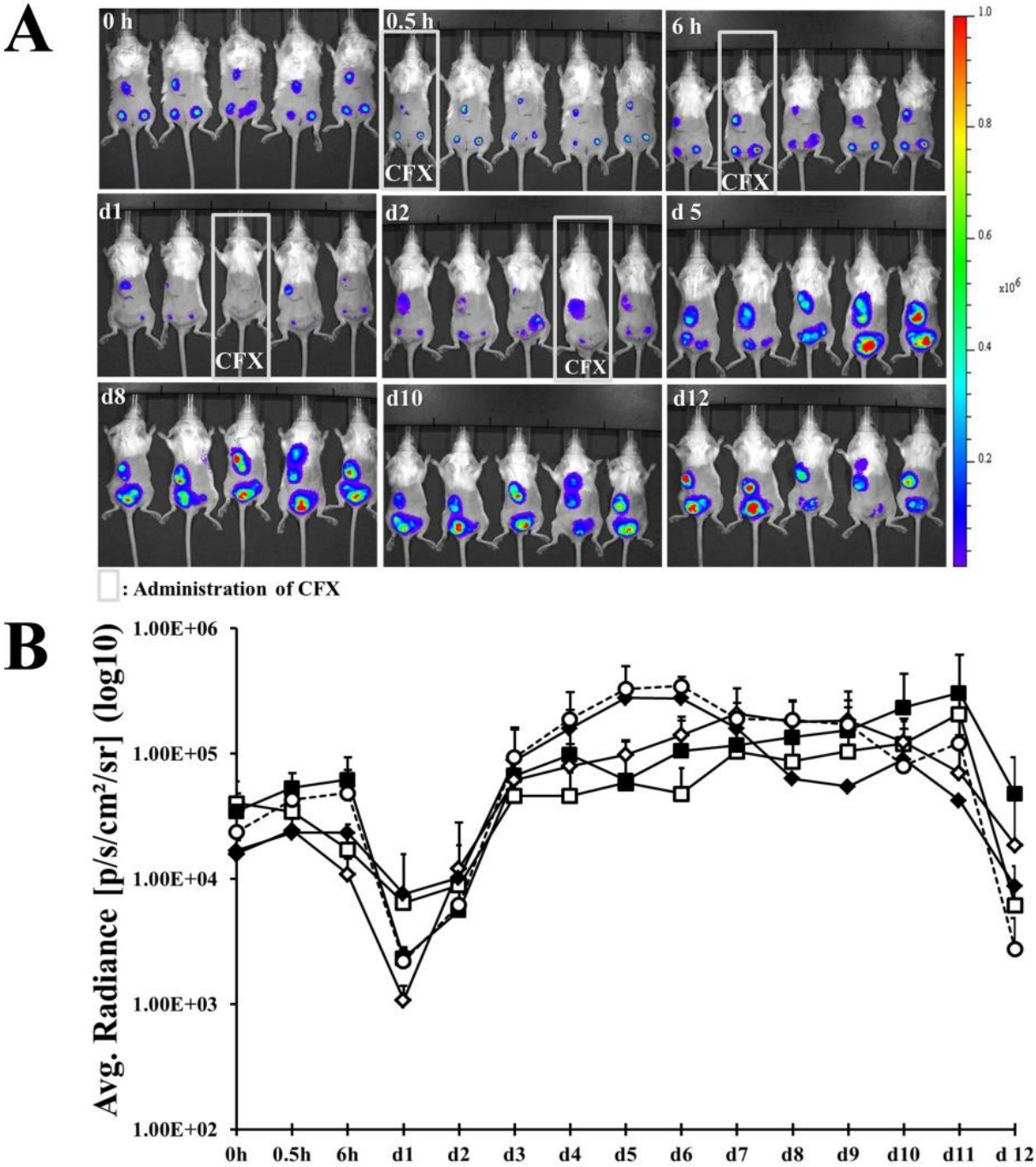

Figure 36: ***P. aeruginosa*** **grown on implant surfaces are antibiotic resistant.** 3 magnesium discs were implanted subcutaneously in each mouse and then 5 µl luminescent *P. aeruginosa* cultures with an OD_{600} of 0.1 were injected on the surface of implants. After infection, systemic administration of 100 µl ciprofloxacin 2 mg/ml was started in each of the framed mouse which was then continued on daily basis at later time points (from left to right). One mouse served as control and received intravenous injection of PBS on daily basis. Bacterial luminescence measured from each animal at indicated time points (A). Average radiance calculated from the mice where systemic ciprofloxacin administration started at 0.5h (empty squares), 6h (filled

squares), day 1 (empty rhombi) and day 2 (filled rhombi) post infection. In control mice PBS was injected daily (empty circles).

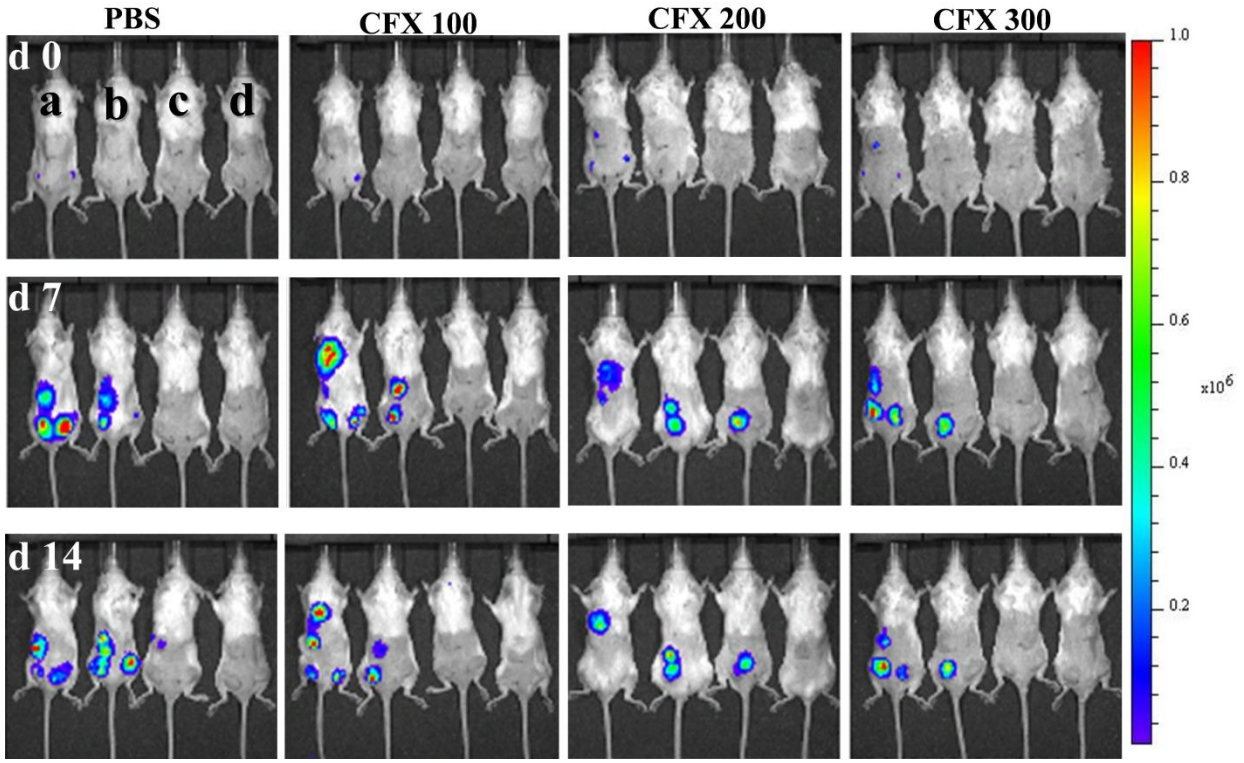

Figure 37: *P. aeruginosa* on magnesium implants pose strong resistance against high systemic doses of ciprofloxacin. 3 magnesium discs were implanted in each animal. Immediately after implantation, $1x10^6$ colony forming units of luminescent *P. aeruginosa* cultures were injected on magnesium implants (a), $1x10^4$ colony forming units were injected on implants (b), $1x10^2$ colony forming units were injected on magnesium (c) while, implants in one animal (d) were kept un-infected. In first group (PBS) of animals 100 µl PBS was injected intravenously in each mouse daily. In second group (CFX 100), immediately after infection, 100µl of 2mg/ml ciprofloxacin was injected daily. In third group (CFX 200), 200µl of 2mg/ml ciprofloxacin was injected daily. In the last group (CFX 300), 300µl of 2mg/ml ciprofloxacin was injected daily. After infection and antibiotic administration, bacterial luminescence was measured daily.

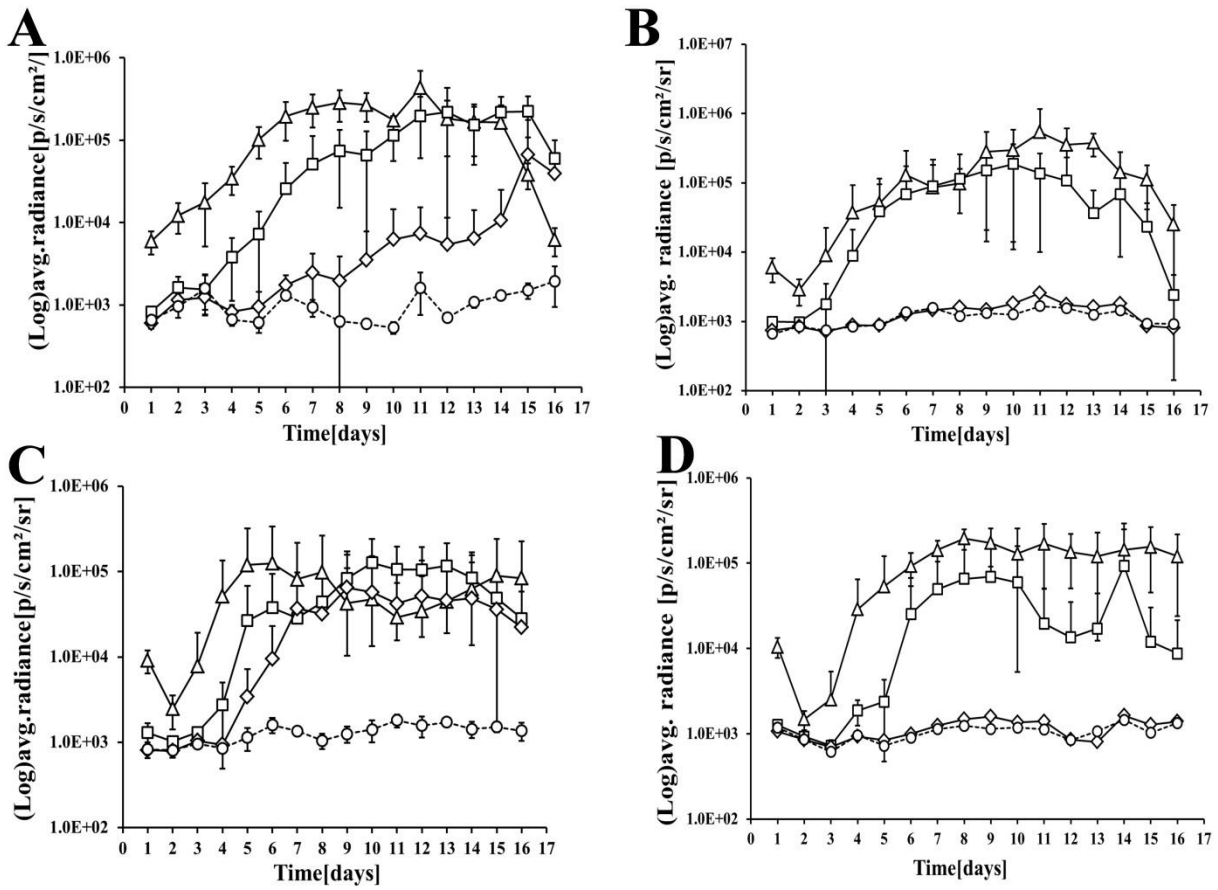

Figure 38: Antibiotic resistance of *P. aeruginosa* against systemic ciprofloxacin. 3 magnesium discs were implanted in each animal and then immediately after implantation infections were done with luminescent *P. aeruginosa*. Bacterial luminescence from each of the infected mice was captured at indicated time points using *in vivo* imaging system. Data was anylzed using a live imaging software and values correspond to the average radiance emitted from bacteria. Average radiance calculated from magnesium implants infected with $1x10^6$ colony forming units of luminescent *P. aeruginosa* cultures (triangles), $1x10^4$ colony forming units (squares), $1x10^2$ colony forming (rhombi) or without infection (circles). Animals receiving intravenous injections of PBS (A), 100 µl of 2mg/ml ciprofloxacin (B), 200 µl of 2mg/ml ciprofloxacin (C) and 300 µl of 2mg/ml ciprofloxacin injections (D).

3.4.3.2 Effect of system antibiotics on established *P. aeruginosa* biofilms

To investigate antibiotic sensitivity of bacteria growing on magnesium implants, an alternative method such as determination of viable bacteria as colony forming units was used after the removal of implants. Magnesium discs were implanted in mice and then immediately after implantation infections were done with luminescent *P. aeruginosa* in each animal. After infection, intravenous injections of high doses of ciprofloxacin were administered in each animal daily for two weeks. One mouse was treated with PBS and

served as control. Bacterial luminescence and weight of mice were measured daily. After two weeks, mice were euthanized and implants were removed. Colony forming units per disc from each of the infected implant were then counted (Figure 39A-C). Ciprofloxacin treatment at high concentrations in mice containing magnesium inoculated with *P. aeruginosa* had no effect on bacterial luminosity which remained same as mice without antibiotic treatment (Figure 39A; b,c,d compare with a). High number of colony forming unit of bacteria were counted from infected implants isolated from mice even after high ciprofloxacin administration comparable to PBS treated (Figure 39B). Mice bearing infected implants showed initial decreases in weight similar to un-infected mice which seemed due to implantation stress (Figure 39C). Over all, these results support that bacteria show a strong resistance to high doses of antibiotics a feature which is typical for bacteria within biofilms.

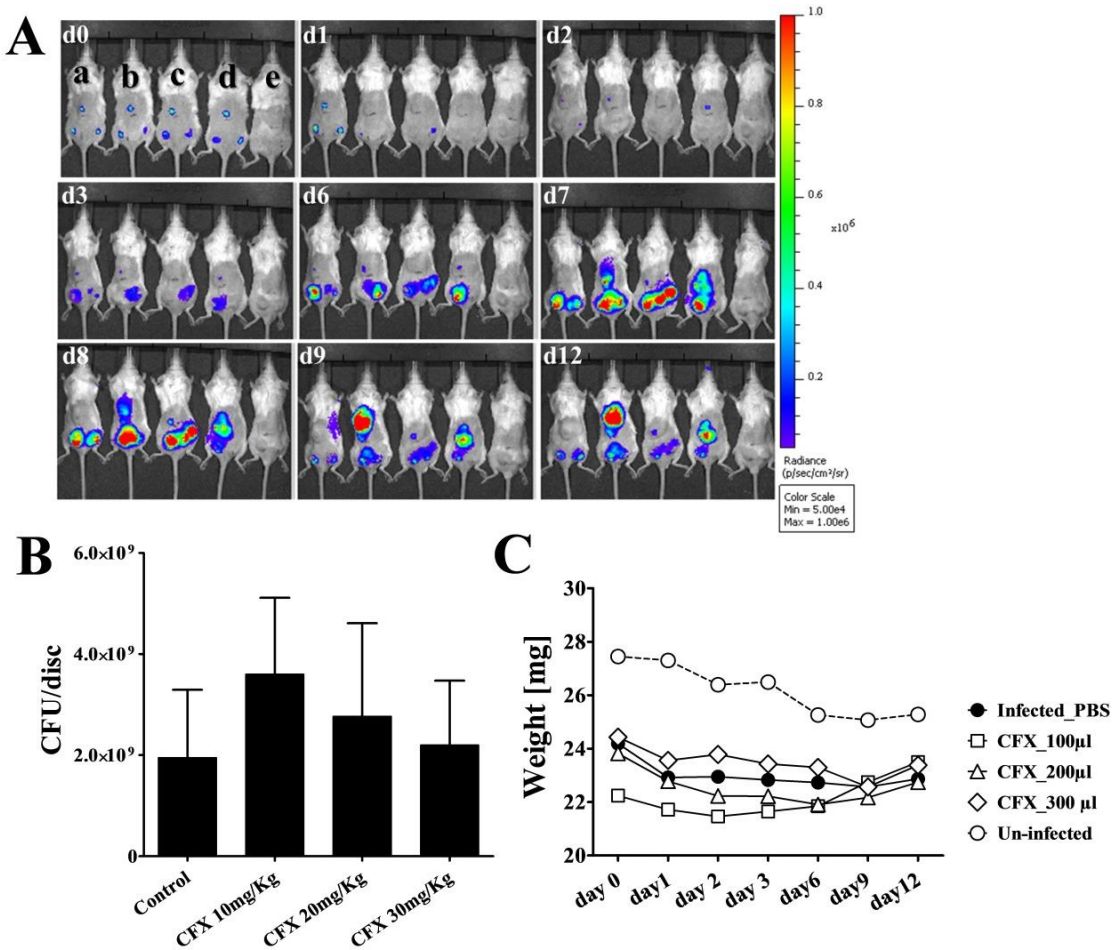

Figure 39: High bacterial numbers on implants after antibiotic treatment. 3 magnesium discs were subcutaneously implanted in each mouse and then these animals were infected with 5µl of approximately

$1x10^6$ CFUs luminescent *P. aeruginosa*. One animal was kept un-infected. After infection, antibiotic or PBS administration was done intravenously as follows: PBS was injected daily in mouse (a), 100µl of 2mg/ml ciprofloxacin in mouse (b), 200µl of 2mg/ml ciprofloxacin in mouse (c), 300µl of 2mg/ml ciprofloxacin in mouse (d), only implantation without infection and treatment (e). After two weeks, mice were euthanized by CO_2 and infected or un-infected implants form each animal were removed and shifted to PBS. Followed by vigorous vortex, tenfold serial dilution in PBS was done individually for each implant and then 10 µl from each dilution were streaked on LB agar plates and overnight incubated at 37°C. Colonies forming units per each implant (CFU/disc) were calculated by the number of colonies counted form overnight incubated LB agar plates. Bacterial luminescence measured at indicated time points (A). Colony forming units counted from implants (B). Changes in weight of mice as indicated (C).

3.4.3.3 Biofilm-like morphology of P. aeruginosa on implants

To reveal morphology of bacterial overgrown magnesium implants and adjacent tissue, electron microscopy was used. Magnesium implants after two weeks of infection were removed from mice and observed under microscope. Scanning electron microscopy (SEM) of tissue adjacent to infected magnesium was densely filled with large populations of *P. aeruginosa* (Figure 40A-L). Bacteria were also embedded in matrix like structures resembling closely to biofilms (Figure 40E,F). Similarly, bacteria were also seen adhering on magnesium discs (Figure 40G-L). Formation of slimy matrix around bacteria was clearly visible (Figure 40L). To reveal in depth biofilm structures, transmission electron microscopy (TEM) was used. TEM of tissue neighboring infected magnesium showed matrix encased *P. aeruginosa* which is typical for biofilm formation (Figure 41A-F). Despite immune cell accumulation the bacterial biofilm remained intact (Figure 41A). This shows biofilm provide a sheath to bacteria against host defense mechanism. In the surrounding *P. aeruginosa* biofilm, many polymorphonuclear leukocytes (PMNs) were seen engulfing single bacteria (Figure 41G-I). Interestingly, white extracellular matrix was only present around cluster of bacteria (J). However, single cells were completely lacking such structures (Figure 41K, L). These analyses proved that prolonged *P. aeruginosa* infection around magnesium implants was due to biofilm formation. In conclusion, electron microscopy analyses clearly revealed that *P. aeruginosa* forming biofilms directly on magnesium as well as in the adjacent tissue.

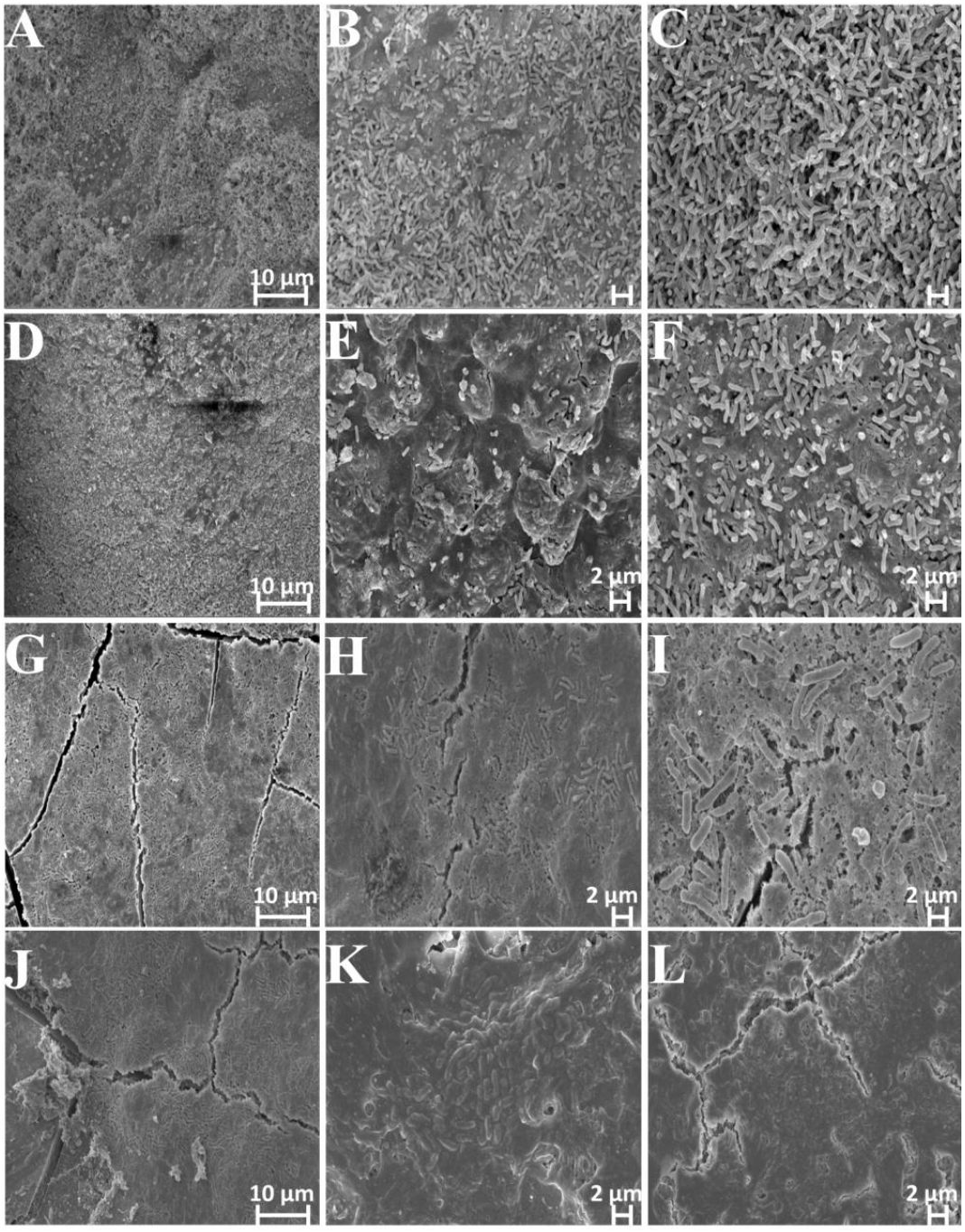

Figure 40: *P. aeruginosa* establish biofilms in peri-implant tissue. Magnesium discs were implanted subcutaneously in mice and then infected with 5µl of suspension with $1x10^6$ CFUs luminescent *P. aeruginosa*. After two weeks, mice were sacrificed and tissue with implants was removed. The samples were fixed with 5% formaldehyde and 2% glutaraldehyde in HEPES buffer followed by washing in TE buffer and then dehydrated with acetone at room temperature. After critical-point drying with CO_2 samples were sputter coated with palladium-gold and imaged in a field emission scanning electron microscope. *P. aeruginosa* infected implant surfaces (A-L). *P. aeruginosa* embedded within peri-implant tissue (K and F). (SEM images courtesy by Manfred Rohde, HZI)

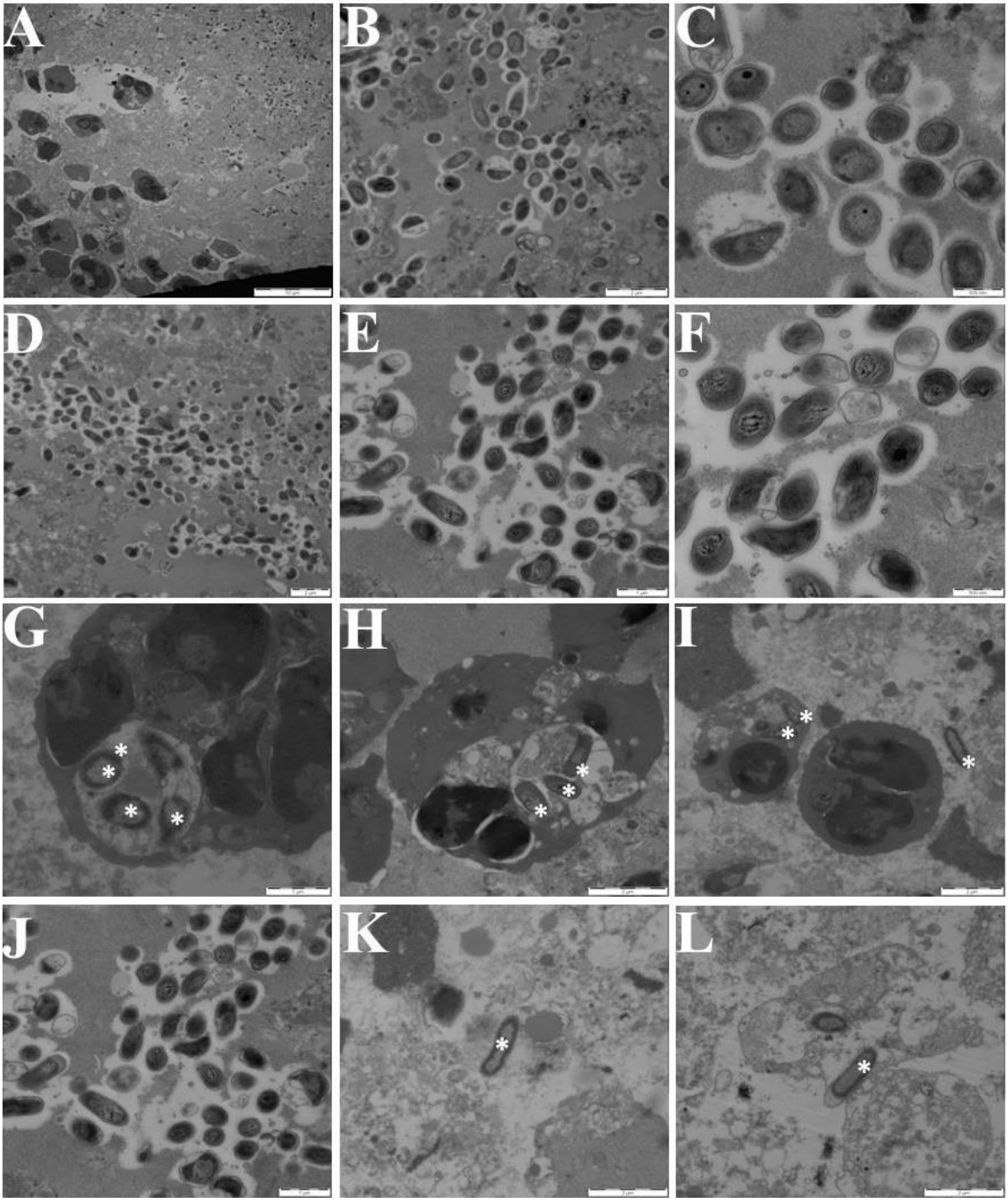

Figure 41: *P. aeruginosa* resistance against host immune cells indicative of biofilm formation. Followed by two weeks of infection with 5µl of 1x10^6 CFUs luminescent *P. aeruginosa* on magnesium, peri-implant tissues were removed, fixed, embedded, cut into sections and then examined under transmission electron microscope. TEM of tissue near *P. aeruginosa* infected magnesium (A-L). Polymorphonuclear leukocytes with *P. aeruginosa* (*)(G-I). (SEM images courtesy by Manfred Rohde, HZI)

3.4.3.4 P. aeruginosa biofilms show strong inflammatory reaction

To determine the host inflammatory response against *P. aeruginosa* histological evaluations were performed (Figure 42A-F). Magnesium implants were infected with *P. aeruginosa* immediately after implantation in mice. Magnesium implants without infection and infection in sham surgical pouches served as control. After a week, histology of tissues surrounding infected magnesium implants showed a severe neutrophilic inflammatory infiltrates surrounding the implant (Figure 42A, B; white arrow). In comparison, there was a mild inflammatory response at the site where infection was done with *P. aeruginosa* alone (Figure 42E, F). There was no increased inflammatory response against un-infected magnesium implants (Figure 42C, D). Hence, Persistent *P. aeruginosa* infections on magnesium lead to strong inflammatory reactions which can be clearly identified by high population of granulocytes.

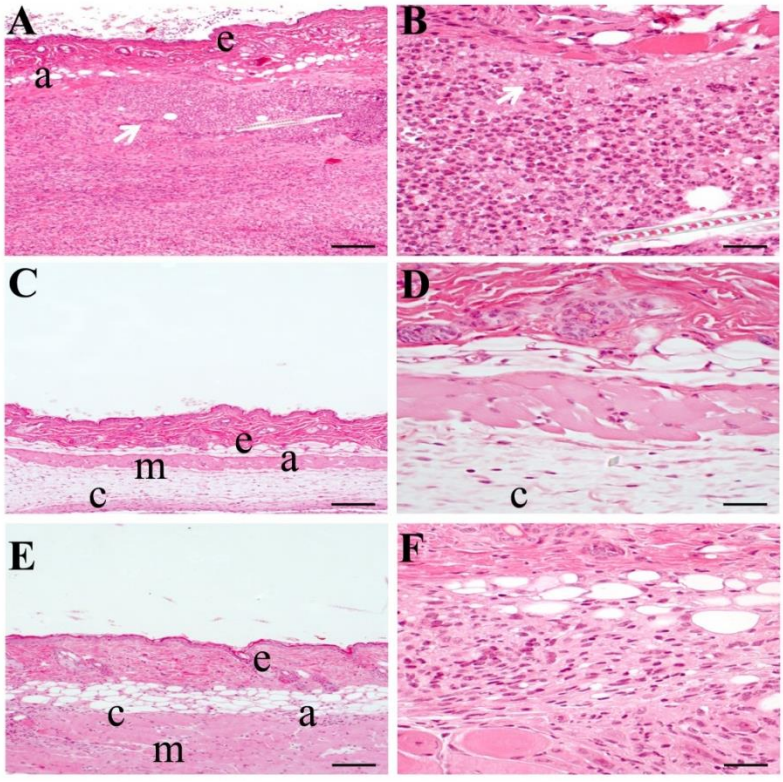

Figure 42: *P. aeruginosa* biofilms induce strong inflammatory reactions. 5µl of 1x10^6 CFUs luminescent *P. aeruginosa* were injected on subcutaneously implanted magnesium discs immediately after implantation (A,B) and in sham surgical pouches (E,F). Magnesium discs implanted and left un-infected served as control (C,D). After 7 days, infected and un-infected magnesium implants along with infected tissues were removed, fixed, paraffin embedded and hematoxylin and eosin (H&E) stained. Peri-implant tissue near *P. aeruginosa* infected magnesium implants (A, B). Peri-implant tissue from un-infected magnesium implants (C, D) and

tissue without implant but infected with *P. aeruginosa* (E, F). The labelled structures are as follows: e (epidermis), a (adipose tissue), m (skeletal muscle) and c (connective tissue). Scale bar corresponds to 50µm. (Staining courtesy by mouse pathology, HZI)

3.4.3.5 P. aeruginosa biofilm matrix composed of exoplysacharide and protein

To confirm the biofilm formation, Periodic Acid Schiff (PAS) staining specifically targeting extracellular polymeric matrix was done (Figure 43A-F). Implants with some surrounding tissue were removed after one week post-infection. Biofilm staining of tissues at the site of *P. aeruginosa* infection on magnesium implants showed the presence of polysacharides and proteins between immune cells (Figure 43A, B) indicating the presence of biofilm. However, such structures were not present in the tissue near un-infected magnesium implants (Figure 43C, D) or in tissues which were infected with *P. aeruginosa* in the absence of implants (Figure 43E, F). These results show that *P. aeruginosa* develop prolonged infections due to biofilm formation.

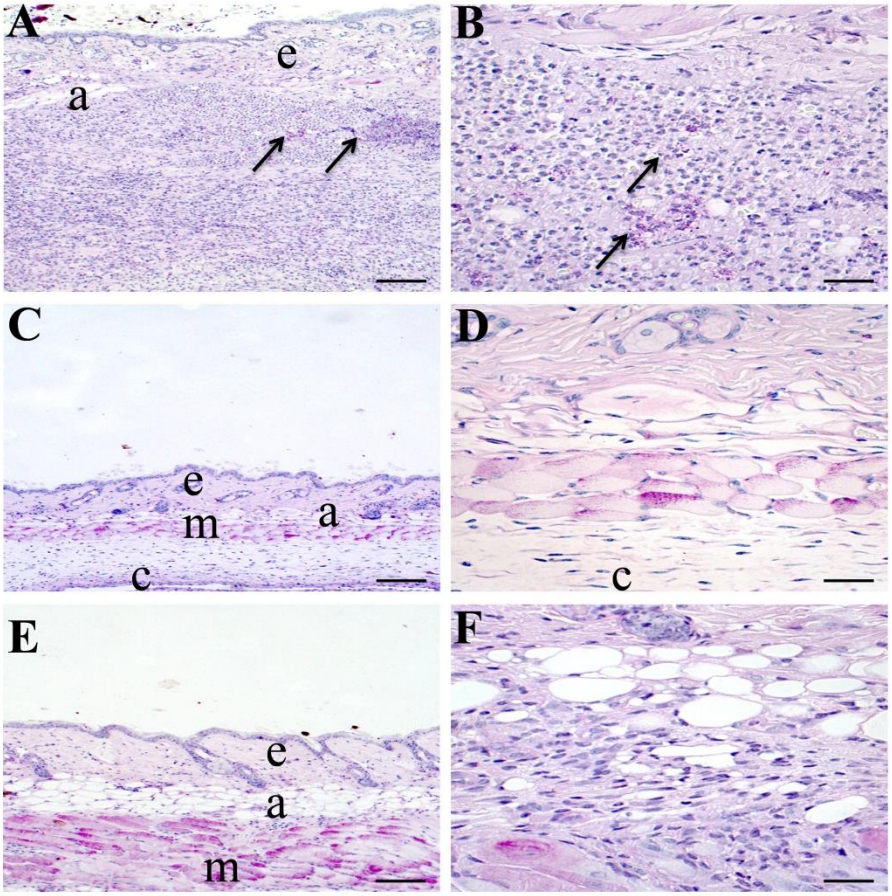

Figure 43: PAS positive biofilm matrix material is detected at the site of infected magnesium implants. As mentioned in Figure 42, tissue near magnesium implants infected with *P. aeruginosa* and stained with

Periodic Acid Schiff (PAS). Photographs of infected peri-implant tissue after implant removal (A, B) positive for polysacharides and proteins (black arrows), un-infected tissue after implant removal (C, D) and infected tissues which were kept un-implanted (E, F). The labelled structures scale bars are same as mentioned in figure 42. (Staining courtesy by mouse pathology, HZI)

3.4.3.6 Immunohistology of P. aeruginosa biofilms

To detect the distribution of *P. aeruginosa* from infected tissues immunohistology of tissue sections specifically targeting *Pseudomonas* was done (Figure 44A-F). Immunohistology of tissues surrounding magnesium implants infected with *P. aeruginosa* clearly revealed a distinct biofilm enriched with *P. aeruginosa* surrounded by high numbers of granulocytes (Figure 44A,B; black arrow). In the absence of infection tissues near magnesium or *P. aeruginosa* infected tissues without implants; bacteria were not present after 1 week (Figure 44C-F). *P. aeruginosa* in the infected tissues after one week indicates that these bacteria can establish persistent biofilms.

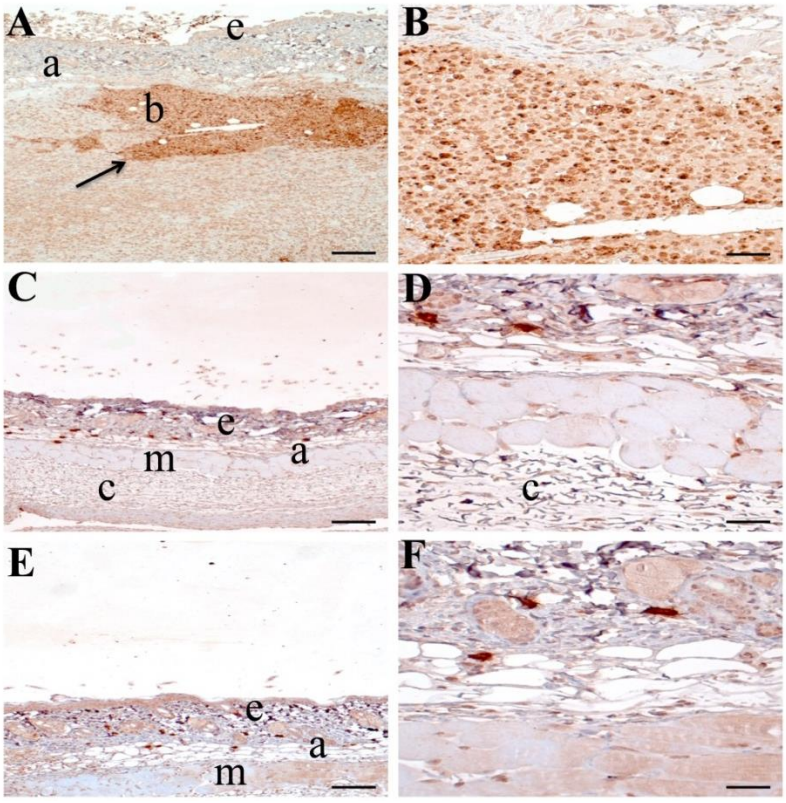

Figure 44: High density *P. aeruginosa* colonization in the tissues near infected magnesium implants. Histology was performed as described in Figure 42, samples were removed and Anti-*Pseudomonas* antibody (1:400) staining was performed after heat-mediated-antigen retrieval of the samples. Light-microscopy images of immunostained tissue sections near *P. aeruginosa* infected magnesium implants (A,B) a distinct region infiltrated with *P. aeruginosa* (A; black arrow). Tissue sections containing un-infected magnesium

implants (C, D) and tissue sections infected with *P. aeruginosa* without implantation (E,F). Magnification, description of labelled structures and scale bars are as explained in Figure 42. (Staining courtesy by mouse pathology, HZI)

3.4.3.7 P. aeruginosa infections induce prolonged interferon production

Type I interferon induction is triggered in response to viral and non- viral infections [162]. Therefore, the induction of Type I interferon in response to biofilm was also tested using β interferon luciferase reporter mice (IFN-$\beta^{+/\Delta\beta\text{-luc}}$) [155]. Wild- type non-luminescent *Pseudomonas aeruginosa* (PAO1) were injected on subcutaneous magnesium implants immediately after implantation. As a control, infection was done at a surgical pouch without implant to differentiate the interferon production in response to bacteria alone. A localized type I interferon production at the site of magnesium infected with *P. aeruginosa* started within a day post-infection (Figure 45A; a). Later, this localized IFN production around infected magnesium became maximum after 1 week of infection and persisted for two weeks. In control where bacteria were injected alone interferon was also detected for three days (Figure 45A; b). No interferon response could be detected around un-infected magnesium implants (Figure 45A; c).

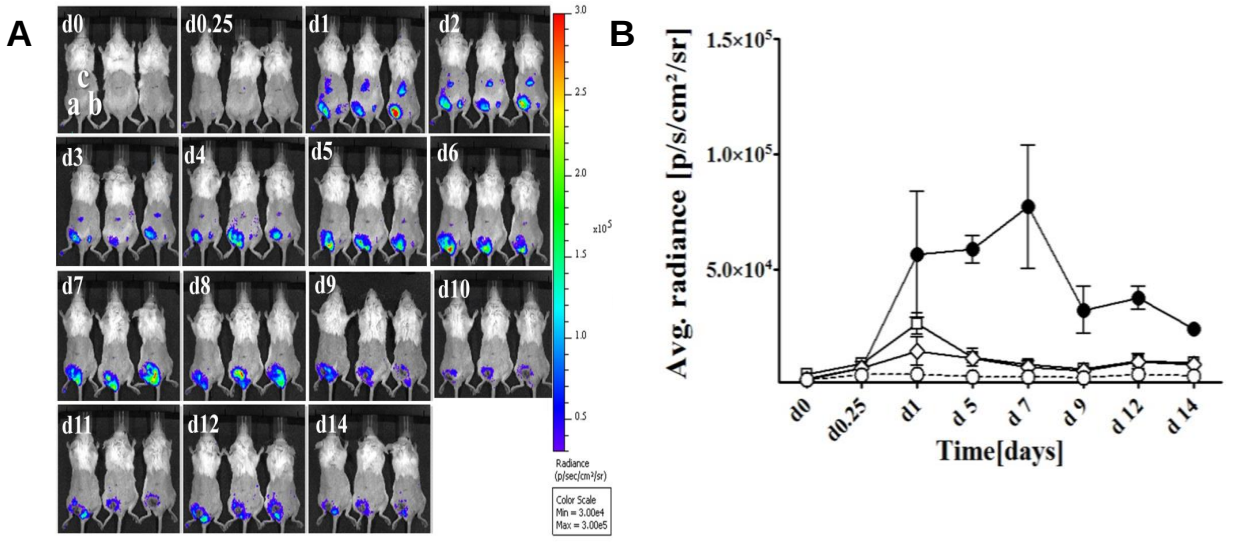

Figure 45: Biofilm formation triggers persistent type I interferon production for over two weeks. β interferon luciferase reporter (IFN-$\beta^{+/\Delta\beta\text{-luc}}$) mice were implanted with magnesium and then immediately after implantation, 5µl ($1x10^3$ CFUs) of wild type *P. aeruginosa* (PAO1) were injected locally on magnesium and in subcutaneous tissues having surgical pouches without implant. Subcutaneously implanted magnesium discs without infection were kept as control. Immediately after infection, luciferin (30 mg/ml) was injected intraperitonealy (i.p.) and after 15 minutes of injection mice were observed under IVIS. Luminescence in

response to localized type I interferon (A) at site of magnesium infected with bacteria (a), infected sham surgical pouch(c), un-infected magnesium (b). Average radiance (B) calculated from infected magnesium (filled circles), infected sham surgical pouch (empty squares), from un-infected magnesium (rhombi) or from the skin as background (empty circles).

3.4.3.8 Bacterial RNA isolation from in vivo grown biofilms

To investigate if intact *P. aeruginosa* RNA can be isolated from infected tissue for RNA sequencing, RNA extraction process was also done. RNA isolated was indeed belonging to prokaryotes and found in good shape and integrity (Figure 46). Further, only a small amount of the isolated RNA was sequenced to evaluate the libraries. Depending upon samples 23 to 53 % of the sequence mapped to *Pseudomonas aeruginosa* (PAO1) (Table 15). In summary, the RNA quality is sufficient for whole genomic gene expression analysis. The major shortcoming in this approach is the lack of a good control culture.

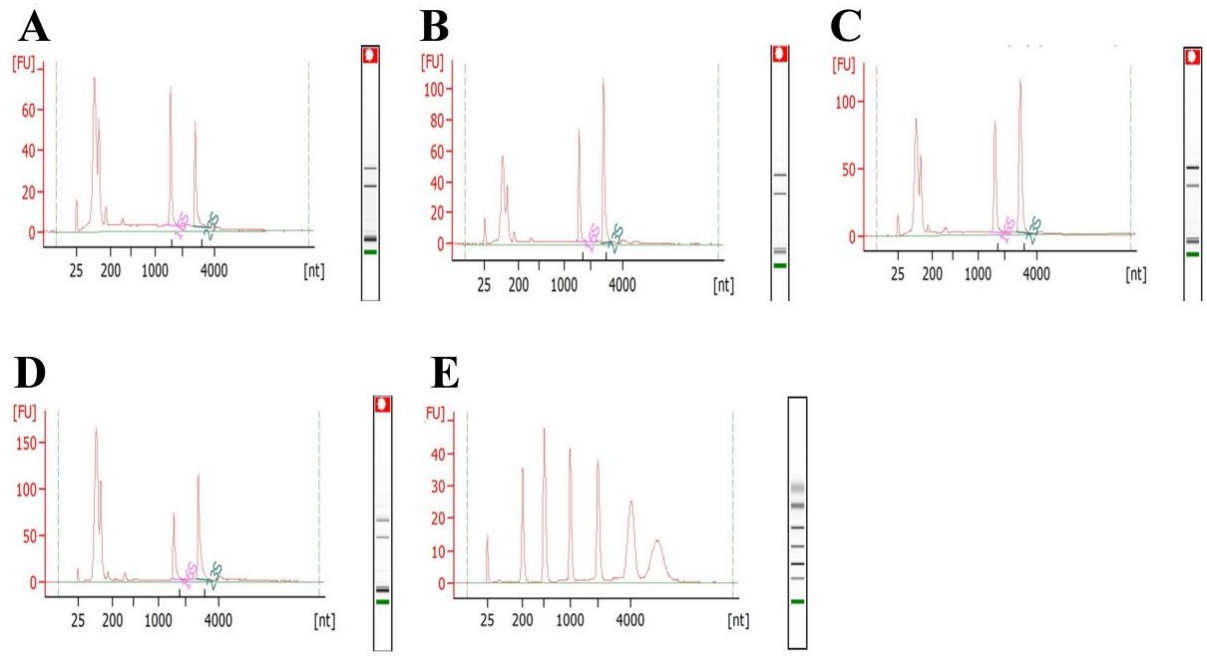

Figure 46: Intact bacterial RNA can be isolated from bacterial biofilms in tissues. Mice bearing magnesium infected with bioluminescent *P. aeruginosa* were euthanized after two weeks and infected tissues were removed and shifted in trizole reagent. RNA was isolated by trizole reagent and stored in RNase free water. This RNA was then subjected to agilent analaysis. Prokaryotic RNA peaks from four independent samples (A-D). RNA Ladder (E). (Agilent analysis in Genome Analytics, HZI)

Table 15: Whole genomic indicates bacterial RNA quality form biofilms suitable for gene expression analysis.

No.	Total reads	Mapped to *Psuedomonas*	% mapped to *Psuedomonas*	mapped to mouse	% mapped to mouse	% rRNA	% Bacterial rRNA	% Euk. rRNA
1	2,130,866	1,142,265	53.6	871,249	40.9	82.60%	53.08	29.33
2	1,669,694	800,130	47.9	754,170	45.2	79.70%	47.48	32.1
3	2,397,579	621,835	25.9	1,578,927	65.9	74.42%	25.84	48.34
4	2,320,781	543,333	23.4	1,561,115	67.3	67.31%	23.18	44.02

3.4.3.9 P. aeruginosa biofilms induce splenomegaly in mice

It is assumed that systemic bacterial infections lead to increase in splenic cellularity due to recruitment and expansion of leukocytes, this results in splenomegaly in the infected host [163]. To see if persistent localized biofilm had any effect on spleen size or on other organs, mice bearing infected magnesium implants treated with or without systemic ciprofloxacin were sacrificed and their organs were examined. Increases in weight and length of spleens from mice bearing magnesium implants with *P. aeruginosa* biofilms was observed (Figure 47A-C). Mice treated systemically with ciprofloxacin had comparatively less increase in weight and length of spleen as compared to PBS treated (Figure 47B and C). However, no gross changes in the shape of other organs could be found. Overall, it indicates that *P. aeruginosa* biofilm leads to the systemic activation of splenic immune cells which cannot eliminate biofilm near magnesium implants.

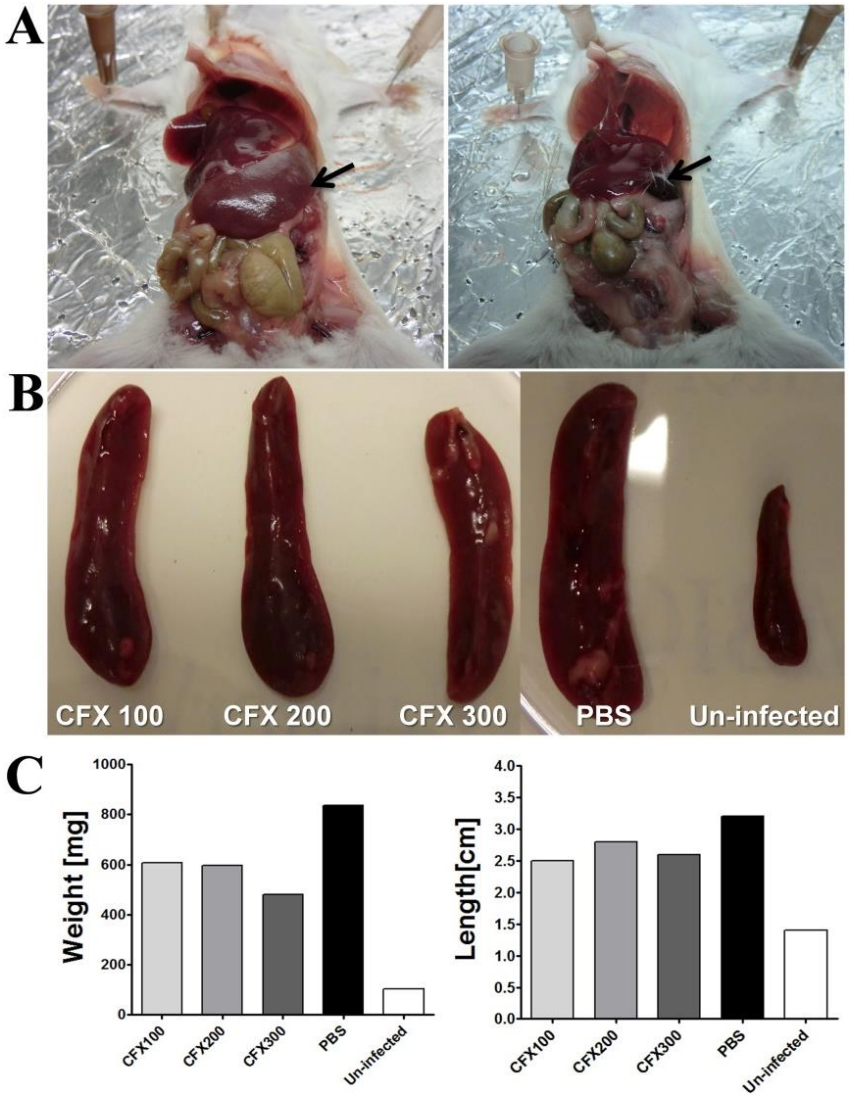

Figure 47: *P. aeruginosa* biofilm infections of implants result in splenomegaly. Mice bearing two weeks old biofilms on magnesium which were treated daily with or without systemic ciprofloxacin (2mg/ml). After two weeks of infection, mice were sacrificed to observe morphology of organs. Spleen (black arrow) of a mouse bearing infected magnesium implant (A; left) and un-infected mouse (A; right). (B) Spleen sizes of infected mice treated daily with intravenous injections of 100 µl of ciprofloxacin (left to right), 200 µl of ciprofloxacin, 300 µl of ciprofloxacin and PBS. Spleen of mice bearing magnesium implants but un-infected (right). (C) Weight of spleen from the mice as indicated (left) and length of spleen (right).

3.4.4 *P. aeruginosa* remain mainly localized within the biofilm

Bacteria are known to migrate from existing biofilm to new surfaces to establish fresh biofilms [164]. To investigate this, magnesium implants were infected with bioluminescent *P. aeruginosa* and in parallel left un-infected with in same mouse. Infection was done immediately or 24h after implantation. *P. aeruginosa* established prolonged infections on

those magnesium which were inoculated immediately or 24h after implantation (Figure 48A,B). Bacteria did not migrate to the neighboring un-infected magnesium implanted in the same mouse as no luminescence could be seen on these implants (Figure 48A,B;Mg1-4). *P. aeruginosa* did not establish infections on any of the titanium implants (Figure 48A,B;Ti). This indicated that *P. aeruginosa* establish localized infections and they do not move in bulk into neighboring tissue.

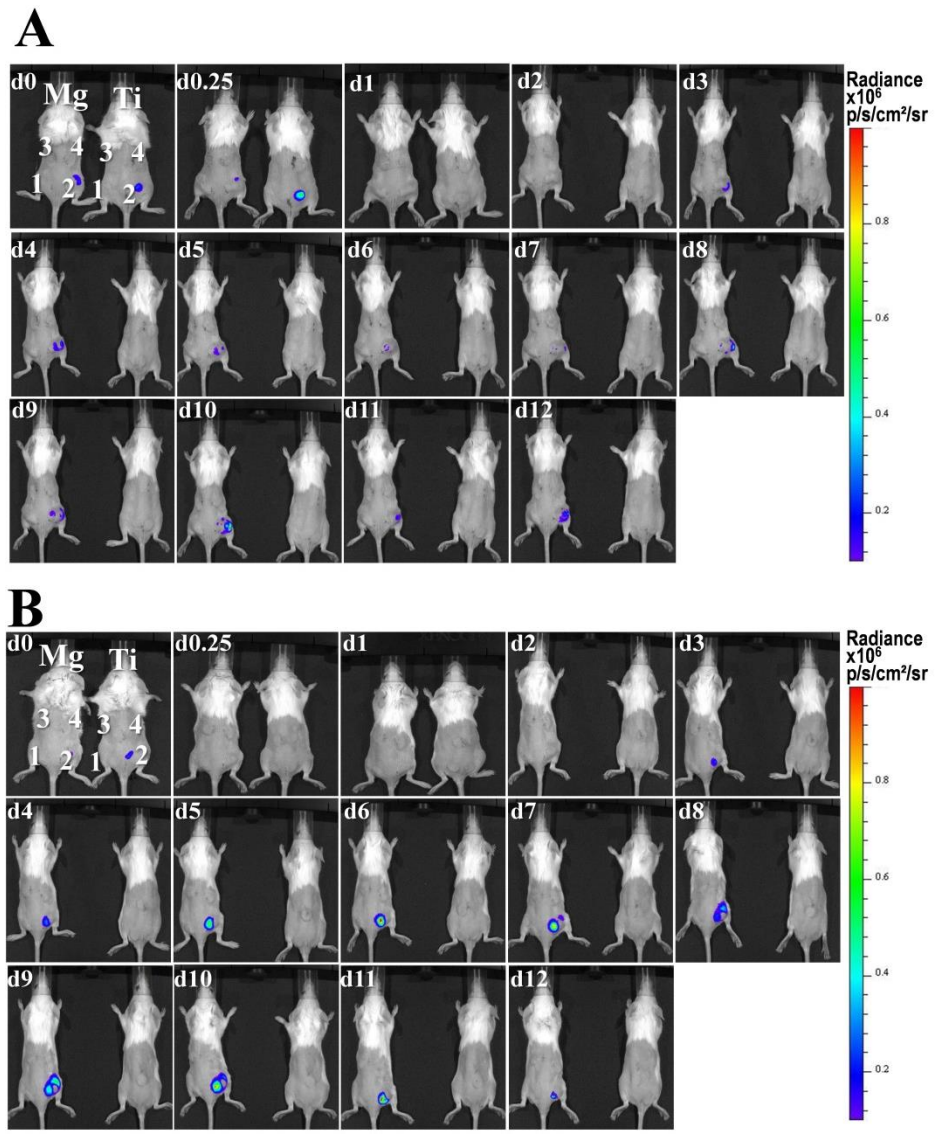

Figure 48: *P. aeruginosa* establish localized infection on magnesium implants. Four magnesium or four titanium discs were implanted subcutaneously in mice. In each mouse, 5µl of approximately $1x10^6$ CFUs luminescent *P. aeruginosa* were injected locally either soon or 24h after implantation on single disc (2) while three discs (1, 3 and 4) were left un-infected. Course of infection was observed using *in vivo* imaging system (IVIS). *P. aeruginosa* luminosity inoculated immediately (A) or 24h after implantation (B) on single implant (2) out of subcutaneously implanted four magnesium (Mg) or titanium discs (Ti).

3.4.5 Contribution of magnesium corrosion products to prolonged infections

Magnesium hydroxide and hydrogen gas are major degradation products of magnesium corrosion. To assess the contribution of these products in prolonged bacterial infection, porous titanium implants were coated with $Mg(OH)_2$ and then implanted into mice. To evaluate role of hydrogen gas, magnesium implants coated with phosphate which suppress gas formation were used. Magnesium implants were infected with *P. aeruginosa* isolated from two weeks *in vivo* grown biofilm to see if these bacteria show any difference from freshly grown cultures. Freshly grown *P. aeruginosa* could be visualized on all implants soon after their administration on respective implants (Figure 49A, a, c, d and e). *P. aeruginosa* inoculated from existing biofilm were not visible (Figure 49A, b) even though same volume was used. However, this may be due to a reduced metabolic activity or due to other reasons. Fresh *P. aeruginosa* showed increased luminosity and established prolonged infections on magnesium (Figure 49B;a). In comparison, these bacteria had decreased luminosity and did not establish permanent infection on phosphate coated magnesium (Figure 49B, c). Interestingly, fresh bacteria showed high luminescence on $Mg(OH)_2$ coated porous titanium discs as compared to un-coated porous titanium (Figure 49B;compare d with e). *P. aeruginosa* (biofilm derived cultures) established prolonged infections on magnesium (Figure 49A, b). Overall, these results indicate that magnesium corrosion products play an important role in the formation of biofilm on metallic magnesium.

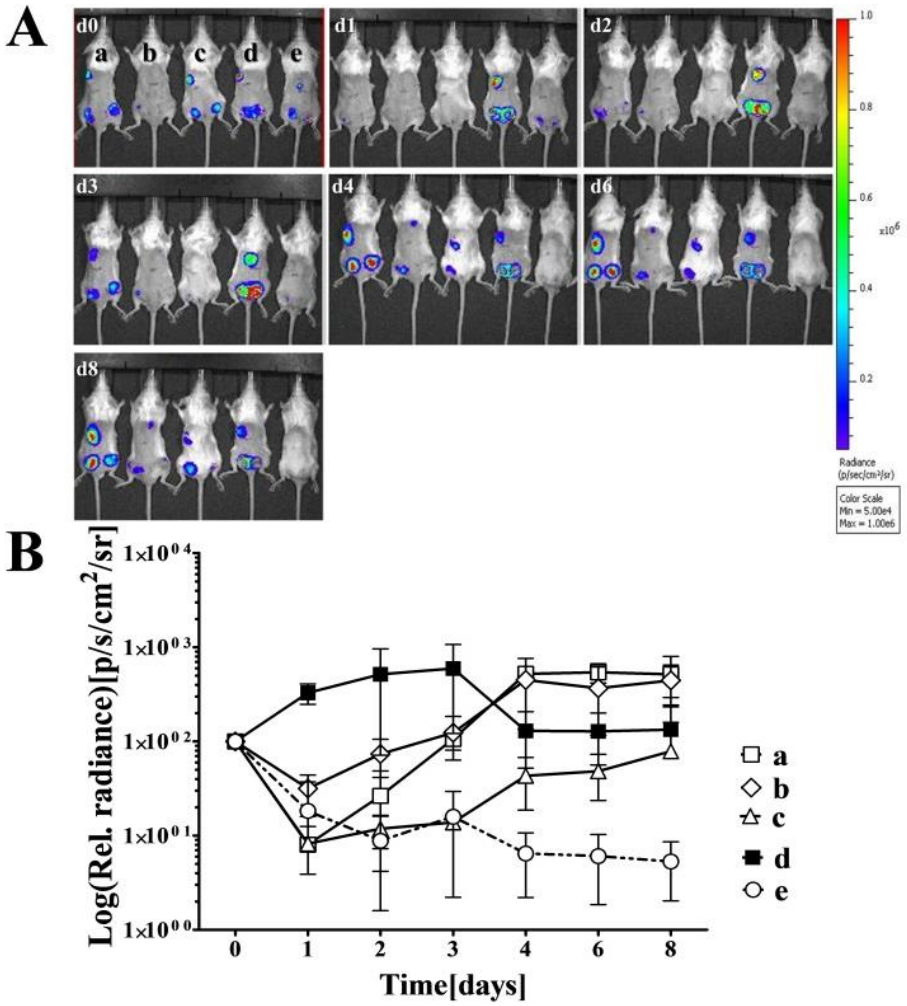

Figure 49: Magnesium corrosion products extend *in vivo* bacterial persistence. Porous titanium discs with 7 mm diameter and 2 mm thickness were filled with $Mg(OH)_2$ and then subcutaneously implanted in mice. Porous titanium implants without coating were implanted as controls. Phosphate coated magnesium discs were also implanted. Immediately after implantation, these discs were infected with 5 µl of $1x10^6$ CFUs freshly grown luminescent *P. aeruginosa.* In parallel, small amount of luminescent *P. aeruginosa* were derived from a two weeks old biofilm established on magnesium in separate mouse. These biofilm extracted bacteria were mixed shortly in LB and then 5 µl were injected on subcutaneously implanted magnesium discs. Bacterial luminescence over the time (A) measured from mice having three magnesium discs (a), mice bearing magnesium discs infected with *P. aeruginosa* isolated form existing biofilm (b), mice implanted with KH_2PO_4 treated magnesium (c), mice implanted with $Mg(OH)_2$ coated porous titanium (d) and mice having un-coated porous titanium (e). Relative radiance calculated from the indicated surfaces over the time (B).

3.4.6 Role of tissue-air interface in biofilm formation

Hollow structures such as catheters support bacterial colonization in experimental animal models [136]. It was speculated that this could be due to the presence of air liquid

interfaces which prevents immune cells invasion. To confirm this, cylindrical tubes were subcutaneously implanted into the mice and then immediately inoculated with bioluminescent *P. aeruginosa* (Figure 50). Bacteria colonized inside tubes for one week post-infection however they disappeared at later time points (Figure 50A;a). In addition, low bacterial luminosity was detected from infected tubes (Figure 50A;a). Comparatively, bacterial luminosity on magnesium implants was high and for extended period of time (Figure 50A;b). This suggests that the formation of an air cavity in tissue cannot be the sole reason for persistent infections of magnesium implants.

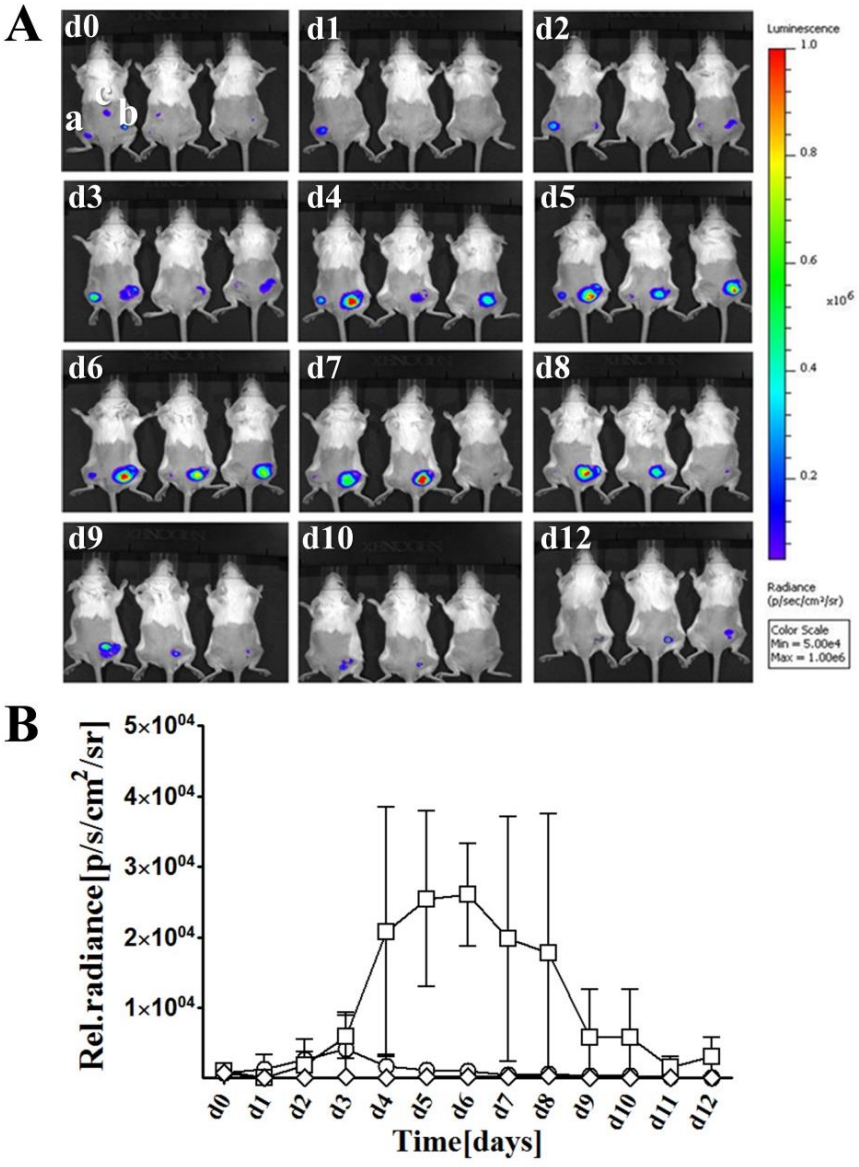

Figure 50: Tubes cannot support bacterial colonization for prolonged time. 5 mm high tubes and magnesium discs were subcutaneously implanted into mice and then 5µl of approximately 1x10^6 CFUs

luminescent *P. aeruginosa* were injected directly into these tubes. Same amount of bacteria were also injected subcutaneously in the tissue without implantation as control. Instantly after infection and later at indicated time points mice were observed under IVIS. Bacterial luminosity from hollow tubes (a), magnesium discs (b) and tissue which was infected without implantation (A). Relative radiance calculated from infected magnesium (squares), infected tubes (circles) and infected tissue without implants (rhombi) at the indicated time points (B).

3.4.7 Role of quorum sensing in persistent bacterial infection

It is assumed that bacteria use quorum sensing system during biofilm formation. To investigate the role of quorum sensing in prolonged infection, a bioluminescent quorum sensing deficient *Pseudomonas aeruginosa* (*pqs* A) was employed. Bioluminescent *P. aeruginosa* with quorum sensing system served as control. Antibiotic sensitivity of both strains was tested using ciprofloxacin. In addition magnesium silver alloy was also infected with *P. aeruginosa* immediately after implantation to see if it was prone to persistent infections. *P. aeruginosa* the quorum sensing mutant strain (*pqs* A) established persistent infections on magnesium implants comparable to wild type *P. aeruginosa* (PAO1, CTX::lux) (Figure 51A; compared d with e). *P. aeruginosa* also established prolonged infections on magnesium silver alloy (Mg6Ag) (Figure 51A; e). Prolonged infections from *P. aeruginosa* (*pqs* A) and (PA01, CTX::lux) strains on magnesium implants also demonstrated resistance against systemic antibiotic treatments (Figure 51A; a,b). These results clearly showed that deficiencies in quorum sensing did not impair the biofilm formation of *P. aeruginosa* on magnesium implants. This is consistent with the notion that quorum sensing is mainly required for rapid establishment of biofilm [120]. Moreover, magnesium silver alloy was susceptible to infection suggesting that the amount of antibacterial silver activity was negligible in this assy.

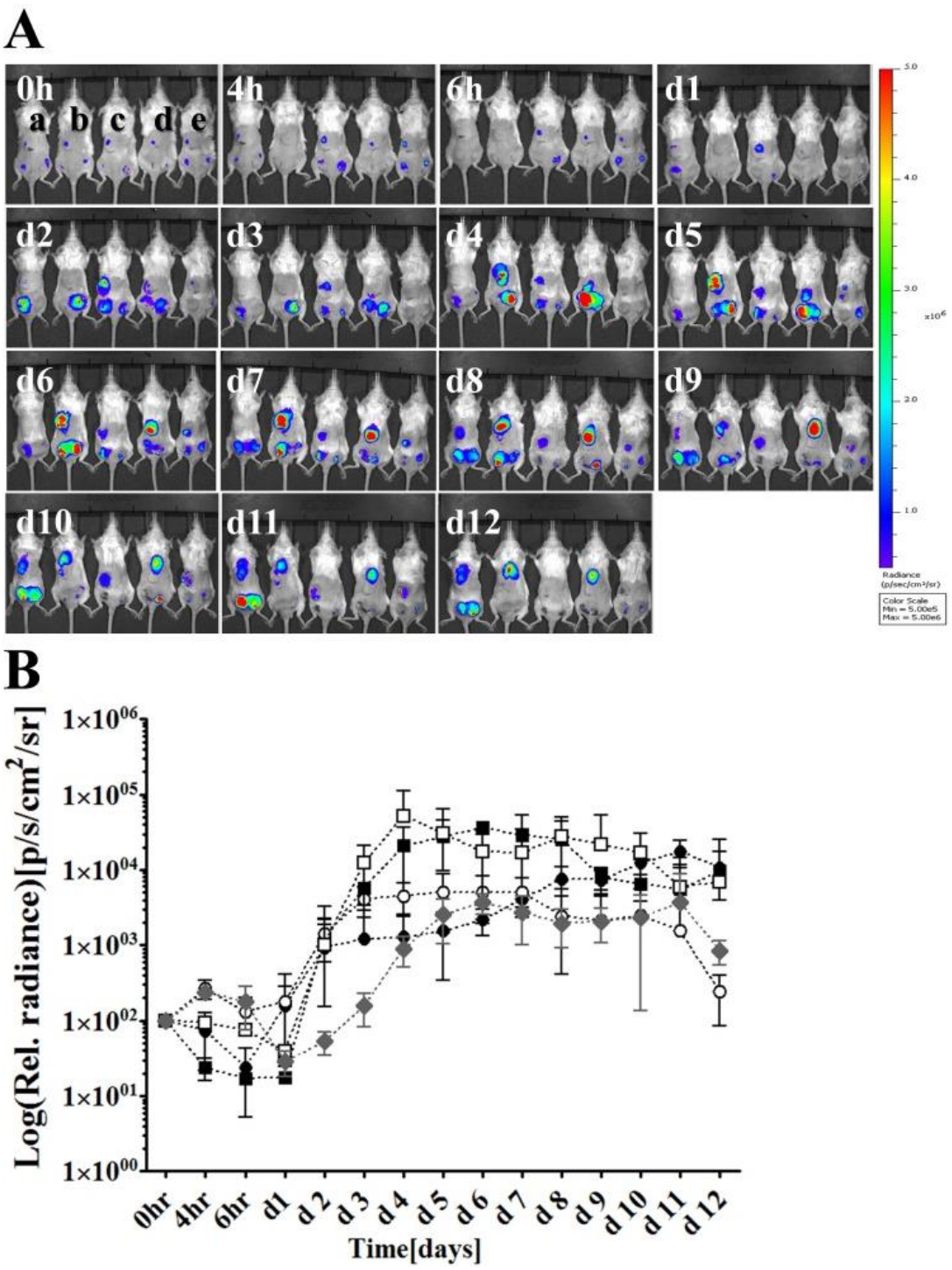

Figure 51: Quorum sensing *P. aeruginosa* mutants can establish prolonged implant infections. 3 magnesium and magnesium silver alloy discs with 5 mm diameter and 2 mm thickness were subcutaneously implanted in mice. Immediately after implantation, 5µl of approximately 1x10^6 CFUs luminescent *P. aeruginosa* (CTX::Lux) or quorum sensing mutant (PA01, *pqs*A) were injected on the surface of magnesium discs. Indicated amounts of bioluminescent *P. aeruginosa* (CTX::Lux) alone were injected on magnesium silver discs. After infection and then daily, 200 µl (2mg/ml) of ciprofloxacin was intravenously injected into the mice bearing magnesium infected with *P. aeruginosa* (CTX::Lux) or quorum sensing mutant (PA01, *pqs*A),

while two mice infected were treated with PBS as controls. Bacterial luminescence (A) measured from mice having magnesium implants infected with *P. aeruginosa* (CTX::Lux) (a), quorum sensing mutant (PAO1, *pqs*A) (b) and treated with ciprofloxacin. Bacterial luminescence from mice having magnesium implants infected with *P. aeruginosa* (CTX::Lux) (c), quorum sensing mutant (PAO1, *pqs*A) (d) and treated with PBS. Bacterial luminescence from mice having magnesium silver implants infected with *P. aeruginosa* (CTX::Lux)(e). Relative radiance (B) calculated from magnesium infected by *pqs* mutant strain injected daily with ciprofloxacin (filled squares) and without ciprofloxacin treatment (empty squares), relative radiance from magnesium infected by *P. aeruginosa* (CTX::Lux) with (filled circles) and without ciprofloxacin (empty circles) and from magnesium silver alloy infected with *P. aeruginosa* (CTX::Lux)(rhombi).

3.4.8 Role of gas cavity formation and antibiotic treatments in prolonged infection

The formation of gas cavities due to magnesium degradation seemed to play an important role in the formation of *P. aeruginosa* biofilms around magnesium implants. To confirm it, phosphate coated magnesium discs (which eliminate early gas cavity generation) in combination with or without ciprofloxacin treatment were subcutaneously implanted and then immediately infected with luminescent *P. aeruginosa.* Previously it was found that bacteria on magnesium implants were resistant to systemic administrated antibiotics. To see the effect of locally produced antibiotic on *P. aeruginosa* infection, magnesium discs were coated with combination of layered double hydroxide (LDH) as slow drug delivery compound and ciprofloxacin. Magnesium coated with LDH alone served as control. Then these discs were implanted subcutaneously and then immediately infected. *P. aeruginosa* injected on the surfaces of phosphate coated magnesium alone and in combination with ciprofloxacin did not establish infections and disappeared shortly after infection (Figure 52 A; a,c). Similarly, bacteria did not survive on magnesium coated with combination of LDH and ciprofloxacin (Figure 52A; d). However, *P. aeruginosa* injected on magnesium implants coated with LDH alone (which do not inhibit gas formation) established prolonged infections (Figure 52A; b). Over all, this experiment shows that the rapidly degrading magnesium is essential for biofilm formation. Local drug delivery system was efficient in inhibiting in bacterial colonization around magnesium implants, presumably due to highly efficacious local antibiotic concentration.

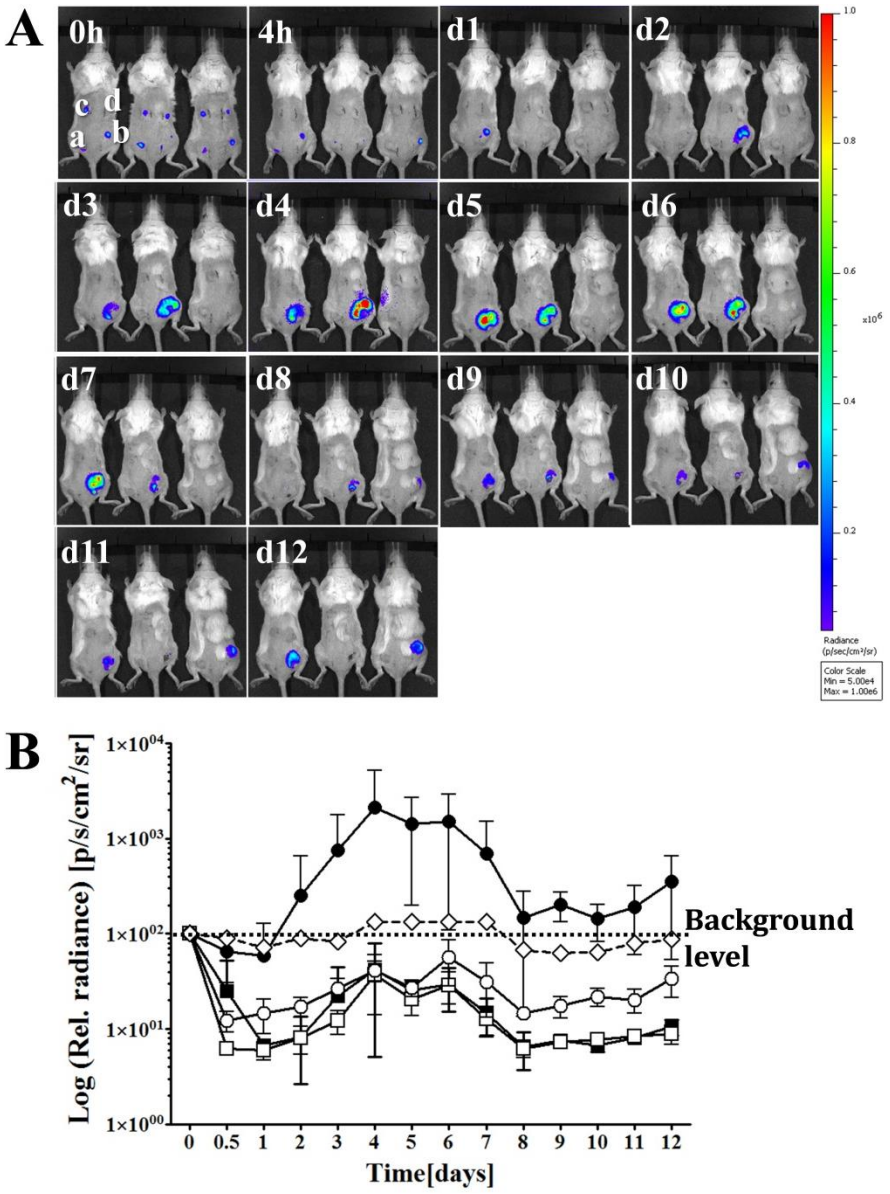

Figure 52: Reduction of magnesium implant corrosion and local antibiotic delivery impede bacterial biofilm formation. A phosphate coating was established on magnesium discs alone and in combination with 250µg of ciprofloxacin. These discs were then implanted subcutaneously in mice and infected with $1x10^6$ CFUs luminescent *P. aeruginosa*. Magnesium discs with Layered double hydroxide (LDH) coating alone as well as in combination with 250µg ciprofloxacin were subcutaneously implanted in mice and then infected *P. aeruginosa.* Luminescence activity (A) of bacteria injected on magnesium coated with phosphate (a) phosphate and ciprofloxacin (c), LDH (b) LDH and ciprofloxacin (d). Relative radiance (B) calculated from magnesium coated with phosphate (filled squares), phosphate and ciprofloxacin (empty squares), LDH (filled circles), LDH and ciprofloxacin (empty circles). Background radiance calculated from un-infected animal (rhombi) as indicated by black line.

3.4.9 Gram-positive *Staphylococcus aureus* can establish prolonged infections on magnesium implants

To investigate if magnesium implants are susceptible to gram positive bacteria, bioluminescent *S. aureus* were employed. Magnesium, titanium and porous glass were infected with *S. aureus* immediately after infection. *S. aureus* established prolonged infections on the surface of magnesium discs which persisted for two weeks (Figure 53A; Mg). However, bacterial luminescence disappeared after one day from titanium and porous glass (Figure 53A; Ti and Pg). These results clearly indicate that magnesium is susceptible to gram negative as well as gram positive bacteria.

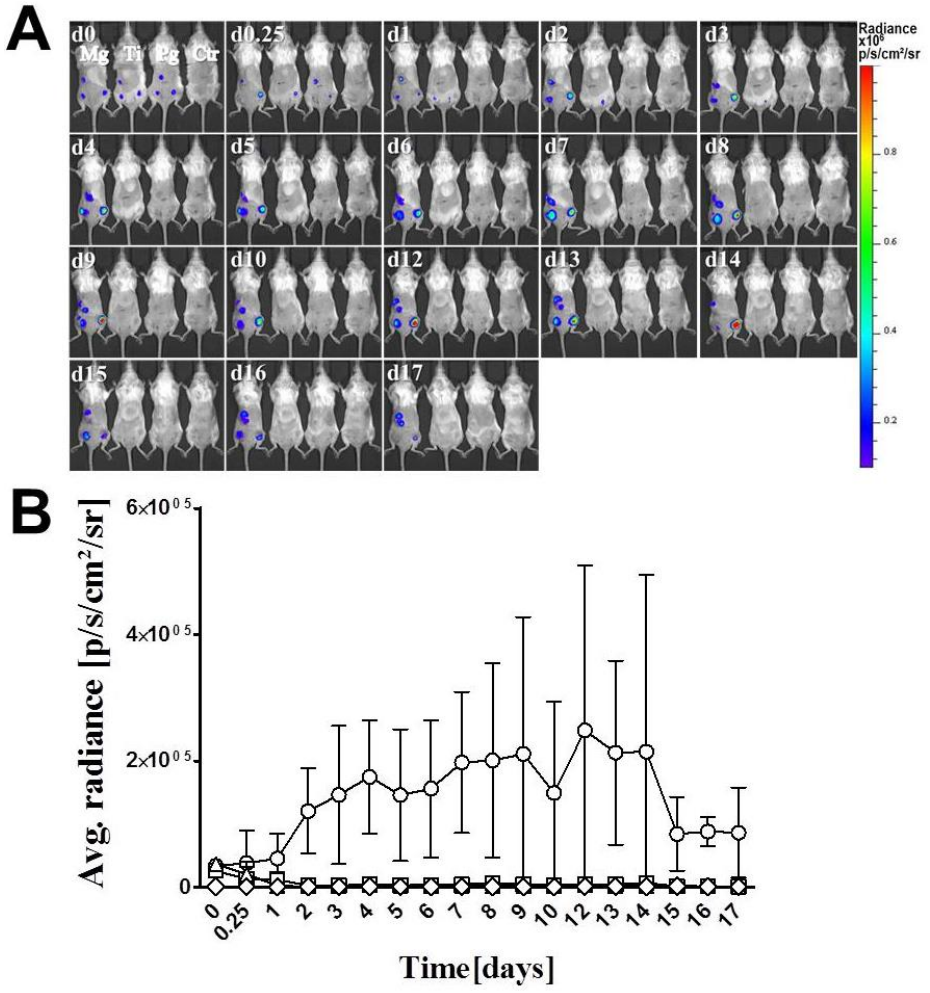

Figure 53: Magnesium implants are prone to persistent gram-positive bacterial infections. 3 magnesium, titanium or porous glass beads were implanted subcutaneously implanted into the mice. Immediately after implantation, 1x10^5 CFUs luminescent *S. aureus* were injected directly on each implant. 3 magnesium implants were implanted subcutaneously (Mg) and left un-infected as control (Ctr). Luminescent activity of *S. aureus* at indicated time points from mice bearing magnesium (Mg), titanium discs (Ti), porous

glass beads (Pg) implants or mice bearing 3 magnesium discs which were not infected (Ctr). Average Radiance calculated from infected magnesium (circles), titanium (squares), porous glass beads (triangles) and un-infected magnesium (rhombi) at indicated time points.

3.4.9.1 Characterization of S. aureus biofilms

To reveal if *S. aureus* were establishing biofilms on magnesium implants, electron microscopy was used. By scanning electron microscopy (SEM) bacteria could not be seen directly on the implants or in peri-implant tissue. However, transmission electron microscopy (TEM) of the tissues adjacent to infected implants showed *S. aureus* embedded within a matrix (white arrows) like structure which seemed typical of bacterial biofilm (Figure 54A-F).

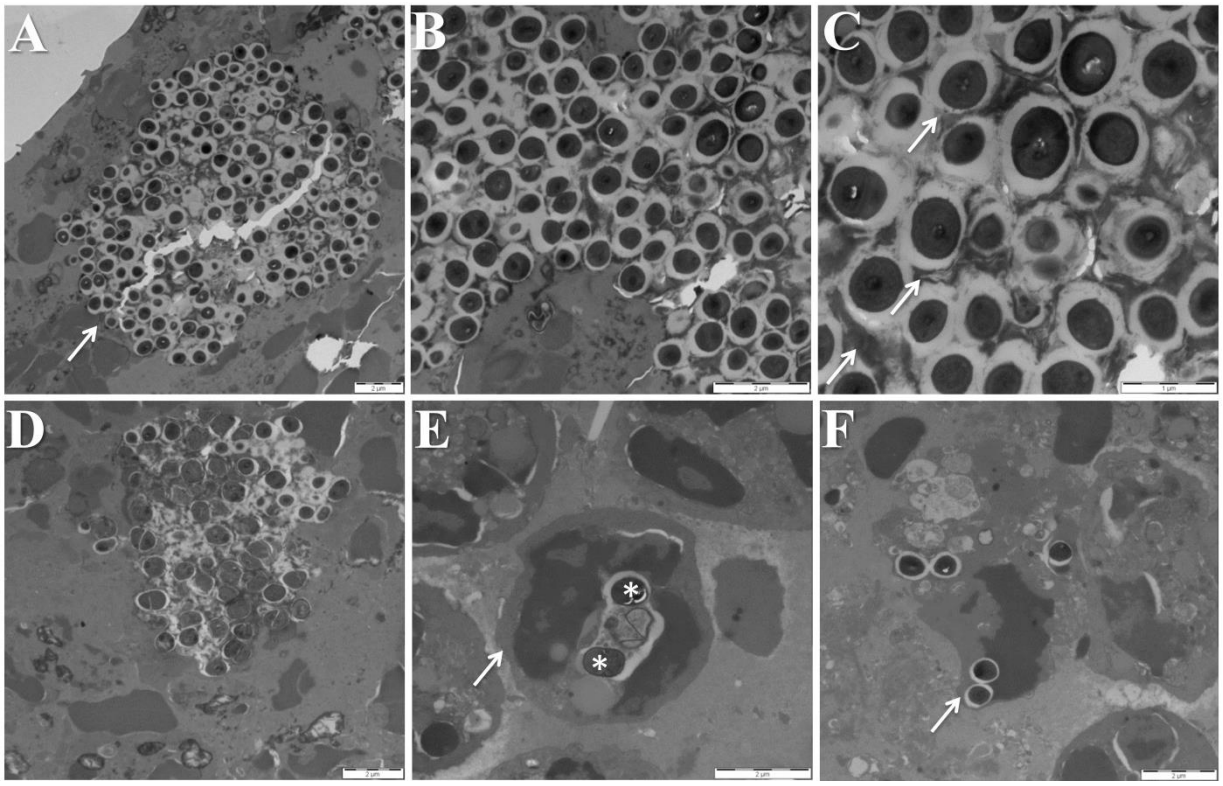

Figure 54: *Staphylococcus aureus* biofilms around magnesium implants. Magnesium implants were subcutaneously implanted in mice and then infected with $1x10^5$ CFUs luminescent *S. aureus*. After two weeks, peri-implant tissues were removed fixed, embedded by epoxy resin and cut into ultrathin sections and examined under transmission electron microscope (A to F). Bacterial biofilms within tissue(A). Exopolysaccharide matrix (white arrows) around bacteria (A-F). Inflammatory cells around biofilms (E) intracellular bacteria (*). (SEM images courtesy by Manfred Rohde, HZI)

3.4.10 Prolonged survival of *Salmonella* on various implant surfaces

Even though Salmonella is not a common biomaterial-associated pathogen, to see if magnesium were susceptible, bioluminescent *S. typhemurium* were employed. Bacteria injected after implantation on magnesium, titanium discs and porous glass beads persisted on all implants for up to two weeks and then started to disappear from magnesium and titanium (Figure 55A). Bacteria continued to persist only on porous glass beads for 34 days (Figure 55A; Pg). This persistence is therefore not specific for magnesium implants and may be related to the nature of bacteria.

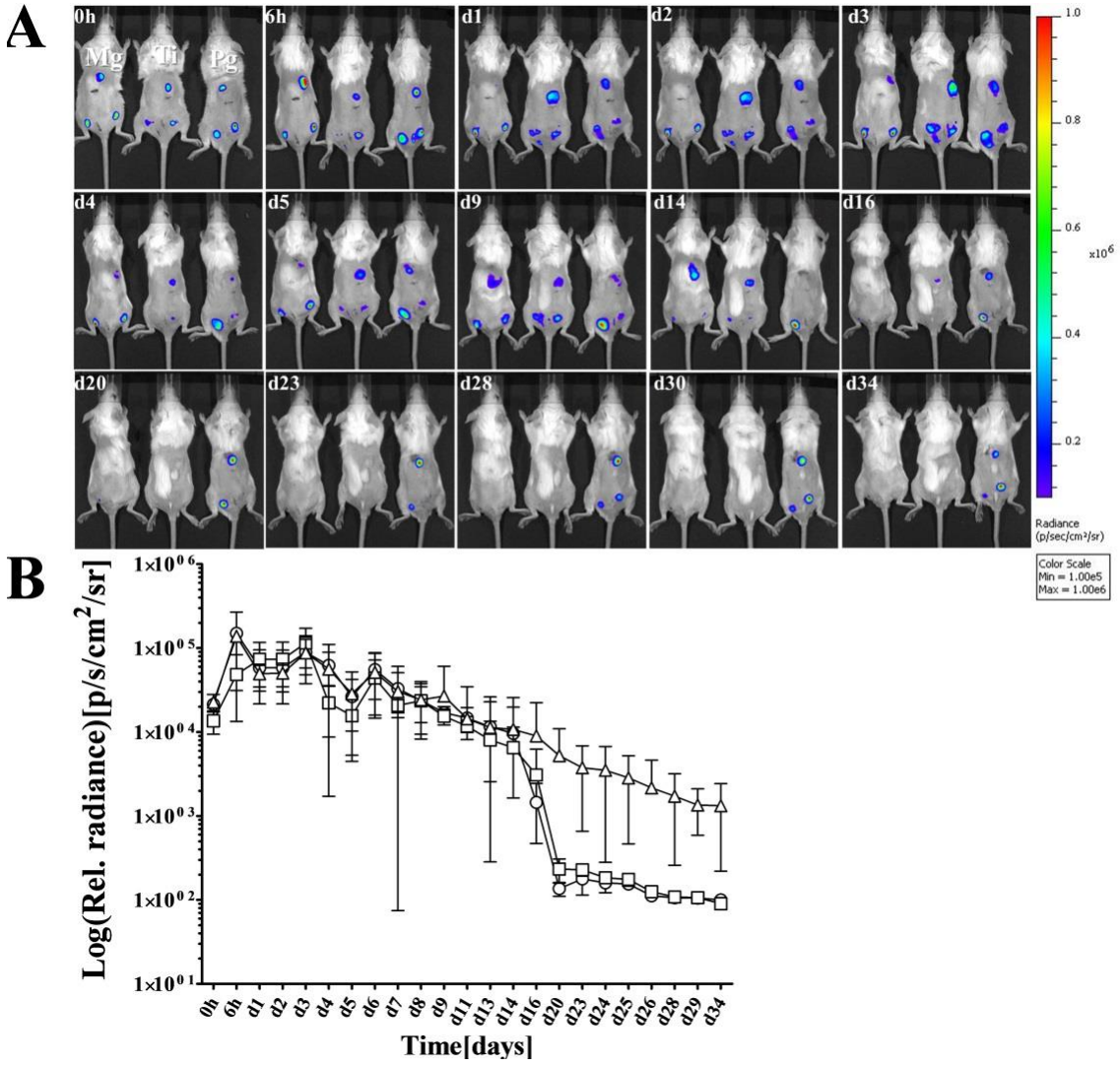

Figure 55: *S. typhimurium* persistence on various implant surfaces. Magnesium, titanium or porous glass beads were subcutaneously implanted in mice. Immediately after implantation, 5µl of bioluminescent *S. typhemurium* at OD_{600}=0.1 in LB suspension were directly injected on the surface of each implant and mice were observed under IVIS. Luminescent activity of bacteria calculated from magnesium (Mg) and titanium

(Ti) and porous glass (Pg). Relative radiance calculated from magnesium (circles), titanium (squares) and porous glass beads (triangles).

3.4.11 Infection by *E. coli* on implant surfaces

Escherichia coli is considered most common implant pathogen around urinary catheter. To investigate its infection kinetics around magnesium, bioluminescent *E. coli* were employed and injected directly on the surfaces of subcutaneously implanted magnesium, titanium and porous glass beads. *E. coli* remained on all implants during early stages however later they disappeared completely from all implants (Figure 56). It could be due to the fact that the employed strain was a laboratory adopted strain that is no longer capable of establishing infections *in vivo.*

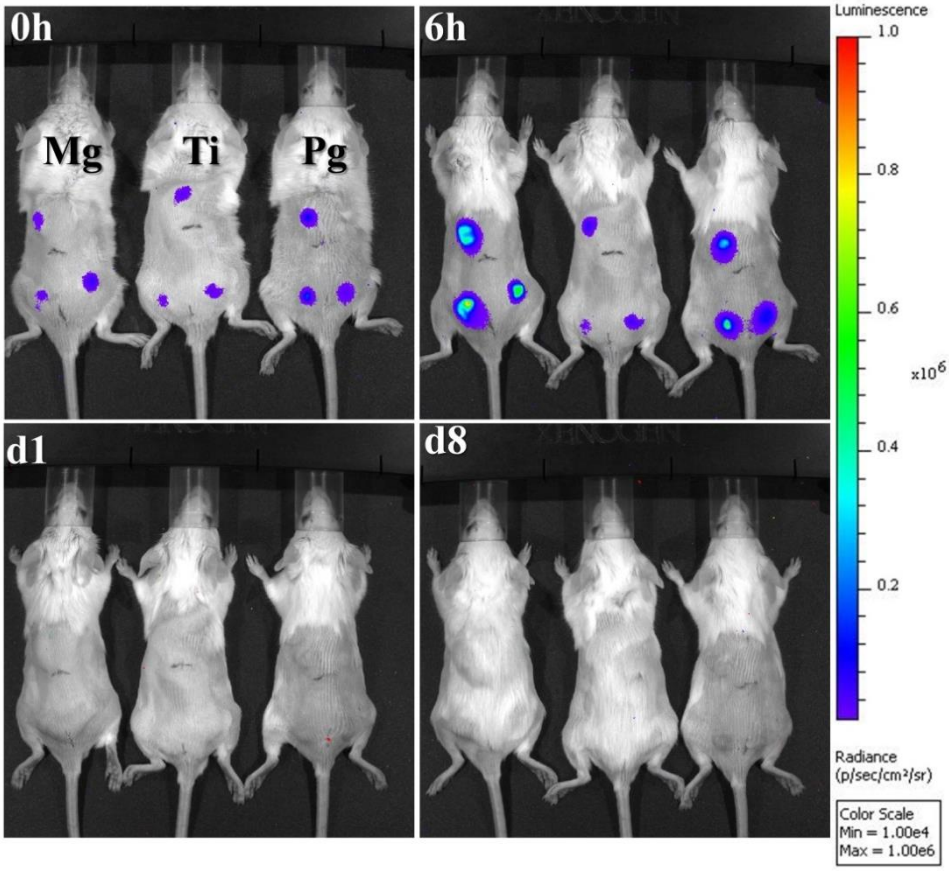

Figure 56: *E. coli* infection and absence of survival on various implants. Mice were implanted subcutaneously with magnesium, titanium and porous glass beads. Immediately after implantation, 5µl of bioluminescent *E. coli* at OD_{600}=0.1 in LB suspension were injected on the surface of each implant and mice were observed by IVIS. Luminescent activity of bacteria observed from magnesium (Mg) and titanium (Ti) and porous glass (Pg) implants.

4 Discussion

4.1 Establishment of *in vitro* corrosion conditions to understand *in vivo* magnesium degradation

Unpredictable corrosion and evolution of gas have been major limitations towards clinical applications of magnesium especially as orthopedic implant. The present study was mainly aimed to establish an *in vitro* model and small animal models to evaluate magnesium for its suitability as implant material in humans. Magnesium is corroding and it starts to degrade immediately after exposure to moist environments resulting magnesium ions (Mg^{2+}), hydroxide (OH^-) and hydrogen (H_2) as primary corrosion products. During corrosion, minerals and elements from the nearby environment accumulate on the surface leading to the formation of a protective corrosion layer. With its establishment, the corrosion layer delays the ongoing degradation process [60]. For in-depth understanding of magnesium degradation, different immersion solutions such as simulated body fluid (SBF), Hank's solution and phosphate buffered saline (PBS) are used [67,31]. However in contrast to body fluids, such *in vitro* solutions are deficient in proteins, and cannot be directly compared with the *in vivo* situation. As described, immediately after implantation, proteins from blood and tissue are adsorbed on implant surfaces [165]. To more closely mimic the *in vivo* situation, cell culture solutions were employed as protein containing media [166]. These solutions mimic the composition of body fluids but they lack living cells. Different murine and human cell lines have previously been cultured with magnesium or its degradation products whereby the emphasis was put on the appropriate cellular response rather than on the degradation kinetics [67]. Under such *in vitro* conditions, cells release metabolic products that might influence the degradation of magnesium. The present study was therefore focused to establish a more reliable *in vitro* corrosion test would be more closely related to the *in vivo* situations. Therefore, a specific conditioned cell culture medium containing cellular secretion products was collected from murine fibroblasts cells (spent cell culture medium). Owing to its specific composition, it appears to be more close to the *in vivo* situation. The degradation rate of magnesium can be assessed by the weight loss method or by the hydrogen generation [167]. In addition, relative pH changes due to hydroxide ions (OH^-), a primary corrosion product was also used as degradation

assessment strategy [166]. These parameters were evaluated and corrosion in spent cell culture medium was compared with various types of solutions under different environmental conditions. Conventionally, weight loss due to degradation is determined by evaluating the end point after a certain time of incubation [167]. However, in present study, weight change in effect to minerals apposition was determined daily under the direct influence of corrosion media. Corrosion layer formation and the subsequent weight change varied with the composition of immersion solution and the incubation environment. As reported in previous studies, cell culture medium had no measureable effect on the weight of magnesium even when incubated at different environmental setups [166]. Magnesium exhibits fast corrosion at physiological pH 7.4-7.6 under standard cell culture conditions [168], which was not the case for cell culture medium DMEM. Given that, proteins and amino acids quickly adsorb on implant surfaces this contributes further to the retardation of corrosion process [169,170]. Magnesium in spent cell culture medium (pH 7.0-7.2) containing cellular excretion products and cellular metabolites showed a more rapid weight loss and increased hydrogen evolution when incubated under standard cell culture conditions. Interestingly, fast degradation of magnesium in the presence of spent cell culture medium was only at standard cell culture conditions. However, magnesium immersed in spent medium at temperature (37°C) within human physiological range did not show any variation in weight. This finding proved that secreted cellular metabolites enhanced corrosion in the presence carbon dioxide [171]. Independent of the environment, a robust weight gain for magnesium incubated in potassium phosphate solution was observed showing that phosphate ions (PO_4^-) accumulated on corroding magnesium [172]. In agreement with previous studies, an increase in the pH of all physiological solutions containing magnesium was observed. Such pH increases occurred mainly during the initial 24h after incubation and became constant at later time points [67]. In the presence of 5% CO_2, pH increases of all media containing metallic magnesium samples was much lower than pH values of same media incubated without CO_2. This could be explained by the acidic effects of CO_2 on aqueous solutions. It is reported that magnesium generally corrodes faster under *in vitro* conditions as compared to *in vivo* situations [71]. Similarly, in present study, pure magnesium wires evidenced weight loss after implantation in soft tissue or tail artery

which was less than wires incubated in spent medium. Enhanced weight loss in spent cell culture medium became more evident at later time points such that magnesium wires degraded completely. Weight loss for magnesium were same in both cases if implantations were done subcutaneously or in tail arteries and it was mainly observed after two weeks of implantation and remained the same at later stages. Corrosion morphologies of magnesium implanted at two mentioned sites were similar suggesting that the tail movement had little influence on the degradation of magnesium. Longtime of implantation resulted in cracking of magnesium wires seemingly due to pitting corrosion [77]. Overall, fast corrosion properties of biological medium containing cellular products were quite evident. Although, there is a need further to investigate the exact composition of spent medium, it can be proposed as best immersion solution to investigate the corrosion properties of degradable magnesium and its alloys under *in vivo*-like conditions.

4.2 Interlocking between corroding magnesium implants and surrounding bone *in vitro*

Intramedullary bone screws synthesized from titanium or stainless steel are widely used for internal fixation of fractured bones. It is expected that stiff fixation of such screws with fragmented bones may prevent micro-motion of fracture lines, enhance bone healing [173]. Magnesium and its alloys have already shown excellent bone morphogenetic properties in small animal models [174,175]. On the basis of these findings, degradable magnesium-based bone fixation screws were manufactured. After implantation in human, such magnesium screws showed promising radio-graphical and clinical properties equivalent to standard titanium [176]. Immediately after exposure to biological environments, degradation of magnesium starts and precipitates form a corrosion layer [74]. Calcium and phosphorus are major components of this layer and these elements are major constituents of natural bone as well. It indicates that magnesium stimulates natural accumulation of calcium and phosphorus that could potentiate the bone healing process. In this context, magnesium based implants were inserted into bones of small animals and strength of internal fixation was assessed using a biomechanical pullout test system [177-179]. Biomechanical pullout tests are a widely used and a reliable method to determine the strength of implant anchorage with the surrounding bone that is conventionally thought to

be due to bone growth. During these studies, increase in bone-implant strength and osseo-integration was significantly evidenced in the presence of living tissue. However, underlying factors responsible for this bone bonding were not previously investigated. It is known that magnesium-based implants can stimulate new bone formation and show increased bone-bonding [37]. Hence, possible factors for the development of rigid fixation between magnesium and bones could either be due to new bone formation or due to the formation of a corrosion layer. During the present study, the contribution of magnesium corrosion in strengthening bone-bonding was investigated in the complete absence of living cells. In the presence of potassium phosphate salt solution, calcium was absent from the corrosion layer thereby confirming that precipitation of calcium is exclusively triggered in the presence of biological media [180]. The surface morphology of corrosion layer on magnesium incubated in biological solutions was different from that incubated in potassium phosphate solution [34,181,182]. Thus, it was confirmed that magnesium promotes the formation of a corrosion layer as soon as it reacts with the biological aqueous solutions. Further, to verify the role of the corrosion layer in promoting the fixation between bone and magnesium implant in the complete absence of live cells. Tibia bones were isolated from mice and dipped in formalin to eliminate live osteocytes that are essential for new bone formation. In the presence of standard cell culture incubation conditions, bone-implant bonding strength significantly increased in the complete absence of live cells. In comparison, standard titanium could not induce strong bone bonding [178]. The interlocking force between magnesium and bone was increasing under the influence different corrosion conditions. The strength of pull-out force was incubation time dependent. This binding force was smaller during early days post-incubation as compared to later time points. Maximum force was determined after one week of incubation and it remained stable thereafter. The elemental composition of the magnesium wires after biomechanical testing seemed to be composed from magnesium (Mg), oxygen (O) and carbon (C). Whereas, calcium and phosphorous could not be detected and apparently was removed due to the mechanical stress. The process of interlocking between magnesium and tibia bones seemed to be in agreement with the *in vitro* corrosion kinetics of magnesium which is fast at initial time points and then slows down with the formation of a precipitation layer. Hence, formation of corrosion layer plays a dominant role in promoting

strong interlocking between magnesium and surrounding bone and is largely independent of new bone formation. As a consequence pull-out experiments are not a valid method to evaluate bone repair or bone growth *in vivo*.

4.3 Preparation and characterization of surface coatings to prevent fast degradation of magnesium

A corrosion resistant coating was established on magnesium which substantially circumvented the initial fast corrosion and hydrogen accumulation in tissues. The degradation process of magnesium in biological media is a dynamic process. In contact with aqueous solutions, magnesium corrosion leads to the generation of (Mg^{2+}) ions and hydrogen gas. At the same time, calcium and phosphorus ions from the surrounding medium start to accumulate on the surface of magnesium. A corrosion layer mainly composed of octacalcium phosphate and hydroxyapatite was established on the surface of magnesium which decelerated the corrosion [183]. We reasoned that if magnesium could be pre-coated with a similar type of corrosion layer before implantation it could avoid the initial rapid corrosion burst. Such coatings would also reduce need for alloying with potentially toxic components. In the present study phosphorus was used as main coating component. Acidic phosphate ions (PO_4^-) could stimulate the degradation of magnesium and form a sturdy corrosion layer [172]. The acidic pH promoted corrosion and coat formation. KH_2PO_4 appeared most promising and was selected as a coating solution for subsequent experiments. KH_2PO_4 resulted in a densely packed amorphous corrosion layer of Newberyite [Mg (HPO_4).3H_2O] on magnesium [184-187]. Such pre-coated magnesium resisted the initial rapid corrosion burst. Magnesium and its alloys induce the precipitation of calcium and phosphorus which may assist the repair of bone tissue. After KH_2PO_4 treatment, calcium and phosphorus were still present on magnesium after corrosion assays in DMEM, plasma and r-SBF [188,189]. Magnesium corrosion generates (OH^-) ions which increase the pH of the surrounding liquid. If the local pH reaches 11, magnesium hydroxide precipitates on the surface of magnesium and slows down the degradation process [190]. Magnesium discs were coated with $Mg(OH)_2$ to investigate if such coatings could prevent fast initial corrosion but it had no protective effects. In living tissue, constant blood circulation may buffer the high pH due to corroding magnesium implants [191]. Still,

alkalization and elevated (Mg^{2+}) ion concentrations may affect cellular and tissue activities near magnesium implants [192]. KH_2PO_4 derived coatings decreased the local concentration of (Mg^{+2}) *in vitro* by reducing magnesium corrosion and also maintained the normal pH level of incubation media. It is essential that medical implant coatings must be non-toxic cell friendly. Immortalized murine fibroblasts and porcine nasal epithelial cells were selected for their potential compatibility with KH_2PO_4 treated magnesium. After implantation, a healing process is triggered to repair the damaged tissue which involves the activation of fibroblasts. These cells then adhere to implant surfaces and secrete collagen and extracellular matrix proteins together forming fibrous tissue capsule around the implants. A direct contact between the test material and cells is critical for the *in vitro* evaluation [193]. Titanium discs were used as standard cell compatible material for comparison. The analysis of cell proliferation, size and number showed that plain magnesium could not support cell growth but after KH_2PO_4 treatment of magnesium fibroblasts demonstrated excellent proliferation. In addition, viability and expression of pro-inflammatory cytokines and chemokines particularly interleukin-8 (IL-8) is another criteria to characterize host-implant interaction [194]. Phosphate coated magnesium significantly increased the viability of nasal epithelial cells. Magnesium promotes IL-8 secretion [195]. We detected an increase in the production of IL-8 in response to magnesium without coatings. However, IL-8 secretion from the cells incubated with phosphate coated magnesium was significantly lower suggesting it has less inflammatory potential. Further, a mouse model was established to examine implant-soft tissue interaction and measure hydrogen gas evolution at implantation site. Subcutaneous implantation allowed the direct observation of gas cavities around implanted discs [78,196,60]. We also established a novel method to measure the volume of these gas cavities formed around the subcutaneous implants. The mice implanted with plain magnesium and $Mg(OH)_2$ coated discs, showed gas pouches about 24h after implantation which later decreased wtih time. No gas bubbles developed in the tissue around phosphate coated magnesium discs. For comparison, fluoride coated discs were implanted, which also diminished the formation of gas cavities. However after one week, small gas cavities around fluoride-coated magnesium persisted for a few days and then disappeared. This could be explained by a high initial corrosion resistance which is only temporal, followed

by the formation of a biological protective corrosion layer. A corrosion layer composed from organic compounds and magnesium corrosion products including calcium phosphate was detected. The microstructure of phosphate based coatings was still intact after short time of implantation. A thick corrosion layer similar in composition was detected on the surface of implants after long period of implantation. This information provides solid evidence that magnesium based implants are rapidly covered by layer of magnesium corrosion products and organic compounds which serves as barrier to slow down the corrosion process [170]. This is in agreement with the common notion that magnesium based implants quickly develop a passivation layer as soon as they are exposed to aqueous environment [184]. It proves that pre-coating process with potassium phosphate generates a barrier and protects magnesium form fast corrosion similar to a natural corrosion layer. Soft tissue compatibility with the implanted discs was evaluated by histological methods [197,65]. Implants were found compatible towards adjacent tissue except with typical foreign-body reaction [198,63]. After prolonged implantation, fibrous tissue formation with infiltration of some giant cells and granulocytes was detected in response to all implanted materials as reported [199]. In addition, a thick corrosion layer was detected around all implants. Recruitment of inflammatory cells (mostly granulocytes, with some macrophages) seemed slightly more pronounced in tissues near fluoride coated magnesium discs indicating an increased inflammatory potential. Phosphate coated magnesium discs showed adequate compatibility with contiguous tissues indicating that these coatings have equivalent protective effect but are more biocompatible than fluoride coatings.

4.4 Establishment of persistent infections around metallic magnesium implants

Magnesium is antibacterial under *in vitro* situations due to increased local alkalinity resulting from its corrosion [62]. Such inherited antibacterial properties of degradable magnesium were further investigated *in vivo*. In this perspective, a recent study reported that pure magnesium intra-medullary nails were antibacterial and anti-biofilm against methicillin resistant *S. aureus* (MRSA) in a rat model of implant related osteomyelitis. Antibacterial efficacy was mainly quantified by counting the bacterial load in colony

forming units (CFUs) [200,201]. The present study was focused to the antibacterial properties of metallic magnesium *in vivo*. A mouse implant-infection model was established whereby metallic discs were inserted subcutaneously and the subsequent infection was done by injecting the bacterial inoculum directly on the surfaces of the implanted discs. For infection, the bacteria *P. aeruginosa* and *S. aureus* (common implant associated pathogens) engineered for bioluminescence (*lux*) were employed. Bacterial luminosity was used as indicator to investigate metabolic activity and viability of bacteria *in vivo*. A sensitive *in vivo* imaging system (IVIS) facilitated the determination of small cultures of bacterial luminescence in direct contact with metallic implants beneath the skin of live animals. The luminescence detection method is prompt and profound as compared to the conventionally used colony counting method which is not only time consuming but is dependent on the explanation of samples at each time point after the sacrifice of animals. Overall, *in vivo* imaging allows imaging procedure in single animal at repeated time points. This reduces the need for larger number of animals whereby the statistics is improved by the collection of multiple data points from same animal and the pathogen load can be quantified without exogenous sampling [202]. Surprisingly and in contrast to previous studies, we detected a gradual increase in the luminosity of *P. aeruginosa* and *S. aureus* specifically on the surfaces of subcutaneously implanted metallic magnesium as compared to titanium and porous glass beads. Bacterial luminescence as a marker for bacterial load and metabolism on metallic magnesium decreased transiently below the initial inoculation during the early time points. After that, a gradual increase was seen which lasted for more than two weeks. This unexpected outcome revealed that magnesium was bactericidal only *in vitro* but infection prone when implanted *in-vivo*. Such stable and prolonged infection occurred on magnesium even if very small numbers (100 CFUs) of bacteria were locally injected. Infection was also productive when bacteria were injected on subcutaneous magnesium implants either immediately after implantation or 24h after implantation. These time courses mimic clinical intraoperative or postoperative contaminations [203]. With both approaches, magnesium seemed to be highly susceptible to locally injected bacteria. However, infections could not be established on magnesium when bacteria were injected intravenously neither soon or 24h after implantation. In some situations, bacterially infected tissues may serve as reservoir and bacteria have been proposed to migrate to

neighboring healthy tissue to establish new infections [204]. On the other hand, *P. aeruginosa* established a localized infection on magnesium and bacteria did not spread to adjacent un-infected magnesium implants in our assays. This may diverge from clinical situations however, the bacterial inoculum required for implant colonization is not known.

4.4.1 Characterization of prolonged infections on magnesium implants

During chronic infections, bacteria organize themselves to biofilms highly stationary cultures surrounded by exoplysacharide matrix. Within biofilms, microbes are held together by self- secreted polysaccharides and proteins, become extremely resistant to antibiotics and host immune system [205]. Different biological and molecular techniques are applied for the detection and visualization of bacterial biofilms. Hence, some of the frequently practiced methods were applied to see if the bacteria were making biofilms on implanted magnesium discs [206]. Scanning electron microscopy of magnesium discs and nearby tissue with *P. aeruginosa* infection, revealed a high density population of bacterial cells inter-connected with filaments of extracellular polymeric (EPS) matrix [207]. *P. aeruginosa* were adhering on the surface of magnesium with well-defined biofilm architecture. Bacteria in free-living form can be eliminated by the innate immune system. The transition to the biofilm form renders bacteria impervious to host defense mechanisms [208]. Transmission electron microscopy was used to detect the infiltration of host immune cells. Bacteria on magnesium implants attracted immune cells mainly polymorphonuclear leukocytes (PMNs). Even though *P. aeruginosa* and *S. aureus* within biofilms were surrounded by the immune cells, the biofilms were not visibly affected. Few bacteria which were outside of the biofilm could be seen being engulfed by polymorphonuclear leukocytes (PMNs) [209]. Moreover, histological findings revealed a strong influx of granulocytes towards *P. aeruginosa* biofilms. These results can be taken as evidence that bacterial biofilms formed on magnesium implants exhibit strong resistance against host immune system. Bacteria within biofilms are known for their resistance against antimicrobial agents [210,211]. This was proved in the current study and a remarkable increase in the antibiotic resistance of *P. aeruginosa* growing on magnesium implants was observed. Bacteria are known to communicate with one another through the exchange of chemical signal molecules called auto inducers. This process is called quorum-sensing and it plays an

important role in biofilm formation [212]. Disabling quorum sensing has been proposed as a potential strategy to prevent biofilm formation and chronic infections [213]. In the current study, the luminescent quorum sensing mutant *P. aeruginosa* (*pqs*A$^-$) showed decreased luminescence and antibiotic sensitivity as compared to wild type luminescent strain only at early time points after infection. However, at later stages the *pqs*A$^-$ mutant strain established prolonged infections on magnesium implants. These results suggest that quorum-sensing is not a critical parameter for *P. aeruginosa* biofilm formation but it may affect the kinetics of early steps. Biofilm extracellular matrix is mainly composed from proteins, exopolysaccharides and extracellular DNA that together function to facilitate cells adherence to surfaces and provide protection [100]. Indeed, proteins and polysaccharides were detected in *P. aeruginosa* infected tissues near magnesium implants with the biofilm specific Periodic acid–Schiff (PAS) staining procedure [214,215]. Type I interferon induction is triggered in response to viral and bacterial infections [162]. *P. aeruginosa* biofilm is reported to promote strong stimulation of type I interferon in β-interferon luciferase reporter mice (IFN-β$^{+/\Delta\beta\text{-luc}}$) [155]. A strong and prolonged production of type I β-interferon was examined in response to magnesium infected with *P. aeruginosa.* Taken together these findings show that *P. aeruginosa* and *S. aureus* establish prolonged infections on magnesium implants. Using different biofilm detection methods, we determined that these extended infections were mainly based upon biofilm formation.

4.4.2 Magnesium corrosion products responsible for prolonged implant infections

When magnesium implants degrade hydroxide ions stimulate the formation of a lowly soluble magnesium hydroxide layer with the inclusion of additional organic and inorganic molecules [31]. In addition, hydrogen gas is produced resulting in the formation of gas cavities. Within these cavities, hydrogen gas is rapidly exchanged with the surrounding air [78]. These observations led us to speculate that these gas cavities could protect bacteria from immune cells. As discussed previously, potassium phosphate treated magnesium impede the development of gas bubbles on corrosion protected magnesium implants. *P. aeruginosa* disappeared quickly from potassium phosphate treated magnesium and infection did not reoccur. This was in agreement with our assumption that magnesium implant degradation promoted bacterial survival. It is thought that surgical damaged tissue

together with blood clots on implant surface may support bacterial initial adherence and biofilm formation [216]. To test the influence of wounding, *P. aeruginosa* were injected on the surface of magnesium after 4 weeks of subcutaneous implantation. Interestingly, bacteria were still capable of establishing prolonged infections on the surfaces of magnesium discs. It can be assumed that under *in vivo* situations the buffering from the blood circulation stabilizes pH near the tissue-magnesium interface. Nevertheless, the elevated pH might be critical to *P. aeruginosa* survival. To this end, magnesium hydroxide coated porous titanium implants were supposed to generate an alkaline environment. *P. aeruginosa* showed a prolonged survival in the presence of magnesium hydroxide loaded porous titanium implants. Therefore, sustained bacterial survival was mainly due to high pH levels. Overall, mainly pH and possibly to minor degree gas cavities may contribute to the initial bacterial survival and immune cell invasion. At later stages, bacteria are enveloped within a self-produced extracellular matrix which acts as barrier against host defense thereby extending their survival.

4.5 Proposed mouse model to understand biofilm formation on implant surfaces

Transformation from planktonic bacteria to the biofilm form is different *in vitro* as compared to *in vivo* [217]. Depending on nutrients supply and surrounding conditions, bacteria can make biofilms *in vitro*. *In vivo* biofilm formation is more complicated. It is thought that bacteria search for suitable substrates like host tissue or inert surfaces like medical implants for initial adherence. To adhere on implanted material, bacteria face tough competition with fibroblasts which are activated to establish first contact with material and completely surround the whole surface. In parallel, bacteria need to cope with the host immune defense [204]. Some bacteria manage to establish *in vivo* biofilms on implants. Such implant infections cannot be cured with conventional antimicrobial treatments and are major cause of persistent clinical infections [218,219]. Laboratory animal models are therefore essential to investigate novel ways to characterize and eliminate *in vivo* biofilms. Such models may provide insight into the molecular mechanisms underlying biofilm formation in biological system and further designing certain drugs capable of disrupting such microbial consortia. Various animal models have been proposed

based on the insertion of pre-colonized solid substrates into animal body [220,221]. A major shortcoming with these models is that the bacteria are already in biofilm mode of growth and invulnerable to immune system. A catheter tube model is centered upon the surgical insertion of small catheter tubes subcutaneously into small animals and then administration of bacteria either before or after implantation into tubes [146]. In clinical situations, catheters provide suitable conditions for the growth of bacterial biofilm [222]. Inside indwelling catheters, bacteria already have no contact with adjacent tissue and blood circulation, hence are protected from tissue-resident macrophages and circulating neutrophils [223]. Bacteria also proliferate on orthopedic and dental implants [224]. Even though, catheter tubes support biofilms they are not perfect models to other types of implant infections in patients. Bacterial survival on magnesium implants in mice appears to be a better model to investigate effective treatments. Bacteria have been proposed to migrate into nearby tissue niches to temporarily hide from the immune attack or from antibiotics. Once the situation becomes more favorable, bacteria return back on implants and cause persistent biomaterial-associated infections [225]. Similarly, during current study, a reduction in bacterial luminosity was monitored at early stages after implantation. At later stages, *P. aeruginosa* and *S. aureus* biofilms clusters were demonstrated in the tissues near magnesium implants. This confirms the notion that bio-material associated infections are not limited to the implant interface but bacteria also grow within peri-implant tissues [226]. It seemed living bacteria within biofilm assemblies were persisting in the tissue near infected implants [225]. Magnesium was infected with low numbers of planktonic bacteria to improve the clinical relevance. However, this reduced the success rate of detectable persistent implant infections. Magnesium implants accessible to the host immune system and polymorphonuclear leukocytes (PMNs) were observed near biofilms. Taken together, magnesium based tissue infection model represents a biofilm formation on medical implants comparable to hospital conditions. It is the first animal model to our knowledge wherein biofilms formation takes place on metallic implants in direct contact with host tissue. Thus, this mouse model could be used in the future to identify intrinsic mechanisms underlying *in vivo* biofilm formation and to develop strategies to eradicate such infections.

5 Conclusion

A major limitation of permanent metallic implant materials for temporal applications is the requirement for secondary surgery for their removal. Medical implants made from degradable metals such as magnesium could overcome this difficulty. This study was conducted to investigate the properties of magnesium and to provide solutions to problems that hinder clinical applications of magnesium-based implants. To understand magnesium degradation *in vitro,* different biological media under various conditions were investigated. It was found that magnesium had the potential to develop strong interlocking with bone even in the absence of cells, a property which was previously thought to indicate the promotion of the healing of fractured bones. Rapid degradation and generation of hydrogen gas cavities in tissue were identified as major problems associated with magnesium implants. Therefore, a biocompatible phosphate based coating found to render magnesium implants corrosion resistant and eliminated the gas cavity formation. Metallic magnesium showed promising antibacterial properties against *P. aeruginosa* and *S. aureus in vitro*. However, *in vivo,* magnesium implants were infection prone and it also proved an appropriate niche for bacteria to establish resistant biofilms and may therefore be useful as *in vivo* model for implant infections.

6 Outlook

In the present study metallic magnesium implants were investigated. Magnesium showed promising degradable properties *in vitro* and in small animals. It was capable of strong bone bonding even in the complete absence of live cells due to the formation of a highly biocompatible corrosion layer. However, problems with rapid corrosion and gas cavities in the tissue associated with magnesium corrosion were solved by potassium phosphate pre-treatment. After this treatment, phosphate coatings around magnesium were compatible with murine cells and tissue. Accumulation of hydrogen gas in tissue and pitting corrosion were completely abrogated for the entire observation period of eight weeks after phosphate coating. The promising properties of phosphate coatings warrant further investigation in larger animals or in the clinics.

Metallic magnesium exhibited bactericidal properties *in vitro*. This property was solely due to alkalization produced near magnesium surface. However, *in vivo*, magnesium was not antibacterial but susceptible to persistent bacterial infections. This was quite contrary to the expectations. Thus, magnesium alloys and coatings which protect magnesium from bacterial colonization need to be established before their clinical applications. Prolonged magnesium infection was clearly due to the formation of biofilms by bacteria which was confirmed by various assays. Hence, magnesium infection closely mimics clinical biomaterial associated infections thereby this can be used as mouse model to understand various aspects of biofilm persistence on medical implants and to test the efficacy of novel anti biofilm compounds.

7 References

1. Concha-Barrientos M, Nelson DI, Fingerhut M, Driscoll T, Leigh J (2005) The global burden due to occupational injury. American Journal of Industrial Medicine 48 (6):470-481.

2. Mathers CD, Loncar D (2006) Projections of global mortality and burden of disease from 2002 to 2030. PLoS medicine 3 (11):e442.

3. Murray CJL, Lopez AD (1997) Global mortality, disability, and the contribution of risk factors: Global Burden of Disease Study. The Lancet 349 (9063):1436-1442.

4. Langer R, Tirrell DA (2004) Designing materials for biology and medicine. Nature 428 (6982):487-492.

5. Disegi JA, Eschbach L (2000) Stainless steel in bone surgery. Injury 31 Suppl 4:2-6

6. Albrektsson T, Branemark PI, Hansson HA, Lindstrom J (1981) Osseointegrated titanium implants. Requirements for ensuring a long-lasting, direct bone-to-implant anchorage in man. Acta orthopaedica Scandinavica 52 (2):155-170

7. Nonami T, Tsutsumi S (1999) Study of diopside ceramics for biomaterials. J Mater Sci: Mater Med 10 (8):475-479.

8. Ivanoff CJ, Widmark G (2001) Nonresorbable versus resorbable sutures in oral implant surgery: a prospective clinical study. Clinical implant dentistry and related research 3 (1):57-60

9. Kulczyk T, Dyszkiewicz Konwinska M, Owecka M, Krzyzostaniak J, Surdacka A (2014) The influence of amalgam fillings on the detection of approximal caries by cone beam CT: in vitro study. Dento maxillo facial radiology 43 (7):20130342.

10. Robb BW, Wachi H, Schaub T, Mecham RP, Davis EC (1999) Characterization of an in vitro model of elastic fiber assembly. Molecular biology of the cell 10 (11):3595-3605.

11. Toita R, Murata M, Tabata S, Abe K, Narahara S, Piao JS, Kang J-H, Hashizume M (2012) Development of Human Hepatocellular Carcinoma Cell-Targeted Protein Cages. Bioconjugate Chemistry 23 (7):1494-1501.

12. Kang YJ, Park DC, Shin H-H, Park J, Kang S (2012) Incorporation of Thrombin Cleavage Peptide into a Protein Cage for Constructing a Protease-Responsive Multifunctional Delivery Nanoplatform. Biomacromolecules 13 (12):4057-4064.

13. Ratner BD, Bryant SJ (2004) BIOMATERIALS: Where We Have Been and Where We are Going. Annual review of biomedical engineering 6 (1):41-75.

14. Brammer KS, Frandsen CJ, Jin S (2012) TiO_2 nanotubes for bone regeneration. Trends in Biotechnology 30 (6):315-322.

15. Crosby JR, DeCook KJ, Tran PL, Smith RG, Larson DF, Khalpey ZI, Burkhoff D, Slepian MJ (2014) Physiological Characterization of the SynCardia Total Artificial Heart in a Mock Circulation System. ASAIO journal.

16. Torregrossa G, Anyanwu A, Zucchetta F, Gerosa G (2014) SynCardia: the total artificial heart. Annals of cardiothoracic surgery 3 (6):612-620.

17. Ruzza A, Czer LSC, Ihnken KA, Sasevich M, Trento A, Ramzy D, Esmailian F, Moriguchi J, Kobashigawa J, Arabia F (2015) Combined Heart-Kidney Transplantation After Total Artificial Heart Insertion. Transplantation proceedings 47 (1):210-212.

18. Kovach KM, LaBarbera MA, Moyer MC, Cmolik BL, van Lunteren E, Sen Gupta A, Capadona JR, Potkay JA (2015) In vitro evaluation and in vivo demonstration of a biomimetic, hemocompatible, microfluidic artificial lung. Lab on a Chip 15(5):1366-75.

19. Gotman I (1997) Characteristics of metals used in implants. Journal of endourology / Endourological Society 11 (6):383-389

20. Geetha M, Singh AK, Asokamani R, Gogia AK (2009) Ti based biomaterials, the ultimate choice for orthopaedic implants – A review. Progress in Materials Science 54 (3):397-425.

21. Harris JD, Siston RA, Brophy RH, Lattermann C, Carey JL, Flanigan DC (2011) Failures, re-operations, and complications after autologous chondrocyte implantation – a systematic review. Osteoarthritis and Cartilage 19 (7):779-791.

22. Senthi S, Munro J, Pitto R (2011) Infection in total hip replacement: meta-analysis. International Orthopaedics (SICOT) 35 (2):253-260.

23. Lendlein A, Langer R (2002) Biodegradable, Elastic Shape-Memory Polymers for Potential Biomedical Applications. Science 296 (5573):1673-1676.

24. Middleton JC, Tipton AJ (2000) Synthetic biodegradable polymers as orthopedic devices. Biomaterials 21 (23):2335-2346.

25. van der Elst M, Klein CP, de Blieck-Hogervorst JM, Patka P, Haarman HJ (1999) Bone tissue response to biodegradable polymers used for intra medullary fracture fixation: a long-term in vivo study in sheep femora. Biomaterials 20 (2):121-128

26. Hermawan H (2012) Biodegradable Metals: State of the Art. In: Biodegradable Metals. SpringerBriefs in Materials. Springer Berlin Heidelberg, pp 13-22.

27. Mueller PP, Arnold S, Badar M, Bormann D, Bach F-W, Drynda A, Meyer-Lindenberg A, Hauser H, Peuster M (2012) Histological and molecular evaluation of iron as degradable medical implant material in a murine animal model. Journal of Biomedical Materials Research Part A 100A (11):2881-2889.

28. Peuster M, Wohlsein P, Brugmann M, Ehlerding M, Seidler K, Fink C, Brauer H, Fischer A, Hausdorf G (2001) A novel approach to temporary stenting: degradable cardiovascular stents produced from corrodible metal-results 6-18 months after implantation into New Zealand white rabbits. Heart 86 (5):563-569.

29. Iron–manganese: new class of metallic degradable biomaterials prepared by powder metallurgy (2008). Powder Metallurgy 51 (1):38-45.

30. Mueller WD, Lucia Nascimento M, Lorenzo de Mele MF (2010) Critical discussion of the results from different corrosion studies of Mg and Mg alloys for biomaterial applications. Acta biomaterialia 6 (5):1749-1755.

31. Mueller W-D, Fernández Lorenzo de Mele M, Nascimento ML, Zeddies M (2009) Degradation of magnesium and its alloys: Dependence on the composition of the synthetic biological media. Journal of Biomedical Materials Research Part A 90A (2):487-495.

32. Song G, Atrens A, John DS, Wu X, Nairn J (1997) The anodic dissolution of magnesium in chloride and sulphate solutions. Corrosion Science 39 (10–11):1981-2004.

33. Wang Y, Wei M, Gao J, Hu J, Zhang Y (2008) Corrosion process of pure magnesium in simulated body fluid. Materials Letters 62 (14):2181-2184.

34. Willumeit R, Fischer J, Feyerabend F, Hort N, Bismayer U, Heidrich S, Mihailova B (2011) Chemical surface alteration of biodegradable magnesium exposed to corrosion media. Acta biomaterialia 7 (6):2704-2715.

35. Xu L, Zhang E, Yin D, Zeng S, Yang K (2008) In vitro corrosion behaviour of Mg alloys in a phosphate buffered solution for bone implant application. Journal of materials science Materials in medicine 19 (3):1017-1025.

36. Huang J, Ren Y, Jiang Y, Zhang B, Yang K (2007) In vivo study of degradable magnesium and magnesium alloy as bone implant. Front Mater Sci China 1 (4):405-409.

37. Witte F, Kaese V, Haferkamp H, Switzer E, Meyer-Lindenberg A, Wirth CJ, Windhagen H (2005) In vivo corrosion of four magnesium alloys and the associated bone response. Biomaterials 26 (17):3557-3563.

38. Badar M, Lunsdorf H, Evertz F, Rahim MI, Glasmacher B, Hauser H, Mueller PP (2013) Formation of an organic coat and release of corrosion microparticles from metallic magnesium implants. Acta biomaterialia.

39. Zhang E, Xu L, Yu G, Pan F, Yang K (2009) In vivo evaluation of biodegradable magnesium alloy bone implant in the first 6 months implantation. Journal of Biomedical Materials Research Part A 90A (3):882-893.

40. Romani A (2007) Regulation of magnesium homeostasis and transport in mammalian cells. Archives of Biochemistry and Biophysics 458 (1):90-102.

41. Vormann J (2003) Magnesium: nutrition and metabolism. Molecular aspects of medicine 24 (1–3):27-37.

42. Romani AM, Scarpa A (2000) Regulation of cellular magnesium. Frontiers in bioscience : a journal and virtual library 5:D720-734.

43. Iannello S, Belfiore F (2001) Hypomagnesemia. A review of pathophysiological, clinical and therapeutical aspects. Panminerva medica 43 (3):177-209.

44. Miller JC, Landesman R (1977) Magnesium deficiency in embryos of Xenopus laevis. Journal of embryology and experimental morphology 39:97-113.

45. Vormann J (2003) Magnesium: nutrition and metabolism. Molecular aspects of medicine 24 (1-3):27-37.

46. Abboud CN, Scully SP, Lichtman AH, Brennan JK, Segel GB (1985) The requirements for ionized calcium and magnesium in lymphocyte proliferation. Journal of cellular physiology 122 (1):64-72.

47. Modiano JF, Kelepouris E, Kern JA, Nowell PC (1988) Requirement for extracellular calcium or magnesium in mitogen-induced activation of human peripheral blood lymphocytes. Journal of cellular physiology 135 (3):451-458.

48. Li FY, Chaigne-Delalande B, Kanellopoulou C, Davis JC, Matthews HF, Douek DC, Cohen JI, Uzel G, Su HC, Lenardo MJ (2011) Second messenger role for Mg2+ revealed by human T-cell immunodeficiency. Nature 475 (7357):471-476.

49. Apel K, Hirt H (2004) REACTIVE OXYGEN SPECIES: Metabolism, Oxidative Stress, and Signal Transduction. Annual Review of Plant Biology 55 (1):373-399.

50. Halliwell B (1991) Reactive oxygen species in living systems: Source, biochemistry, and role in human disease. The American Journal of Medicine 91 (3, Supplement 3):S14-S22.

51. Wolf FI, Trapani V, Simonacci M, Boninsegna A, Mazur A, Maier JA (2009) Magnesium deficiency affects mammary epithelial cell proliferation: involvement of oxidative stress. Nutrition and cancer 61 (1):131-136.

52. Wang FL, Wang R, Khairallah EA, Schwartz R (1971) Magnesium depletion during gestation and lactation in rats. The Journal of nutrition 101 (9):1201-1209

53. Hurley LS, Cosens G, Theriault LL (1976) Teratogenic effects of magnesium deficiency in rats. The Journal of nutrition 106 (9):1254-1260.

54. Venu L, Padmavathi IJ, Kishore YD, Bhanu NV, Rao KR, Sainath PB, Ganeshan M, Raghunath M (2008) Long-term effects of maternal magnesium restriction on adiposity and insulin resistance in rat pups. Obesity 16 (6):1270-1276.

55. Makrides M, Crowther CA (2001) Magnesium supplementation in pregnancy. The Cochrane database of systematic reviews (4):CD000937.

56. Elin RJ (1988) Magnesium metabolism in health and disease. Disease-a-month : DM 34 (4):161-218

57. Jahnen-Dechent W, Ketteler M (2012) Magnesium basics. Clinical Kidney Journal 5 (Suppl 1):i3-i14.

58. Eliezer D, Aghion E, Froes FH (1998) Magnesium Science, Technology and Applications. Advanced Performance Materials 5 (3):201-212.

59. Brar H, Platt M, Sarntinoranont M, Martin P, Manuel M (2009) Magnesium as a biodegradable and bioabsorbable material for medical implants. JOM 61 (9):31-34.

60. Staiger MP, Pietak AM, Huadmai J, Dias G (2006) Magnesium and its alloys as orthopedic biomaterials: a review. Biomaterials 27 (9):1728-1734.

61. Busscher HJ, van der Mei HC, Subbiahdoss G, Jutte PC, van den Dungen JJAM, Zaat SAJ, Schultz MJ, Grainger DW (2012) Biomaterial-Associated Infection: Locating the Finish Line in the Race for the Surface. Science Translational Medicine 4 (153):153rv110.

62. Robinson DA, Griffith RW, Shechtman D, Evans RB, Conzemius MG (2010) In vitro antibacterial properties of magnesium metal against Escherichia coli, Pseudomonas aeruginosa and Staphylococcus aureus. Acta biomaterialia 6 (5):1869-1877.
63. Higgins DM, Basaraba RJ, Hohnbaum AC, Lee EJ, Grainger DW, Gonzalez-Juarrero M (2009) Localized immunosuppressive environment in the foreign body response to implanted biomaterials. The American journal of pathology 175 (1):161-170.
64. Dalal A, Pawar V, McAllister K, Weaver C, Hallab NJ (2012) Orthopedic implant cobalt-alloy particles produce greater toxicity and inflammatory cytokines than titanium alloy and zirconium alloy-based particles in vitro, in human osteoblasts, fibroblasts, and macrophages. Journal of Biomedical Materials Research Part A 100A (8):2147-2158.
65. Xu L, Pan F, Yu G, Yang L, Zhang E, Yang K (2009) In vitro and in vivo evaluation of the surface bioactivity of a calcium phosphate coated magnesium alloy. Biomaterials 30 (8):1512-1523.
66. Xu L, Yamamoto A (2012) Characteristics and cytocompatibility of biodegradable polymer film on magnesium by spin coating. Colloids and Surfaces B: Biointerfaces 93 (0):67-74.
67. Gu X, Zheng Y, Cheng Y, Zhong S, Xi T (2009) In vitro corrosion and biocompatibility of binary magnesium alloys. Biomaterials 30 (4):484-498.
68. Zhang S, Li J, Song Y, Zhao C, Zhang X, Xie C, Zhang Y, Tao H, He Y, Jiang Y, Bian Y (2009) In vitro degradation, hemolysis and MC3T3-E1 cell adhesion of biodegradable Mg–Zn alloy. Materials Science and Engineering: C 29 (6):1907-1912.
69. Gu X, Zheng Y, Zhong S, Xi T, Wang J, Wang W (2010) Corrosion of, and cellular responses to Mg–Zn–Ca bulk metallic glasses. Biomaterials 31 (6):1093-1103.
70. Liu L, Li N, Lei T, Li K, Zhang Y (2014) The in vitro biological properties of Mg-Zn-Sr alloy and superiority for preparation of biodegradable intestinal anastomosis rings. Medical science monitor : international medical journal of experimental and clinical research 20:1056-1066
71. Witte F, Fischer J, Nellesen J, Crostack H-A, Kaese V, Pisch A, Beckmann F, Windhagen H (2006) In vitro and in vivo corrosion measurements of magnesium alloys. Biomaterials 27 (7):1013-1018.
72. Huehnerschulte TA, Reifenrath J, von Rechenberg B, Dziuba D, Seitz JM, Bormann D, Windhagen H, Meyer-Lindenberg A (2012) In vivo assessment of the host reactions to the biodegradation of the two novel magnesium alloys ZEK100 and AX30 in an animal model. Biomedical engineering online 11:14.
73. Waizy H, Diekmann J, Weizbauer A, Reifenrath J, Bartsch I, Neubert V, Schavan R, Windhagen H (2014) In vivo study of a biodegradable orthopedic screw (MgYREZr-alloy) in a rabbit model for up to 12 months. Journal of biomaterials applications 28 (5):667-675.
74. Badar M, Lunsdorf H, Evertz F, Rahim MI, Glasmacher B, Hauser H, Mueller PP (2013) The formation of an organic coat and the release of corrosion microparticles from metallic magnesium implants. Acta biomaterialia 9 (7):7580-7589.
75. Altun H, Sen S (2004) Studies on the influence of chloride ion concentration and pH on the corrosion and electrochemical behaviour of AZ63 magnesium alloy. Materials & Design 25 (7):637-643.

76. Tunold R, Holtan H, Berge M-BH, Lasson A, Steen-Hansen R (1977) The corrosion of magnesium in aqueous solution containing chloride ions. Corrosion Science 17 (4):353-365.
77. Zeng R-c, Zhang J, Huang W-j, Dietzel W, Kainer KU, Blawert C, Ke W (2006) Review of studies on corrosion of magnesium alloys. Transactions of Nonferrous Metals Society of China 16, Supplement 2 (0):s763-s771.
78. Kuhlmann J, Bartsch I, Willbold E, Schuchardt S, Holz O, Hort N, Höche D, Heineman WR, Witte F (2013) Fast escape of hydrogen from gas cavities around corroding magnesium implants. Acta biomaterialia 9 (10):8714-8721.
79. Witte F (2010) The history of biodegradable magnesium implants: A review. Acta biomaterialia 6 (5):1680-1692.
80. Kraus T, Fischerauer SF, Hänzi AC, Uggowitzer PJ, Löffler JF, Weinberg AM (2012) Magnesium alloys for temporary implants in osteosynthesis: In vivo studies of their degradation and interaction with bone. Acta biomaterialia 8 (3):1230-1238.
81. Song G (2007) Control of biodegradation of biocompatable magnesium alloys. Corrosion Science 4 (49):1696–1701.
82. C.K. Seal KVaMAH (2009) Biodegradable Surgical Implants based on Magnesium Alloys - A Review of Current Research. IOP Conference Series: Materials Science and Engineering 4 (1).
83. Iskandar ME, Aslani A, Liu H (2013) The effects of nanostructured hydroxyapatite coating on the biodegradation and cytocompatibility of magnesium implants. Journal of Biomedical Materials Research Part A 101A (8):2340-2354.
84. Foster TJ, Höök M (1998) Surface protein adhesins of Staphylococcus aureus. Trends in microbiology 6 (12):484-488.
85. Zberg B, Uggowitzer PJ, Loffler JF (2009) MgZnCa glasses without clinically observable hydrogen evolution for biodegradable implants. Nat Mater 8 (11):887-891.
86. Feyerabend F, Fischer J, Holtz J, Witte F, Willumeit R, Drücker H, Vogt C, Hort N (2010) Evaluation of short-term effects of rare earth and other elements used in magnesium alloys on primary cells and cell lines. Acta biomaterialia 6 (5):1834-1842.
87. Wong HM, Yeung KWK, Lam KO, Tam V, Chu PK, Luk KDK, Cheung KMC (2010) A biodegradable polymer-based coating to control the performance of magnesium alloy orthopaedic implants. Biomaterials 31 (8):2084-2096.
88. Gristina AG (1987) Biomaterial-centered infection: microbial adhesion versus tissue integration. Science 237 (4822):1588-1595.
89. Rohde H, Frankenberger S, Zähringer U, Mack D (2010) Structure, function and contribution of polysaccharide intercellular adhesin (PIA) to Staphylococcus epidermidis biofilm formation and pathogenesis of biomaterial-associated infections. European journal of cell biology 89 (1):103-111.

90. Cazander G, van Veen KB, Bouwman L, Bernards A, Jukema G (2009) The Influence of Maggot Excretions on PAO1 Biofilm Formation on Different Biomaterials. Clinical orthopaedics and related research 467 (2):536-545.

91. Legeay G, Poncin-Epaillard F, Arciola CR (2006) New surfaces with hydrophilic/hydrophobic characteristics in relation to (no)bioadhesion. The International journal of artificial organs 29 (4):453-461

92. Grilo IR, Ludovice AM, Tomasz A, de Lencastre H, Sobral RG (2014) The glucosaminidase domain of Atl - the major Staphylococcus aureus autolysin - has DNA-binding activity. MicrobiologyOpen 3 (2):247-256.

93. Weinstein RA, Darouiche RO (2001) Device-Associated Infections: A Macroproblem that Starts with Microadherence. Clinical Infectious Diseases 33 (9):1567-1572.

94. Vuong C, Saenz HL, Götz F, Otto M (2000) Impact of the agr Quorum-Sensing System on Adherence to Polystyrene in Staphylococcus aureus. Journal of Infectious Diseases 182 (6):1688-1693.

95. Gristina AG (1994) Implant failure and the immuno-incompetent fibro-inflammatory zone. Clinical orthopaedics and related research (298):106-118.

96. An YH, Friedman RJ (1998) Concise review of mechanisms of bacterial adhesion to biomaterial surfaces. Journal of biomedical materials research 43 (3):338-348.

97. Schierholz JM, Beuth J (2001) Implant infections: a haven for opportunistic bacteria. The Journal of hospital infection 49 (2):87-93.

98. Costerton JW, Stewart PS, Greenberg EP (1999) Bacterial biofilms: a common cause of persistent infections. Science 284 (5418):1318-1322

99. Vlamakis H, Chai Y, Beauregard P, Losick R, Kolter R (2013) Sticking together: building a biofilm the Bacillus subtilis way. Nat Rev Micro 11 (3):157-168.

100. Flemming H-C, Wingender J (2010) The biofilm matrix. Nat Rev Micro 8 (9):623-633

101. O'Neill E, Pozzi C, Houston P, Humphreys H, Robinson DA, Loughman A, Foster TJ, O'Gara JP (2008) A novel Staphylococcus aureus biofilm phenotype mediated by the fibronectin-binding proteins, FnBPA and FnBPB. J Bacteriol 190 (11):3835-3850.

102. Cramton SE, Gerke C, Schnell NF, Nichols WW, Gotz F (1999) The intercellular adhesion (ica) locus is present in Staphylococcus aureus and is required for biofilm formation. Infection and immunity 67 (10):5427-5433

103. Sutherland IW (2001) The biofilm matrix – an immobilized but dynamic microbial environment. Trends in microbiology 9 (5):222-227.

104. Yarwood JM, Bartels DJ, Volper EM, Greenberg EP (2004) Quorum Sensing in Staphylococcus aureus Biofilms. Journal of Bacteriology 186 (6):1838-1850.

105. Arciola CR, Campoccia D, Speziale P, Montanaro L, Costerton JW (2012) Biofilm formation in Staphylococcus implant infections. A review of molecular mechanisms and implications for biofilm-resistant materials. Biomaterials 33 (26):5967-5982.

106. Klausen M, Heydorn A, Ragas P, Lambertsen L, Aaes-Jørgensen A, Molin S, Tolker-Nielsen T (2003) Biofilm formation by Pseudomonas aeruginosa wild type, flagella and type IV pili mutants. Molecular Microbiology 48 (6):1511-1524.

107. Kraus-Haas M, Mielke M, Simon A (2015) [Update on outbreaks reported from neonatal intensive care units: Serratia marcescens, Klebsiella pneumoniae, Acinetobacter baumannii, and Pseudomonas aeruginosa. Bundesgesundheitsblatt, Gesundheitsforschung, Gesundheitsschutz 58(3):308-22.

108. Hentzer M, Teitzel GM, Balzer GJ, Heydorn A, Molin S, Givskov M, Parsek MR (2001) Alginate Overproduction Affects Pseudomonas aeruginosa Biofilm Structure and Function. Journal of Bacteriology 183 (18):5395-5401.

109. Prabhawathi V, Thirunavukarasu K, Doble M (2014) A study on the long term effect of biofilm produced by biosurfactant producing microbe on medical implant. Materials science & engineering C, Materials for biological applications 40:212-218.

110. Schurr MJ, Okkotsu Y, Little AS (2014) The Pseudomonas aeruginosa AlgZR Two-Component System Coordinates Multiple Phenotypes. Frontiers in Cellular and Infection Microbiology 4:82.

111. Davies DG, Geesey GG (1995) Regulation of the alginate biosynthesis gene algC in Pseudomonas aeruginosa during biofilm development in continuous culture. Applied and environmental microbiology 61 (3):860-867.

112. Stickler DJ, Morris NS, McLean RJ, Fuqua C (1998) Biofilms on indwelling urethral catheters produce quorum-sensing signal molecules in situ and in vitro. Applied and environmental microbiology 64 (9):3486-3490.

113. Kashimura N, Kusachi S, Konishi T, Shimizu J, Kusunoki M, Oka M, Wakatsuki T, Sumiyama Y (2012) Impact of surgical site infection after colorectal surgery on hospital stay and medical expenditure in Japan. Surg Today 42 (7):639-645.

114. Veerachamy S, Yarlagadda T, Manivasagam G, Yarlagadda PK (2014) Bacterial adherence and biofilm formation on medical implants: A review. Proceedings of the Institution of Mechanical Engineers, Part H: Journal of Engineering in Medicine 228 (10):1083-1099.

115. Cucarella C, Solano C, Valle J, Amorena B, Lasa Í, Penadés JR (2001) Bap, a Staphylococcus aureus Surface Protein Involved in Biofilm Formation. Journal of Bacteriology 183 (9):2888-2896.

116. Houston P, Rowe SE, Pozzi C, Waters EM, O'Gara JP (2011) Essential role for the major autolysin in the fibronectin-binding protein-mediated *Staphylococcus aureus* biofilm phenotype. Infection and immunity 79 (3):1153-1165.

117. Boles BR, Horswill AR (2008) agr-Mediated Dispersal of *Staphylococcus aureus* Biofilms. PLoS pathogens 4 (4):e1000052.

118. Whitchurch CB, Tolker-Nielsen T, Ragas PC, Mattick JS (2002) Extracellular DNA Required for Bacterial Biofilm Formation. Science 295 (5559):1487.

119. Davies DG, Parsek MR, Pearson JP, Iglewski BH, Costerton JW, Greenberg EP (1998) The Involvement of Cell-to-Cell Signals in the Development of a Bacterial Biofilm. Science 280 (5361):295-298.

120. De Kievit TR, Gillis R, Marx S, Brown C, Iglewski BH (2001) Quorum-Sensing Genes in Pseudomonas aeruginosa Biofilms: Their Role and Expression Patterns. Applied and environmental microbiology 67 (4):1865-1873.

121. Costerton JW, Stewart PS, Greenberg EP (1999) Bacterial Biofilms: A Common Cause of Persistent Infections. Science 284 (5418):1318-1322.

122. Barraud N, Hassett DJ, Hwang S-H, Rice SA, Kjelleberg S, Webb JS (2006) Involvement of Nitric Oxide in Biofilm Dispersal of Pseudomonas aeruginosa. Journal of Bacteriology 188 (21):7344-7353.

123. Darouiche RO (2004) Treatment of infections associated with surgical implants. The New England journal of medicine 350 (14):1422-1429.

124. Hetrick EM, Schoenfisch MH (2006) Reducing implant-related infections: active release strategies. Chemical Society Reviews 35 (9):780-789.

125. Wu P, Grainger DW (2006) Drug/device combinations for local drug therapies and infection prophylaxis. Biomaterials 27 (11):2450-2467.

126. Stigter M, Bezemer J, de Groot K, Layrolle P (2004) Incorporation of different antibiotics into carbonated hydroxyapatite coatings on titanium implants, release and antibiotic efficacy. Journal of Controlled Release 99 (1):127-137.

127. Huh AJ, Kwon YJ (2011) "Nanoantibiotics": A new paradigm for treating infectious diseases using nanomaterials in the antibiotics resistant era. Journal of Controlled Release 156 (2):128-145.

128. Pauksch L, Hartmann S, Rohnke M, Szalay G, Alt V, Schnettler R, Lips KS (2014) Biocompatibility of silver nanoparticles and silver ions in primary human mesenchymal stem cells and osteoblasts. Acta biomaterialia 10 (1):439-449.

129. Jin G, Qin H, Cao H, Qian S, Zhao Y, Peng X, Zhang X, Liu X, Chu PK (2014) Synergistic effects of dual Zn/Ag ion implantation in osteogenic activity and antibacterial ability of titanium. Biomaterials 35 (27):7699-7713.

130. Lu Y, Slomberg DL, Schoenfisch MH (2014) Nitric oxide-releasing chitosan oligosaccharides as antibacterial agents. Biomaterials 35 (5):1716-1724.

131. Barraud N, J. Kelso M, A. Rice S, Kjelleberg S (2015) Nitric Oxide: A Key Mediator of Biofilm Dispersal with Applications in Infectious Diseases. Current Pharmaceutical Design 21 (1):31-42.

132. Hook AL, Chang C-Y, Yang J, Luckett J, Cockayne A, Atkinson S, Mei Y, Bayston R, Irvine DJ, Langer R, Anderson DG, Williams P, Davies MC, Alexander MR (2012) Combinatorial discovery of polymers resistant to bacterial attachment. Nat Biotech 30 (9):868-875.

133. de la Fuente-Núñez C, Reffuveille F, Haney EF, Straus SK, Hancock REW (2014) Broad-Spectrum Anti-biofilm Peptide That Targets a Cellular Stress Response. PLoS pathogens 10 (5):e1004152.

134. Balaban N, Giacometti A, Cirioni O, Gov Y, Ghiselli R, Mocchegiani F, Viticchi C, Del Prete MS, Saba V, Scalise G, Dell'Acqua G (2003) Use of the Quorum-Sensing Inhibitor RNAIII-Inhibiting Peptide to Prevent Biofilm Formation In Vivo by Drug-Resistant Staphylococcus epidermidis. Journal of Infectious Diseases 187 (4):625-630.

135. Christensen GD, Simpson WA, Bisno AL, Beachey EH (1983) Experimental foreign body infections in mice challenged with slime-producing Staphylococcus epidermidis. Infection and immunity 40 (1):407-410.

136. Chauhan A, Lebeaux D, Decante B, Kriegel I, Escande M-C, Ghigo J-M, Beloin C (2012) A Rat Model of Central Venous Catheter to Study Establishment of Long-Term Bacterial Biofilm and Related Acute and Chronic Infections. PloS one 7 (5):e37281.

137. Rupp ME, Ulphani JS, Fey PD, Mack D (1999) Characterization of Staphylococcus epidermidisPolysaccharide Intercellular Adhesin/Hemagglutinin in the Pathogenesis of Intravascular Catheter-Associated Infection in a Rat Model. Infection and immunity 67 (5):2656-2659.

138. Ebert T, Smith S, Pancari G, Wu X, Zorman J, Clark D, Cook J, Burns C, Antonello JM, Cope L, Nagy E, Meinke A, McNeely T (2011) Development of a rat central venous catheter model for evaluation of vaccines to prevent Staphylococcus epidermidis and Staphylococcus aureus early biofilms. Human Vaccines 7 (6):630-638.

139. Langerman L, Chaimsky G, Golomb E, Tverskoy M, Kook AI, Benita S (1990) A Rabbit Model for Evaluation of Spinal Anesthesia: Chronic Cannulation of the Subarachnoid Space. Anesthesia & Analgesia 71 (5):529-535.

140. Andriole VT, Nagel DA, Southwick WO (1973) A paradigm for human chronic osteomyelitis. The Journal of bone and joint surgery American volume 55 (7):1511-1515

141. Lucke M, Wildemann B, Sadoni S, Surke C, Schiller R, Stemberger A, Raschke M, Haas NP, Schmidmaier G (2005) Systemic versus local application of gentamicin in prophylaxis of implant-related osteomyelitis in a rat model. Bone 36 (5):770-778.

142. Inglis TJ, Millar MR, Jones JG, Robinson DA (1989) Tracheal tube biofilm as a source of bacterial colonization of the lung. Journal of Clinical Microbiology 27 (9):2014-2018.

143. Gil-Perotin S, Ramirez P, Marti V, Sahuquillo JM, Gonzalez E, Calleja I, Menendez R, Bonastre J (2012) Implications of endotracheal tube biofilm in ventilator-associated pneumonia response: a state of concept. Critical Care 16 (3):R93-R93.

144. Garrigós C, Murillo O, Lora-Tamayo J, Verdaguer R, Tubau F, Cabellos C, Cabo J, Ariza J (2013) Fosfomycin-Daptomycin and Other Fosfomycin Combinations as Alternative Therapies in Experimental Foreign-Body Infection by Methicillin-Resistant Staphylococcus aureus. Antimicrobial agents and chemotherapy 57 (1):606-610.

145. Rupp ME, Fey PD (2001) In Vivo Models to evaluate adhesion and biofilm formation by staphylococcus epidermidis. In: Ron JD (ed) Methods in Enzymology, vol Volume 336. Academic Press, pp 206-215.

146. Kadurugamuwa JL, Sin L, Albert E, Yu J, Francis K, DeBoer M, Rubin M, Bellinger-Kawahara C, Parr J, T. R., Contag PR (2003) Direct Continuous Method for Monitoring Biofilm Infection in a Mouse Model. Infection and immunity 71 (2):882-890.

147. Beenken KE, Dunman PM, McAleese F, Macapagal D, Murphy E, Projan SJ, Blevins JS, Smeltzer MS (2004) Global Gene Expression in Staphylococcus aureus Biofilms. Journal of Bacteriology 186 (14):4665-4684.

148. Ensing GT, Roeder BL, Nelson JL, van Horn JR, van der Mei HC, Busscher HJ, Pitt WG (2005) Effect of pulsed ultrasound in combination with gentamicin on bacterial killing of biofilms on bone cements in vivo. Journal of applied microbiology 99 (3):443-448.

149. Darouiche RO, Mansouri MD, Meade R (2002) In-vitro and in-vivo activity of antimicrobial-coated prosthetic heart valve sewing cuffs. The Journal of heart valve disease 11 (1):99-104.

150. Cirioni O, Mocchegiani F, Cacciatore I, Vecchiet J, Silvestri C, Baldassarre L, Ucciferri C, Orsetti E, Castelli P, Provinciali M, Vivarelli M, Fornasari E, Giacometti A (2013) Quorum sensing inhibitor FS3-coated vascular graft enhances daptomycin efficacy in a rat model of staphylococcal infection. Peptides 40 (0):77-81.

151. Becher A, Schweizer HP (2000) Integration-proficient Pseudomonas aeruginosa vectors for isolation of single-copy chromosomal lacZ and lux gene fusions. BioTechniques 29 (5):948-950, 952.

152. Fletcher MP, Diggle SP, Camara M, Williams P (2007) Biosensor-based assays for PQS, HHQ and related 2-alkyl-4-quinolone quorum sensing signal molecules. Nature protocols 2 (5):1254-1262.

153. Stern C, Kasnitz N, Kocijancic D, Trittel S, Riese P, Guzman CA, Leschner S, Weiss S (2015) Induction of CD4+ and CD8+ anti-tumor effector T cell responses by bacteria mediated tumor therapy. International Journal of Cancer: 137: 2019–2028.

154. Leschner S, Weiss S (2010) Salmonella—allies in the fight against cancer. J Mol Med 88 (8):763-773.

155. Lienenklaus S, Cornitescu M, Zietara N, Lyszkiewicz M, Gekara N, Jablonska J, Edenhofer F, Rajewsky K, Bruder D, Hafner M, Staeheli P, Weiss S (2009) Novel reporter mouse reveals constitutive and inflammatory expression of IFN-beta in vivo. Journal of immunology 183 (5):3229-3236.

156. Materials. ASfTa (2004) ASTM-G31-72: Standard practice for laboratory immersion corrosion testing of metals. . Annual Book of ASTM Standards. American Society for Testing and Materials, Philadelphia, PA:

157. Lienenklaus S, Cornitescu M, Ziętara N, Łyszkiewicz M, Gekara N, Jabłońska J, Edenhofer F, Rajewsky K, Bruder D, Hafner M, Staeheli P, Weiss S (2009) Novel Reporter Mouse Reveals Constitutive and Inflammatory Expression of IFN-β In Vivo. The Journal of Immunology 183 (5):3229-3236.

158. Spurr AR (1969) A low-viscosity epoxy resin embedding medium for electron microscopy. Journal of ultrastructure research 26 (1):31-43.

159. Bancroft JD, Gamble M (2008) Theory and Practice of Histological Techniques. Churchill Livingstone 6th Ed.

160. Mulisch M, Welsch U (2010) Romeis Mikroskopische Technik. Spektrum Akademischer Verlag,

161. Castellani C, Lindtner RA, Hausbrandt P, Tschegg E, Stanzl-Tschegg SE, Zanoni G, Beck S, Weinberg A-M (2011) Bone–implant interface strength and osseointegration: Biodegradable magnesium alloy versus standard titanium control. Acta biomaterialia 7 (1):432-440.

162. Bogdan C, Mattner J, Schleicher U (2004) The role of type I interferons in non-viral infections. Immunological reviews 202:33-48.

163. Jackson A, Nanton MR, O'Donnell H, Akue AD, McSorley SJ (2010) Innate Immune Activation during Salmonella Infection Initiates Extramedullary Erythropoiesis and Splenomegaly. Journal of immunology (Baltimore, Md : 1950) 185 (10):6198-6204.

164. Parsek MR, Singh PK (2003) Bacterial biofilms: an emerging link to disease pathogenesis. Annual review of microbiology 57:677-701.

165. Wilson CJ, Clegg RE, Leavesley DI, Pearcy MJ (2005) Mediation of biomaterial-cell interactions by adsorbed proteins: a review. Tissue engineering 11 (1-2):1-18.

166. Naddaf Dezfuli S, Huan Z, Mol JMC, Leeflang MA, Chang J, Zhou J (2014) Influence of HEPES buffer on the local pH and formation of surface layer during in vitro degradation tests of magnesium in DMEM. Progress in Natural Science: Materials International 24 (5):531-538.

167. Xin Y, Hu T, Chu PK (2011) In vitro studies of biomedical magnesium alloys in a simulated physiological environment: A review. Acta biomaterialia 7 (4):1452-1459.

168. Mc BE (1938) Absorbable metal in bone surgery: A further report on the use of magnesium alloys. Journal of the American Medical Association 111 (27):2464-2467.

169. Killian MS, Wagener V, Schmuki P, Virtanen S (2010) Functionalization of Metallic Magnesium with Protein Layers via Linker Molecules. Langmuir 26 (14):12044-12048.

170. Liu C, Xin Y, Tian X, Chu PK (2007) Degradation susceptibility of surgical magnesium alloy in artificial biological fluid containing albumin. Journal of Materials Research 22 (07):1806-1814.

171. Lindström R, Johansson L-G, Thompson GE, Skeldon P, Svensson J-E (2004) Corrosion of magnesium in humid air. Corrosion Science 46 (5):1141-1158.

172. Xin Y, Huo K, Tao H, Tang G, Chu PK (2008) Influence of aggressive ions on the degradation behavior of biomedical magnesium alloy in physiological environment. Acta biomaterialia 4 (6):2008-2015.

173. Song KS, Kang CH, Min BW, Bae KC, Cho CH, Lee JH (2008) Closed Reduction and Internal Fixation of Displaced Unstable Lateral Condylar Fractures of the Humerus in Children, 90(12):2673-81.

174. Chen D, He Y, Tao H, Zhang Y, Jiang Y, Zhang X, Zhang S (2011) Biocompatibility of magnesium-zinc alloy in biodegradable orthopedic implants. International journal of molecular medicine 28 (3):343-348.

175. Chaya A, Yoshizawa S, Verdelis K, Myers N, Costello BJ, Chou D-T, Pal S, Maiti S, Kumta PN, Sfeir C In vivo study of magnesium plate and screw degradation and bone fracture healing. Acta biomaterialia 18:262-9.

176. Windhagen H, Radtke K, Weizbauer A, Diekmann J, Noll Y, Kreimeyer U, Schavan R, Stukenborg-Colsman C, Waizy H (2013) Biodegradable magnesium-based screw clinically equivalent to titanium screw in hallux valgus surgery: short term results of the first prospective, randomized, controlled clinical pilot study. Biomedical engineering online 12:62.

177. Lindtner RA, Castellani C, Tangl S, Zanoni G, Hausbrandt P, Tschegg EK, Stanzl-Tschegg SE, Weinberg AM (2013) Comparative biomechanical and radiological characterization of osseointegration of a biodegradable magnesium alloy pin and a copolymeric control for osteosynthesis. Journal of the mechanical behavior of biomedical materials 28:232-243.

178. Castellani C, Lindtner RA, Hausbrandt P, Tschegg E, Stanzl-Tschegg SE, Zanoni G, Beck S, Weinberg AM (2011) Bone-implant interface strength and osseointegration: Biodegradable magnesium alloy versus standard titanium control. Acta biomaterialia 7 (1):432-440.

179. Thomann M, Krause C, Bormann D, von der Höh N, Windhagen H, Meyer-Lindenberg A (2009) Comparison of the resorbable magnesium . alloys LAE442 und MgCa0.8 concerning their mechanical properties, their progress of degradation and the bone-implant-contact after 12 months implantation duration in a rabbit model. Materialwissenschaft und Werkstofftechnik 40 (1-2):82-87.

180. Lin X, Yang X, Tan L, Li M, Wang X, Zhang Y, Yang K, Hu Z, Qiu J (2014) In vitro degradation and biocompatibility of a strontium-containing micro-arc oxidation coating on the biodegradable ZK60 magnesium alloy. Applied Surface Science 288 (0):718-726.

181. Yang L, Hort N, Laipple D, Hoche D, Huang Y, Kainer KU, Willumeit R, Feyerabend F (2013) Element distribution in the corrosion layer and cytotoxicity of alloy Mg-10Dy during in vitro biodegradation. Acta biomaterialia 9 (10):8475-8487.

182. Rettig R, Virtanen S (2009) Composition of corrosion layers on a magnesium rare-earth alloy in simulated body fluids. Journal of biomedical materials research Part A 88 (2):359-369.

183. Jang Y, Collins B, Sankar J, Yun Y (2013) Effect of biologically relevant ions on the corrosion products formed on alloy AZ31B: An improved understanding of magnesium corrosion. Acta biomaterialia 9 (10):8761-8770.

184. Willumeit R, Fischer J, Feyerabend F, Hort N, Bismayer U, Heidrich S, Mihailova B (2011) Chemical surface alteration of biodegradable magnesium exposed to corrosion media. Acta biomaterialia 7 (6):2704-2715.

185. Hassane Assaaoudi ZF, Ian S. Butler, Dominic, H. Ryan, Janusz A. Kozinski (2007) Characterization of a new magnesium hydrogen orthophosphate salt, $Mg_3.5H_2(PO_4)_3$, synthesized in supercritical water. Solid state sciences 9:385-393.

186. Bartl H, Catti M, Joswig W, Ferraris G (1983) Investigation of the crystal structure of newberyite, MgHPO4·3H2O, by single crystal neutron diffraction. TMPM Tschermaks Petr Mitt 32 (2-3):187-194.

187. Abbona F, Lundager Madsen HE, Boistelle R (1982) Crystallization of two magnesium phosphates, struvite and newberyite: Effect of pH and concentration. Journal of Crystal Growth 57 (1):6-14.

188. Kirkland N, Waterman J, Birbilis N, Dias G, Woodfield TF, Hartshorn R, Staiger M (2012) Buffer-regulated biocorrosion of pure magnesium. J Mater Sci: Mater Med 23 (2):283-291.
189. Huan ZG, Leeflang MA, Zhou J, Fratila-Apachitei LE, Duszczyk J (2010) In vitro degradation behavior and cytocompatibility of Mg–Zn–Zr alloys. J Mater Sci: Mater Med 21 (9):2623-2635.
190. Witte F, Hort N, Vogt C, Cohen S, Kainer KU, Willumeit R, Feyerabend F (2008) Degradable biomaterials based on magnesium corrosion. Current Opinion in Solid State and Materials Science 12 (5–6):63-72.
191. Seuss F, Seuss S, Turhan MC, Fabry B, Virtanen S (2011) Corrosion of Mg alloy AZ91D in the presence of living cells. Journal of Biomedical Materials Research Part B: Applied Biomaterials 99B (2):276-281.
192. Song G, Song S (2007) A possible biodegradable magnesium implant material. Advanced Engineering Materials 9 (4):298-302.
193. Purnama A, Hermawan H, Champetier S, Mantovani D, Couet J (2013) Gene expression profile of mouse fibroblasts exposed to a biodegradable iron alloy for stents. Acta biomaterialia 9 (10):8746-8753.
194. Drynda A, Deinet N, Braun N, Peuster M (2009) Rare earth metals used in biodegradable magnesium-based stents do not interfere with proliferation of smooth muscle cells but do induce the upregulation of inflammatory genes. Journal of Biomedical Materials Research Part A 91A (2):360-369.
195. Schumacher S, Roth I, Stahl J, Bäumer W, Kietzmann M (2014) Biodegradation of metallic magnesium elicits an inflammatory response in primary nasal epithelial cells. Acta biomaterialia 10 (2):996-1004.
196. Salunke P, Shanov V, Witte F (2011) High purity biodegradable magnesium coating for implant application. Materials Science and Engineering: B 176 (20):1711-1717.
197. Bartsch I, Willbold E, Rosenhahn B, Witte F (2014) Non-invasive pH determination adjacent to degradable biomaterials in vivo. Acta biomaterialia 10 (1):34-39.
198. Kim J, Dadsetan M, Ameenuddin S, Windebank AJ, Yaszemski MJ, Lu L (2010) In vivo biodegradation and biocompatibility of PEG/sebacic acid-based hydrogels using a cage implant system. Journal of biomedical materials research Part A 95 (1):191-197.
199. Chinn JA, Sauter JA, Phillips RE, Kao WJ, Anderson JM, Hanson SR, Ashton TR (1998) Blood and tissue compatibility of modified polyester: Thrombosis, inflammation, and healing. Journal of biomedical materials research 39 (1):130-140.
200. Li Y, Liu G, Zhai Z, Liu L, Li H, Yang K, Tan L, Wan P, Liu X, Ouyang Z, Yu Z, Tang T, Zhu Z, Qu X, Dai K (2014) Antibacterial properties of magnesium in an in vitro and in vivo model of implant-associated MRSA infection. Antimicrobial agents and chemotherapy 58(12):7586-91.
201. Zeng J, Ren L, Yuan Y, Wang Y, Zhao J, Zeng R, Yang K, Mei X (2013) Short-term effect of magnesium implantation on the osteomyelitis modeled animals induced by Staphylococcus aureus. Journal of materials science Materials in medicine 24 (10):2405-2416.

202. Komor U, Bielecki P, Loessner H, Rohde M, Wolf K, Westphal K, Weiss S, Häussler S (2012) Biofilm formation by Pseudomonas aeruginosa in solid murine tumors – a novel model system. Microbes and Infection 14 (11):951-958.
203. Fang A, Hu SS, Endres N, Bradford DS (2005) Risk Factors for Infection After Spinal Surgery. Spine 30 (12):1460-1465.
204. Mulvey MA, Schilling JD, Hultgren SJ (2001) Establishment of a persistent Escherichia coli reservoir during the acute phase of a bladder infection. Infection and immunity 69 (7):4572-4579.
205. Berk V, Fong JC, Dempsey GT, Develioglu ON, Zhuang X, Liphardt J, Yildiz FH, Chu S (2012) Molecular architecture and assembly principles of Vibrio cholerae biofilms. Science 337 (6091):236-239.
206. Hannig C, Follo M, Hellwig E, Al-Ahmad A (2010) Visualization of adherent micro-organisms using different techniques. Journal of medical microbiology 59 (1):1-7.
207. Whiteley M, Bangera MG, Bumgarner RE, Parsek MR, Teitzel GM, Lory S, Greenberg EP (2001) Gene expression in Pseudomonas aeruginosa biofilms. Nature 413 (6858):860-864.
208. Singh PK, Parsek MR, Greenberg EP, Welsh MJ (2002) A component of innate immunity prevents bacterial biofilm development. Nature 417 (6888):552-555.
209. van Gennip M, Christensen LD, Alhede M, Qvortrup K, Jensen PO, Hoiby N, Givskov M, Bjarnsholt T (2012) Interactions between polymorphonuclear leukocytes and Pseudomonas aeruginosa biofilms on silicone implants in vivo. Infection and immunity 80 (8):2601-2607.
210. Davies D (2003) Understanding biofilm resistance to antibacterial agents. Nat Rev Drug Discov 2 (2):114-122.
211. Brooun A, Liu S, Lewis K (2000) A dose-response study of antibiotic resistance in Pseudomonas aeruginosa biofilms. Antimicrobial agents and chemotherapy 44 (3):640-646.
212. Bassler BL (2002) Small talk. Cell-to-cell communication in bacteria. Cell 109 (4):421-424.
213. O'Loughlin CT, Miller LC, Siryaporn A, Drescher K, Semmelhack MF, Bassler BL (2013) A quorum-sensing inhibitor blocks Pseudomonas aeruginosa virulence and biofilm formation. Proceedings of the National Academy of Sciences 110 (44):17981-17986.
214. Fulcher TP, Dart JKG, McLaughlin-Borlace L, Howes R, Matheson M, Cree I (2001) Demonstration of biofilm in infectious crystalline keratopathy using ruthenium red and electron microscopy. Ophthalmology 108 (6):1088-1092.
215. Anderson GG, Palermo JJ, Schilling JD, Roth R, Heuser J, Hultgren SJ (2003) Intracellular bacterial biofilm-like pods in urinary tract infections. Science 301 (5629):105-107. doi:10.1126/science.1084550.
216. Donlan RM, Costerton JW (2002) Biofilms: Survival Mechanisms of Clinically Relevant Microorganisms. Clinical Microbiology Reviews 15 (2):167-193.
217. Hall-Stoodley L, Costerton JW, Stoodley P (2004) Bacterial biofilms: from the Natural environment to infectious diseases. Nat Rev Micro 2 (2):95-108.
218. Xu KD, McFeters GA, Stewart PS (2000) Biofilm resistance to antimicrobial agents. Microbiology 146 (Pt 3):547-549.

219. Park HR, Hong MK, Hwang SY, Park YK, Kwon KH, Yoon JW, Shin S, Kim JH, Park YH (2014) Characterisation of Pseudomonas aeruginosa related to bovine mastitis. Acta veterinaria Hungarica 62 (1):1-12.

220. Patrick CC, Plaunt MR, Hetherington SV, May SM (1992) Role of the Staphylococcus epidermidis slime layer in experimental tunnel tract infections. Infection and immunity 60 (4):1363-1367.

221. Nejadnik MR, Engelsman AF, Saldarriaga Fernandez IC, Busscher HJ, Norde W, van der Mei HC (2008) Bacterial colonization of polymer brush-coated and pristine silicone rubber implanted in infected pockets in mice. The Journal of antimicrobial chemotherapy 62 (6):1323-1325.

222. Stickler DJ (2008) Bacterial biofilms in patients with indwelling urinary catheters. Nat Clin Pract Urol 5 (11):598-608.

223. Davies LC, Jenkins SJ, Allen JE, Taylor PR (2013) Tissue-resident macrophages. Nat Immunol 14 (10):986-995.

224. Koseki H, Yonekura A, Shida T, Yoda I, Horiuchi H, Morinaga Y, Yanagihara K, Sakoda H, Osaki M, Tomita M (2014) Early Staphylococcal Biofilm Formation on Solid Orthopaedic Implant Materials: In Vitro Study. PloS one 9 (10):e107588.

225. Broekhuizen CAN, de Boer L, Schipper K, Jones CD, Quadir S, Feldman RG, Dankert J, Vandenbroucke-Grauls CMJE, Weening JJ, Zaat SAJ (2007) Peri-Implant Tissue Is an Important Niche for Staphylococcus epidermidis in Experimental Biomaterial-Associated Infection in Mice. Infection and immunity 75 (3):1129-1136.

226. Moriarty F, Zaat SAJ, Busscher HJ (2012) Biomaterials Associated Infection: Immunological Aspects and Antimicrobial Strategies. Springer New York.

8 Appendix

8.1 List of abbreviations

Abbreviations	Explanations
µ	micro; 10^{-6}
θ	diffraction angle
ATCC	American type culture collection
ATP	Adenosine triphosphate
agr	accessory gene regulator
AIP	Auto inducing peptide
AI	auto inducers
AgNPs	Silver nanoparticles
AECGM	Airway epithelial cell growth medium
Al	Aluminum
Bap	biofilm associated proteins
Ca	Calcium
cm	centimeter
CVC	central venous catheter
CFSE	Carboxyfluorescein diacetate succinimidyl ester
CR	corrosion rate
CFU	colony forming unit
CTR	control
CFX	Ciprofloxacin
DMEM	Dulbecco's modified Eagle's medium
DNA	Deoxyribonucleic acid

DMSO	Dimethyl sulfoxide
DNase	Deoxyribonuclease
d	day(s)
ECM	Extra cellular matrix
EPS	Exopolysaccharide
eDNA	extracellular DNA
EDX	Energy-dispersive X-ray spectroscopy
ELISA	Enzyme-linked immunosorbent assay
FCS	Fetal calf serum
FnBPs	fibronectin-binding proteins
g	gram
GTP	guanosine triphosphate
h	hour(s)
H_2	hydrogen
H&E	hematoxylin and eosin
HBSS	Hank's balanced salt solution
IL	interleukin
IVC	intravascular venous catheter
IVIS	in vivo imaging system
IFN	interferon
i.p	intraperitoneal
i.v.	Intravenous
I	relative X-ray reflection intensity
Kg	Kilo gram
K	potassium

KH_2PO_4	Potassium dihydrogen phosphate
K_2HPO_4	Potassium monohydrogen phosphate
LDH	Layered double hydroxide
LB	Lysogeny broth
Mg	Magnesium
ml	milliliter(s)
mRNA	messenger RNA
mmol	millimole
MAGT	Magnesium transporter gene
MSCRAMMS	Microbial surface components recognizing adhesive matrix molecules
M	Molar
min	min
MgF_2	Magnesium fluoride
MRSA	methicillin resistant *S. aureus*
Na	Sodium
NK	Natural killer
NO	Nitric oxide
N	Newton
OH	Hydroxide
OD	Optical density
PBS	Phosphate buffer saline
Pg	Porous glass
PIA	polysaccharide intercellular adhesion
PJI	prosthetic joint infections

PLLA	Poly L lactic acid
PCR	Polymerase chain reaction
PNEC	Porcine nasal epithelial cells
PAS	Periodic acid-Schiff
PMNs	Polymorphonuclear leukocytes
QS	quorum sensing
RNA	Ribonucleic acid
ROS	Reactive oxygen species
RNase	Ribonuclease
RT	Room temperature
rpm	revolution per minute
sarA	staphylococcal accessory regulator
SBF	Simulated body fluid
Ti	Titanium
TCR	T-cell receptor
TIVAP	Totally implantable venous access ports
w.t.	wild type
XRD	X-ray diffraction

8.2 List of figures

8.3 List of tables

Acknowledgement

I am indebted to pay my best regards and special thanks to all those who helped me to finish this work. First of all, I am thankful to my supervisor **Prof. Dr. Peter Paul Mueller** for giving me an opportunity to complete this work, his excellent guidance and substantial support, for the provision of freedom to do independent research, being magnanimous for discussions and being motivation for me. I am thankful to my co-supervisors **Prof. Dr. Manfred Kietzmann** (TiHo, Hannover) and **Dr. Wolf-Rainer Abraham** for their consistent and illuminating instructions. I would like to express my deepest gratitude to **Dr. Hansjörg Hauser** for his open and friendly attitude and always having time for discussion. My profound regards are for **Ms. Angela Walter** for her continuous support and help regarding my visa and residence issues. I pay heart filled thanks to my graduate school for organizing courses, seminars and presentations which were helpful for me.

This thesis work was funded by the German Research Foundation (DFG) within the Collaborative Research Program (SFB 599, Project D1, D8, R8 and DR1). I am thankful to Higher Education Commission (HEC) of Pakistan and the German Academic Exchange Service (DAAD) for their financial support. I am thankful to the people from SFB-599 especially **Prof Dr. Peter Behrens, Marc Kieke, Andreas Weizbauer, Florian Evertz, Ranier Eifler** and **Jan-Martin Seitz** for their enthusiastic attitude and fruitful collaboration.

I am especially thankful to Anshu Babbar for her constant support, nice company, fruitful guidance and precious advices. I am thankful to Stefan Lienenklaus for his guidance and cooperation. I would like to thank all of my colleagues from department of gene regulation and differentiation specially Bushra Rais, Shawal Spencer and Vinay Pawar for being cooperative and friendly with me. My Special thanks go to Muhammad Akram Khan, his whole family and Muhammad Zaraar Ali Khan for their prayers and best wishes.

The completion of this project would not have been possible without the help and support of my father Rahim Bux, my mother, brothers Bilal Anjum, Adnan Rahim, Farhan Rahim and my sisters who deserve my deepest gratitude and appreciation.